PhD thesis
Jointly awarded at the

Institut National des Sciences appliquées de Lyon

Ecole doctorale : Mécanique, Energétique, Génie Civil, Acoustique (MEGA)

Doctorat en Mécanique

and at the

University "La Sapienza" of Rome

Dottorato in Meccanica Teorica ed Applicata
XXIV ciclo

Tribological activation of tactile receptors by vibrations induced at the finger contact surface

Ramona FAGIANI

on December 16 2011

PhD committee:

Yves BERTHIER	Research Director CNRS (LaMCoS,CNRS, INSA of Lyon)	(Examiner)
Francesco MASSI	Maître de Conférence (LaMCoS, INSA of Lyon)	(Co-Director)
Aldo SESTIERI	Professor (DIMA, University "La Sapienza" of Rome)	(Co-Director)
Antonio CULLA	Researcher (DIMA, University "La Sapienza" of Rome)	(Examiner)
Adnan AKAY	Professor (ME, Bilkent University of Ankara)	(Examiner)
Marie Ange BUENO	Professor (LPMT, ENSISA of Mulhouse)	(Reviewer)
George DEBREGÉAS	Chargé de recherche HDR (CNRS, LPS)	(Reviewer)
Eric CHATELET	Maître de Conférence (LaMCoS, INSA of Lyon)	(Guest)

Research Laboratory:
Laboratoire de Méchanique des Contacts et des Solids (LaMCoS)
Dipartimento di Meccanica e Aeronautica (DMA)

SIGLE	ECOLE DOCTORALE	NOM ET COORDONNEES DU RESPONSABLE
CHIMIE	CHIMIE DE LYON http://www.edchimie-lyon.fr Insa : R. GOURDON	M. Jean Marc LANCELIN Université de Lyon – Collège Doctoral Bât ESCPE 43 bd du 11 novembre 1918 69622 VILLEURBANNE Cedex Tél : 04.72.43 13 95 directeur@edchimie-lyon.fr
E.E.A.	ELECTRONIQUE, ELECTROTECHNIQUE, AUTOMATIQUE http://edeea.ec-lyon.fr Secrétariat : M.C. HAVGOUDOUKIAN eea@ec-lyon.fr	M. Gérard SCORLETTI Ecole Centrale de Lyon 36 avenue Guy de Collongue 69134 ECULLY Tél : 04.72.18 60 97 Fax : 04 78 43 37 17 Gerard.scorletti@ec-lyon.fr
E2M2	EVOLUTION, ECOSYSTEME, MICROBIOLOGIE, MODELISATION http://e2m2.universite-lyon.fr Insa : H. CHARLES	Mme Gudrun BORNETTE CNRS UMR 5023 LEHNA Université Claude Bernard Lyon 1 Bât Forel 43 bd du 11 novembre 1918 69622 VILLEURBANNE Cédex Tél : 04.72.43.12.94 e2m2@biomserv.univ-lyon1.fr
EDISS	INTERDISCIPLINAIRE SCIENCES- SANTE http://ww2.ibcp.fr/ediss Sec : Safia AIT CHALAL Insa : M. LAGARDE	M. Didier REVEL Hôpital Louis Pradel Bâtiment Central 28 Avenue Doyen Lépine 69677 BRON Tél : 04.72.68 49 09 Fax :04 72 35 49 16 Didier.revel@creatis.uni-lyon1.fr
INFOMATHS	INFORMATIQUE ET MATHEMATIQUES http://infomaths.univ-lyon1.fr	M. Johannes KELLENDONK Université Claude Bernard Lyon 1 INFOMATHS Bâtiment Braconnier 43 bd du 11 novembre 1918 69622 VILLEURBANNE Cedex Tél : 04.72. 44.82.94 Fax 04 72 43 16 87 infomaths@univ-lyon1.fr
Matériaux	MATERIAUX DE LYON Secrétariat : M. LABOUNE PM : 71.70 –Fax : 87.12 Bat. Saint Exupéry Ed.materiaux@insa-lyon.fr	M. Jean-Yves BUFFIERE INSA de Lyon MATEIS Bâtiment Saint Exupéry 7 avenue Jean Capelle 69621 VILLEURBANNE Cédex Tél : 04.72.43 83 18 Fax 04 72 43 85 28 Jean-yves.buffiere@insa-lyon.fr
MEGA	MECANIQUE, ENERGETIQUE, GENIE CIVIL, ACOUSTIQUE Secrétariat : M. LABOUNE PM : 71.70 –Fax : 87.12 Bat. Saint Exupéry mega@insa-lyon.fr	M. Philippe BOISSE INSA de Lyon Laboratoire LAMCOS Bâtiment Jacquard 25 bis avenue Jean Capelle 69621 VILLEURBANNE Cedex Tél :04.72.43.71.70 Fax : 04 72 43 72 37 Philippe.boisse@insa-lyon.fr
ScSo	ScSo* M. OBADIA Lionel Sec : Viviane POLSINELLI Insa : J.Y. TOUSSAINT	M. OBADIA Lionel Université Lyon 2 86 rue Pasteur 69365 LYON Cedex 07 Tél : 04.78.69.72.76 Fax : 04.37.28.04.48 Lionel.Obadia@univ-lyon2.fr

*ScSo : Histoire, Geographie, Aménagement, Urbanisme, Archéologie, Science politique, Sociologie, Anthropologie

CONVENZIONE PER UNA CO-TUTELA DI TESI DI DOTTORATO DI RICERCA

L'INSA di Lione rappresentata dal Professore Daniel BARBIER, Addetto alla Direzione della Ricerca, che opera in virtù dei poteri che gli sono conferiti, da una parte

e

L'Università degli Studi di Roma "La Sapienza" con sede in Roma (Italia), Piazzale Aldo Moro, 5 rappresentata dal Rettore Prof. LUIGI FRATI , che opera in virtù dei poteri che gli sono conferiti, dall'altra parte

Visti, per la parte francese,
- La delibera del 6 gennaio 2005 relativo alla procedura internazionale per la cotutela di tesi (Francia);
- La delibera del 7 agosto 2006 relativo al dottorato (Francia);
- La convenzione franco-italiana tra la Conférence des Présidents d'Université (CPU) e la Conferenza dei Rettori delle Università Italiane (CRUI) sul riconoscimento dei diplomi e della validità dei titoli universitari siglata in data 18 gennaio 1996;
- La convenzione franco-italiana tra la Conférence des Présidents d'Université (CPU) e la Conferenza dei Rettori delle Università Italiane (CRUI) sulla cotutela di tesi siglata li 13 febbraio 1998;

E

Per la parte italiana:
- VISTA la Legge 210 del 3 luglio 1998 art. 4 – dottorato di ricerca;
- VISTO il D.M. 224/99 recante norme in materia di dottorato di ricerca
- VISTO il D.M. 509/99 recante norme concernenti l'autonomia didattica degli Atenei;
- VISTO il Regolamento di Ateneo in materia di dottorato di ricerca;
- VISTA la delibera del Senato Accademico del 2 ottobre 2003;

nell'intento di contribuire ad instaurare e/o sviluppare la cooperazione scientifica tra équipe di ricerca italiana e straniere attraverso la mobilità dei dottorandi

convengono e stipulano quanto segue

Parte prima – Modalità amministrative

Art. 1 – L'INSA di Lione e L'Università degli Studi di Roma "La Sapienza" denominati qui di seguito "Istituzioni" concordano, nel rispetto delle leggi e dei regolamenti in vigore in ciascun Paese e/o Istituzione, di organizzare congiuntamente una co-tutela di tesi di dottorato a beneficio della dottoranda sottoindicata:
nome e cognome: Ramona FAGIANI
iscritta al corso di Dottorato di Ricerca in Meccanica Teorica e Applicata presso l'Università La Sapienza di Roma e in "Mecanique" presso l' "ecole doctoral MEGA".
Soggetto di tesi: Attivazione tribologica dei recettori tattili causata dalle vibrazioni indotte dal contatto dito/superficie.

Lo studio della sensazione tattile dovuta all'attrito tra la pelle e la superficie é molto importante sia per caratterizzare il contatto con gli oggetti d'uso quotidiano (i tasti della tastiera del computer, i tessuti degli indumenti, plancie di bordo degli aereoveicoli...), sia per riprodurre la percezione reale, come avviene nella realtà virtuale, che per incrementarla (

realtà aumentata). Dal punto di vista fisiologico, quattro tipi di sensori, i meccanoreceptori, disposti a differenti profondità, all'interno della pelle, consentono la trasmissione delle informazioni ai centri nervosi. Ogni tipo di sensore reagisce a differenti intervalli di frequenze definendo cosi' i parametri sensoriali.

Fino ad ora, l'attivazione di questi sensori é stata connessa alla rugosità della pelle e della superficie con la quale é in contatto.

I risultati ottenuti da studi tribologici, numerici e sperimentali, hanno evidenziato che l'attrito di due corpi in contatto é accompagnato da vibrazioni che si sviluppano in un ampio range di frequenze. Si ritiene, pertanto, che siano queste vibrazioni ad attivare, a differenti frequenze e differenti profodità, i sensori della pelle.

Recenti pubblicazioni riguardanti la realtà virtuale e quella aumentata hanno messo in luce la possibilità di indurre la sensazione del contatto e le ondulazioni di una superficie sottoponendo il dito ad una vibrazione adeguata.

In questo contesto, la tesi proposta é indirizzata verso gli aspetti tribologici e dinamici della sensazione tattile. In un primo momento si realizzerà un dito modello in materiale fotoelastico al fine di determinare la dinamica locale al contatto.

Inoltre, sensori di forza e accelerazione verranno posizionati al di sotto della superficie di contatto e sul modello del dito in modo da consentire il monitoraggio del comportamento delle forze globali di contatto e dei vibrazioni del sistema.

In seguito verrà sviluppato un modello numerico non lineare per la simulazione nel tempo al fine di introdurre la rugosità del dito e della superficie in contatto e, conseguentemente, di riprodurre le vibrazioni indotte dall'interno del dito. L'analisi numerica potrà essere validata dalla comparazione con i risultati sperimentali e consentirà la caratterizzazione del legame « caratteristiche della superficie di contatto/frequenze delle vibrazioni indotte/segnali emessi dai recettori ».

Una volta noto il comportamento del dito modello, l'analisi sperimentale potrà essere estesa al dito reale. Il collegamento tra le misure locali e globali, stabilito per il modello, verrà utilizzato per interpretare le misure delle forze globali e delle vibrazioni ottenute sul dito reale.

Come ultimo passo, la sensazione tattile percepita al contatto verrà quindi collegata alle vibrazioni indotte dallo scorrere del dito su una superficie. Il modello numerico, testato sul modello di dito, verrà utilizzato per quantificare le vibrazioni indotte dall'attrito.

L'analisi sperimentale, condotta in parallelo a quella numerica, permetterà di stabilire la connessione tra le proprietà della superficie e la percezione tattile, per mezzo delle vibrazioni indotte dal contatto.

I principi e le modalità amministrative e didattiche di tale co-tutela sono definiti dalla presente convenzione.

Art. 2 - La durata per la preparazione della tesi è di 3 anni, a partire dall'anno accademico 2008/2009.
In caso di necessità tale durata potrà essere prorogata in conformità con la regolamentazione vigente nelle due Istituzioni.

Art. 3 -. La preparazione della tesi si effettuerà in periodi alterni, pressoché equivalenti, in ciascuna delle due Istituzioni. La durata di tali periodi sarà fissata in comune accordo dai due Direttori di tesi.

Art. 4 –La dott.ssa Ramona Fagiani sarà iscritta in entrambe le Istituzioni. Corrisponderà i regolari diritti di iscrizione all'INSA di Lione e ne sarà esonerata presso l' Università "La Sapienza" di Roma

Art. 5 - Per tutto il periodo di preparazione della tesi la dott.ssa Ramona Fagiani
beneficerà di quanto disposto dalla delibera del 7 Agosto 2006 e della carta dei tesisti de l'INSA de Lyon.

Art.6-Per la durata della sua iscrizione, la dottoranda dovrà fornire giustificazione relativamente alle sue risorse, alla sua coperta sanitaria così come alla sua assicurazione sugli incidenti di lavoro, in ognuno dei paesi.

Parte seconda – Modalità didattiche

Art. 1 – La dott.ssa preparerà la tesi sotto la direzione comune dei professori:
- Yves RENARD (Docente presso il Laboratorio di Meccanica dei Contatti e delle strutture), direttore di tesi all'INSA di Lione
- Aldo SESTIERI (Docente presso il dipartimento di Meccanica e Aeronautica), direttore di tesi a L'Università La Sapienza di Roma

che si impegnano ad esercitare pienamente la funzione di tutori della dottoranda e si impegnano a valutarne, ciascuno con propria relazione scritta, la tesi di Dottorato.
Il giudizio positivo di entrambi i Direttori di Tesi è condizione necessaria per l'ammissione all'esame finale.

Art. 2 - La discussione della tesi, unica e riconosciuta dalle due istituzioni, avrà luogo presso l'INSA di Lione. La Commissione giudicatrice, nominata dai Rettori delle due Università, sarà composta da un numero pari di studiosi appartenenti alle due Istituzioni e designati congiuntamente da esse, oltre a membri esterni alle due Istituzioni. Essa dovrà essere composta da un minimo di quattro membri ed un massimo di otto, appartenenti ai settori scientifico-disciplinari del Dottorato, tra cui, a meno di derogazioni, i due direttori di tesi.

Art. 3 – La tesi sarà redatta e discussa in inglese; un riassunto sostanziale sarà redatto in lingua francese.

Art. 4 – Ognuna delle due Istituzioni si impegna a conferire il titolo di dottore di ricerca per la stessa tesi, in seguito ad una relazione favorevole della Commissione giudicatrice.
L'Università degli Studi di Roma "La Sapienza" conferirà il titolo di dottore di ricerca in Meccanica Teorica e Applicata.
L'INSA di Lione conferirà il titolo di dottore di ricerca in Meccanica.

Art. 5- In caso la dottoranda deve convalidare le formazioni complementari (scientifiche o mirate alla sua inserzione professionale), le Istituzioni (l'Ecole Doctorale MEGA pour l'INSA) specificheranno le modalità di riconoscimento reciproco di queste formazioni, in accordo con i direttori di tesi ed la dottoranda.

Parte terza – Conclusione

Art. 1 – La dottoranda dovrà rispettare i regolamenti e le consuetudini dell'Istituzione ospitante.

Art. 2 – Le Istituzioni contraenti, attraverso l'intermediazione dei rispettivi direttori di tesi, si impegnano a comunicarsi rispettivamente tutte le informazioni e la documentazione utile per l'organizzazione della co-tutela di tesi oggetto della presente convenzione.

Art. 3 – Le modalità di presentazione, di deposito e riproduzione della tesi saranno effettuati in ogni paese secondo i regolamenti in vigore.
La protezione dell'oggetto della tesi, così come la pubblicazione, lo sfruttamento e la protezione dei risultati ottenuti con lo studio di ricerca della dottoranda nelle Istituzioni contraenti saranno assoggettati alla normativa in vigore e assicurati conformemente alle procedure specifiche di ciascun Paese coinvolto nella co-tutela.
Qualora richiesto, le disposizioni relative alla protezione dei diritti di proprietà intellettuale potranno costituire oggetto di protocolli o documenti specifici.

Art. 4 – La presente convenzione entra in vigore dalla data di firma del rappresentante legale di ciascuna Istituzione contraente e sarà valida fino alla fine dell'anno accademico nel corso del quale la tesi o lo studio saranno discussi.
Nel caso in cui la dottoranda non fosse iscritto in una e/o l'altra delle Istituzioni contraenti, oppure rinunciasse per iscritto a proseguire, oppure, in virtù della decisione di almeno uno dei due direttori di tesi, non fosse autorizzato a proseguire la preparazione della tesi in co-tutela, le Istituzioni contraenti porranno fine, congiuntamente e senza ritardo, alle disposizioni del presente accordo.

Art. 5 – La presente convenzione è redatta in quattro esemplari originali, di cui due in lingua italiana e due in lingua francese ,aventi valore legale.

Villeurbanne, li _____ 0 7 OCT. 2008   Roma, li _____

Per il Direttore dell'INSA de Lyon   Per il Rettore dell'Università
Professore Daniel BARBIER   La Sapienza di Roma
Addetto alla Direzione della Ricerca   Prof. Luigi Frati

_____   _____

Il Responsabile del Dottorato di Ricerca   Il Responsabile del Dottorato di Ricerca
Jean-Louis GUYADER   Carlo Massimo CASCIOLA

_____   _____

Il Direttore del laboratorio
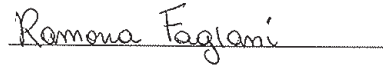Alain COMBESCURE

_____
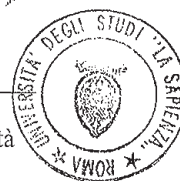
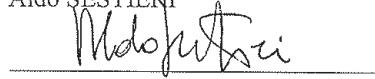Co-direttori di tesi
Yves RENARD

Francesco MASSI

La Dottoranda
Ramona FAGIANI

Co-direttore di tesi
Aldo SESTIERI

ACCORD DE COOPERATION POUR LA MISE EN ŒUVRE D'UNE COTUTELLE DE THESE

L'INSA de LYON, représenté par le Professeur Daniel BARBIER, Directeur Adjoint de la Recherche, agissant en-qualités et en vertu des pouvoirs qui lui sont conférés, d'une part
ET
L'Université de Rome "La Sapienza" ayant son siège à Rome (Italie), Piazzale Aldo Moro 5, représentée par son Recteur Professeur LUIGI FRATI agissant en-qualité et en vertu des pouvoirs qui lui sont conférés d'autre part

Vu pour la part française :
- L'arrêté du 6 janvier 2005 relatif à la procédure de cotutelle internationale de thèse (France);
- L'arrêté du 7 août 2006 relatif aux études doctorales (France);
- La convention cadre franco-italienne entre la Conférence des Présidents d'Université (CPU) et la Conferenza dei Rettori delle Università Italiane (CRUI) sur la reconnaissance des diplômes et validation des titres universitaires signée en date 18 janvier 1996;
- La convention cadre franco-italienne entre la Conférence des Présidents d'Université (CPU) e la Conferenza dei Rettori delle Università Italiane (CRUI) sur la co-tutelle de thèse signée le 13 février 1998;

Et

Pour la partie italienne :
- Vue la Loi n. 210 du 3 juillet 1998 art. 4 – doctorat de recherche ;
- Vu le D.M. 224/99 relatif aux normes en matière de doctorat de recherche ;
- Vu le D.M. 509/99 relatif aux normes en matière d'autonomie didactique des Universités ;
- Vu le Règlement de l'Université en matière de doctorat de recherche ;
- Vue la délibération du Sénat Académique du 2 octobre 2003 ;

désireux (désireuses) de contribuer à l'instauration et/ou au développement de la coopération scientifique entre équipes de recherche italiennes et étrangères en favorisant la mobilité des doctorants

sont convenu(e)s des dispositions suivantes

Titre I – Modalités administratives

Art. 1 –L'INSA de Lyon et L'Université de Rome "La Sapienza" désignées ci-après "les établissements", décident dans le respect des lois et des règlements en vigueur dans chacun des pays et/ou établissements, d'organiser conjointement une cotutelle de thèse au bénéfice de l'étudiante désignée ci-après :
Prénom et nom : Ramona FAGIANI
spécialité : ingenieur Mecanique – Doctorat en Meccanica Teorica ed Applicata
sujet de thèse : Activation tribologique des capteurs sensoriels par les vibrations induites par le contact frottant doigt - surface.

Les aspects sensoriels, liés au frottement de la peau, sont de plus en plus pris en compte notamment pour étudier le « contact » avec les objets de la vie de tous les jours (touches d'un clavier, vêtements, surface d'une planche de bord...) et pour reproduire la perception réelle (virtual reality) ou augmenter artificiellement la perception humaine (augmented reality). Physiologiquement, ce sont quatre types de capteurs (mécano-récepteurs) situés à différentes profondeurs sous la peau (derme, épiderme) qui transmettent les informations sensorielles au centre nerveux. Chaque type de capteur réagit à différentes gammes de fréquences qui seront exploitées pour définir les paramètres sensoriels.

Jusque là, l'activation fréquentielle de ces capteurs a été corrélée à la rugosité de la peau et des objets frottés. Dans les faits, les résultats récents de tribologie numérique ont mis en évidence que le frottement de deux corps en contact s'accompagnait toujours de vibrations induites dans un large spectre de fréquences. Ces vibrations locales font qu'il y a tout lieu de penser que ce sont elles qui activent ces capteurs à différentes fréquences et profondeurs, ce qui permet de sélectionner les informations provenant du frottement peau-objet. Des récents publications concernant la réalité virtuelle et la réalité augmentée ont mis en évidence la possibilité d'induire la sensation tactile d'ondulation d'une surface avec une excitation vibratoire appropriée du doigt. Toutefois, une analyse des vibrations induites par le contact frottant doigt–surface et la conséquente activation de mecano-receptors de la peau doit être encore exploitée.

Dans ce contexte, cette allocation de recherche permettra de reposer la problématique tribologique du toucher, incluant les aspects tribologiques et dynamiques.

Dans un premier temps un doigt modèle sera réalisé dans un matériau photo.élastique afin de déterminer, en dynamique, les champs de contraintes produits en surface et dans l'épaisseur du doigt modèle. Des capteurs de force et accélération seront introduits dans la surface en contact et sur le doigt modèle pour suivre le comportement des forces globales de contact et la vibration du système. Un modèle numérique nonlinéaire pour la simulation temporelle sera développé pour introduire la rugosité du doigt et du corps en contact et donc reproduire les vibrations induites à l'intérieur du doigt. Les résultats seront exploités expérimentalement et numériquement pour comprendre le lien « propriétés de la surface en contact / fréquences des vibrations induites / signaux émis par les quatre types de capteurs ».

Une fois le fonctionnement du doigt modèle compris, les résultats seront étendus au doigt réel; le lien entre les mesure locales et globale développé sur le doigt modèle seront utilisées pour interpréter les mesures globales sur le doigt réel et lier la sensation tactile aux vibrations induites par le frottement de la peau sur la surface. Le modèle numérique, un fois validé sur le doigt modèle, sera utilisé pour calculer les vibrations locales induites par le contact frottant. En fin, les caractéristiques de surfaces et de vibrations induites par le balayage du doigt seront liées à la sensation du toucher, à travers l'exploitation expérimentale et la simulation numérique.

Les principes et les modalités administratives et pédagogiques de cette cotutelle sont définis par le présent accord.

Art. 2 - La durée prévue pour la préparation de la thèse en cotutelle est de 3 ans, à partir de l'année scolaire 2008/2009.
En cas de nécessité, cette durée peut être prolongée en conformité avec la réglementation en vigueur dans les deux établissements.

Art. 3 - La préparation de la thèse s'effectue par périodes alternées, à peu près équivalentes, dans chacun des deux établissements partenaires. La durée de ces périodes sera déterminée de commun accord par les deux directeurs de thèse.

Art. 4 – L'étudiante Ramona FAGIANI
est tenue à s'inscrire régulièrement dans les deux établissements. L'étudiante paiera les droits d'inscriptions à l' INSA de Lyon et en sera dispensée près l' Université La Sapienza de Rome.

Art. 5 –Pour les périodes d'études effectuées en France et pour la soutenance, la doctorante bénéficie de l'ensemble des dispositions de l'arrêté du 7 août 2006 susvisé, et de la charte des thèses de l'INSA de Lyon.

Art.6 –Lors de son inscription, la doctorante devra fournir les justificatifs relatifs à ses ressources, à sa couverture sociale ainsi qu'à son assurance relative aux accidents du travail, dans chacun des pays.

Titre II – Modalités pédagogiques

Art. 1 – Le travail de thèse de l'étudiante sera réalisé sous la supervision commune de deux directeurs de thèse :
- Yves RENARD (Professeur au Laboratoire de Mécanique des Contacts et des Structures), directeur de thèse à l' INSA de Lyon ;
- Aldo SESTIERI (Professeur du Département de Meccanica e Aeronautica), directeur de thèse à l'Université "La Sapienza" ;

qui s'engagent à exercer pleinement la fonction de tuteurs de la candidate ainsi qu'à formuler chacun un avis écrit sur la thèse de Doctorat.
L'avis favorable des deux Directeurs de Thèse est une condition nécessaire à l'admission à l'examen final.

Art. 2- La thèse donnera lieu à une soutenance unique, reconnue par les deux établissements concernés. La soutenance aura lieu à l'INSA de Lyon.Le jury de soutenance est composé sur la base d'une proportion équilibrée de membres de chaque établissement désignés conjointement par les établissements contractants et comprend, en outre, des personnalités extérieures à ces établissements.
Il comprendra au moins quatre membres et au maximum huit membres, dont, sauf dérogation, les deux directeurs de thèse.

Art. 3-La thèse sera rédigée et discuté en Anglais. Elle comportera un résumé substantiel rédigé en français.

Art. 4 – En cas de rapport favorable du Jury, chacun des deux établissements s'engage à conférer le titre de docteur de recherche pour la même thèse.
L'Université de Rome "La Sapienza" s'engage à conférer le grade de docteur de recherche en en Meccanica Teorica e Applicata.
L'INSA de Lyon s'engage à conférer le grade de docteur de recherche en Mécanique.

Art. 5-Lorsque la doctorante doit valider des formations complémentaires (scientifiques ou visant à son insertion professionnelle), les établissements (l'Ecole Doctorale MEGA pour l'INSA) préciseront les modalités de reconnaissance mutuelle de ces formations, en accord avec les directeurs de thèse et la doctorante.

Titre III – Conclusions

Art. 1 – L'étudiante est tenu de respecter les règlements et les usages de l'établissement d'accueil.

Art. 2 – Par l'intermédiaire de leurs directeurs de thèses respectifs, les établissements signataires s'engagent à se communiquer toutes les informations et la documentation utiles à l'organisation de la cotutelle de thèse faisant l'objet du présent accord.

Art. 3 – Les modalités de présentation, de dépôt et de reproduction de la thèse seront établies dans chaque pays dans le respect de la réglementation en vigueur.
La protection du sujet de thèse, ainsi que la publication, l'exploitation et la protection des résultats issus des travaux de recherche du doctorant dans les deux établissements signataires seront assujetties à la réglementation en vigueur et assurées conformément aux procédures spécifiques à chacun des pays impliqués dans la cotutelle.
Sur demande, les dispositions concernant la protection des droits de propriété intellectuelle pourront faire l'objet de protocoles ou de documents spécifiques.
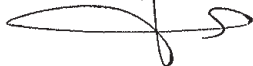
Art. 4 – Le présent accord entre en vigueur à partir de la date de signature du représentant légal de chaque établissement signataire et le reste jusqu'à la fin de l'année universitaire au cours de laquelle la thèse ou les travaux seront soutenus.
Dans le cas où l'étudiante ne serait pas inscrite dans l'un et/ou l'autre des établissements signataires, ou bien renoncerait par écrit à poursuivre, ou bien n'est pas autorisée à poursuivre la préparation de sa thèse en vertu de la décision de l'un au moins des deux directeurs de thèse, les deux établissements signataires mettront fin conjointement et sans délai, aux dispositions du présent accord.

Art. 5 – Le présent accord est rédigé en quatre exemplaires originaux, dont deux en italien et deux en française, faisant également foi.

07 OCT. 2008   Fait à Villeurbanne, le

Pour le directeur de l'INSA de Lyon   Pour le Recteur de l'Université
Professeur Daniel BARBIER   La Sapienza de Rome
Directeur Adjoint de la Recherche   Prof. Luigi Frati

Le Responsable de l'École Doctorale   Il Coordinatore del Dottorato di Ricerca
Jean-Louis GUYADER   Carlo Massimo CASCIOLA

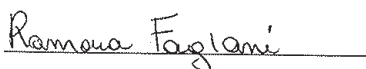Le Directeur du laboratoire
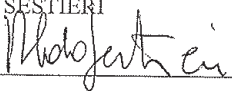Alain COMBESCURE

Co-directeur (s) de thèse
Yves RENARD

Francesco MASSI

La Doctorante
Ramona FAGIANI

Il Co-direttore di tesi
Aldo SESTIERI

Happiness is real when shared
quote from INTO THE WILD movie

Acknowledgements

This thesis has been developed in cotutelle at the "Laboratoire de Mécanique des Contacts et des Solides" (LaMCoS) of the INSA of Lyon and at the " Dipartimento di Ingegneria Meccanica e Aerospaziale" (DIMA) of the University of Rome "La Sapienza", in the framework of a french-italian agreement between the doctoral school MEGA (Mécanique, Energétique, Génie Civil, Acoustique) of Lyon and the doctoral course in Theoretical and Applied Mechanics of the University of Rome "La Sapienza", so I acknowledge the directors of the two doctoral schoola for accepting and supporting this program.

I would like to express my gratitude to Professors Francesco Massi, Yves Renard, Eric Chatelet and Aldo Sestieri for their guidance throughout the development of this work and the scientific and personal support during my research in Lyon and Rome. My thanks go also to Professor Berthier for his precious support, to Claude Godeau, George Roche and Pierre Aeby for the excellent realization of the experimental set-up.

A special thanks is due to the members of the committee and in particular to Professors George Debregéas and Marie Ange Bueno for their careful revision of the thesis, and to Professor Adnan Akay for his interest in my work.

I would like to extend my thanks to all the people and friends who shared with me these years, and naturally to my family.

i

Abstract

This thesis deals with the tribological and dynamic aspects of tactile perception given by the scanning of the finger on a surface. The attention is focused on a direct analysis of the vibration spectrum characteristics, induced by the surface features. Indeed, while great attention has been paid in the literature to the analysis of skin properties (both frictional and mechanical [1, 2]) and to the finger position and normal load effects on skin friction [3, 4], the relationship between friction induced vibrations, surface features and tactile perception is a relatively new research field. In fact, it is accepted that vibrations activate the tactile afferents and their essential role for the perception of fine textures (duplex theory of tactile texture perception [5]) but it is still unknown the link with the surface texture characteristics and the features of the induced vibration spectra.

The work is aimed to contribute to the definition of objective indexes of the surface perception (softness, textile quality, perceived roughness, etc.) and to understand more deeply the mechanisms of the tactile sense, that is basilar for manifold different applications: textile quality quantification, ergonomics of everyday objects (which largely affects their commercial competitiveness), identification of surface imperfections, the design of tactile communication devices, the development of artificial tactile sensors for intelligent prostheses or robotic assistants, the development of human-machine interfaces for interaction with virtual realities or teleoperation systems, such as for telediagnosis or microsurgery, reproducing real perception (virtual reality), increasing the human perception (augmented reality), development of tests for evaluation of tactile sensitivity during diagnosis or monitoring process in rehabilitation. Human tactile sensory perception is due to the nerve fibers contained in the skin. In fact, while the interactions between the environment and the humans consist of mechanical and thermal stimuli, brain codes are based on electrical impulses transported by the nervous system. The two code types are linked by the cutaneous sensory neurons that, activated by the physical stimulus (mechanical and/or thermal), respond producing an electrical signal sent to the brain.

Focusing the attention on the mechanical stimuli detection, when fingertip and object surface are in contact with a relative motion, the sliding between the two surfaces generate vibrations that propagate into the skin and cause a continuous change of the skin stress state. Four types of tactile sensors, named mechanoreceptors, located at different depths under the skin (dermis, epidermis), transduce skin deformations throughout their discharge rate, permitting the perception of the surface characteristics.

These tactile units are made by an afferent fiber and its unmyelinated ending that distinguishes them as Merkel disk, Meissner's corpuscles, Ruffini endings and Pacinian corpuscles [6, 7]. Each of these endings is associated with tactile afferents populations, classified, on the basis of receptive field size and response to sustained stimulation, respectively in: the SA I (slowly adapting type I), the FA I (fast adapting type I), the FA II (fast adapting type II) and SA II (slowly adapting type II). The capabilities of discerning single object surface information are linked to their form and location, that confer them specific response properties and, in consequence, specific tactile functions. With respect to the tactile information coded, the SA I reacts from about 1 Hz to 16 Hz and are responsible for the detection of object spatial structure, texture and form; the FA I, easily excited between 3 Hz and 40 Hz, gives the perception of the motion (fundamental for grip control); the FA II, reacting in a range of 40-500 Hz, transmits vibration sensation and the SA II, responding from 100 Hz to 500 Hz, gives the skin stretch sensation [8].

The study of a finger that moves on a surface involves different difficulties that are related to the material characteristics and to the measurements themselves. For example, it is impossible to measure and to maintain the fidelity of the contact between finger and object surface at the same time. Moreover, each finger and each hand have specific mechanical properties, mechanoreceptors density and distribution and, in consequence, different sensitivity. One major issue is due to the difficulty to analyze the vibrations induced by the scanning, which are very low in magnitude, and to isolate them from the noise coming out from an experimental set-up, in order to detect them without significant alteration.

For these reasons, as a first step, of the presented work, a new experimental set-up, named TriboTouch, has been developed to reproduce the finger/surface scanning phenomena under real values of the contact feature (scanning velocity and amplitude, surface roughness, etc...), avoiding undesired vibrations. The contact forces are acquired by means of two triaxial force transducers placed below the surface sample while the induced vibrations by a light accelerometer placed on the finger nail. The test bench has been designed to guarantee the measurements reproducibility and to perform measurements without introducing external noise. In fact, the relative motion between finger and surface is obtained, without any other interface under sliding contact, by a compliant system and a linear voice coil actuator which, through a feed-back control and a TTL linear encoder, allows for imposing the desired scanning velocity.

The set-up permits to carry out both measurements of the global dynamics, meaning that an accelerometer is mounted on the finger nail to detect the induced vibrations, and local ones (at the contact zone) employing a silicone fake finger. In both cases, the fingertip, which is the main point of measurement, is fixed while the scanning of the surface is allowed by the sample translation, to have a better control of the applied normal force and of the scanning speed. The fake finger is realized in RTV (Room Temperature Vulcanizing) silicone which allows to reproduce fingerprints and fingertip shape by molding technique. An aluminum lever, representing the finger bones, allows to fix the finger on the set-up struc-

ture and confers stiffness to the finger. A fast camera is employed to record the finger motions at the contact zone during the scanning of the fake finger on the surface.

In the presented analysis, the behavior of the right hand index finger scanning on the surface sample with periodical and isotropic roughness and on textiles has been investigated for different scanning speed. Experimental tests characterizing the vibration spectra with respect to scanning speed and surface roughness are developed highlighting the role of fingerprints (that discriminates the frequency distribution of the vibration spectra) and confirming the "duplex model of tactile roughness perception" [5, 9, 10, 11, 12, 13, 14]. This model makes distinction between the perception of fine textures (spatial period smaller than 100 μm), highlighted by vibrations, and the coarse ones (spatial period bigger than 200 μm), characterized by a "single spatial intensive code", mediated by SA I afferents. Both aspects play important role for transition textures, meaning a characteristic size of about 100-200 μm.

With respect to the periodic roughness samples, the carried out measurements show well defined frequency peaks that depend on the spatial periods of both the fingerprints and roughness sample. As expected, the frequency peak values are a function of the relationship between the surface sample, the fingertip roughness and the scanning speed. Specifically, the frequency peak value increases linearly with the increase of the scanning velocity. With respect to the sample roughness width, it is possible to distinguish three different behaviors in function of the fingerprints wavelength:

I: the surface sample wavelength is smaller than the fingerprint one: the frequency peak value depends primarily on the roughness wavelength of the sample.

II: the surface sample wavelength is comparable with the fingerprint one: the frequency peak is function of the ratio between the wavelengths of the sample and of the fingertip. This behavior is due to the excitation mechanism provided by the sliding between the two quasi-sinusoidal surfaces.

III: the surface sample wavelength is larger than the fingerprint one: the frequency peak value depends primarily on the roughness wavelength of the fingerprints. In this case the measured frequencies are, for the same subject, almost constant for all the sample roughness.

The same behaviors have been found for different subjects; nevertheless, even if the global trend of the spectra in function of roughness and scanning velocity is the same, the values of the peak frequencies and the slope of the curves change because of the different fingertip characteristics.

These results allow to distinguish two different perception mechanism of the surface roughness as a function of the roughness wavelength: while in I and II the spectra of the scanning induced vibrations are affected by the surface roughness, in III the spectra of the induced vibrations do not give information about the surface, because they are only function of the fingerprints width.

The amplitude of the frequency peaks rises by increasing the scanning speed and shows a nonlinear dependence on the normal load applied during the scan-

ning. The tests show that for the same speed, the amplitude, starting from a high value, decreases until the load of 0.25 N is reached; it remains almost constant for values between 0.25 and 1 N and, finally, and it rises for higher force values. These results agree with the neurophysiologic studies asserting that people tactile pattern recognition is independent of contact forces ranging from 0.2 to 1 N [15] while, for greater values, the normal load applied from the fingertip on the object surface influences the perceived roughness [16]; higher applied forces correspond to higher perceived roughness. This is due to both the vibration magnitude increase and to the change of the contrasts in the roughness pattern in contact. In fact, increasing the force, the finger deformations rise modifying the contact area and the finger pattern.

The tests have been carried out with surface samples having isotropic roughness, i.e. without any preferential direction. Measurements of induced vibrations coming from the scanning between fingertip and isotropic roughness show that the induced vibration spectra stay in the activation frequency range of mechanoreceptors. In this case, the vibration spectra show a large band frequency distribution rather than a main frequency peak, like with periodic roughness. Nevertheless, like for the periodic roughness surfaces, from the obtained spectra it is possible to observe that, increasing the scanning velocity, both the frequencies and the amplitude of the induced vibrations increase. The vibration spectra obtained when scanning textiles show a frequency behavior that is a combination of the spectra previously described. In fact, there are well defined frequency peaks, characteristic of periodical surface roughness, and a larger frequency distribution, characteristic of isotropic roughness. This behavior is due to the structure of the textile: the main frequency peaks are due to the fingerprints periodicity and to the periods of the fabric texture, while the higher frequency distribution is related to the roughness of the wires composing the texture. This particular feature of the induced vibration spectra, when scanning a textile, opens a new interest field of investigation to link the different components of the spectra with the quality perception when touching a textile.

Like for the periodical and random roughness surfaces, it is possible to observe that, increasing the scanning velocity, the amplitude of the vibration increases and the induced vibrations move to higher frequencies. The measurements developed with the fake finger show a high compatibility of the global behavior with respect to the ones performed on the real finger employed for the molding technique.

A simple numerical model have been developed for reproducing the behavior of the induced vibrations when sliding two periodical surfaces and the numerical results have been compared with the experimental ones. A finite element model has been realized with the code PLASTD, developed at the LaMCoS for transient simulation of contact problems between deformable bodies. The scanning between fingertip and sample surfaces has been simulated numerically for reproducing the experimental tests and investigating the local behavior at the contact surfaces.

The presented work has shown the possibility to obtain objective indexes for

the tactile perception characterization, by means of the friction induced vibration spectrum analysis, in agreement with the neurophysiological studies present in literature. This opens a wide range of perspectives for the characterization of the tactile perception, and in consequence, this work can serve as a basis for the formalization of the link among tactile perception, induced vibrations and surface properties.

Keywords: Tactile perception, mechanoreceptors, textiles, roughness, friction induced vibrations, tribology.

Résumé

Cette thèse traite des aspects tribologiques et dynamiques de la perception tactile donnée par un doigt lors du balayage d'une surface. Une attention particulière est portée à l'analyse directe des spectres des vibrations induites par contact entre le doigt et la surface touchée. Jusqu'alors, une grande attention a été portée à l'analyse des propriétés de la peau (coefficient de frottement, propriétés mécaniques [1, 2]) et aux effets des paramètres locaux au contact (charge normale, vitesse relative, etc.) sur le frottement de peau. Ainsi, la relation entre les vibrations induites par frottement, les propriétés de la surface et la perception tactile représente un nouveau champ de recherche. En fait, si le fait que les vibrations activent les afférentes tactiles et leur rôle essentiel pour la perception des textures fines est une chose acquise (duplex theory of tactile texture perception [5]), le lien entre les caractéristiques de la surface, leur perception et les caractéristiques des spectres des vibrations induites est encore inconnu.

Ces travaux de recherche s'inscrivent donc dans l'exploration de ces aspects encore inconnus et sont animés par la volonté de contribuer de la définition d'indices objectifs à la perception de surfaces (douceur, qualité du textile, rugosité perçue...) et de comprendre les mécanismes à la base du toucher, élément clé de nombreuses applications touchant différents domaines : la quantification de la qualité des textiles, l'ergonomie des objets du quotidien (affectant grandement leur compétitivité commerciale), l'identification des imperfections de surface ; la conception de dispositifs tactiles de communication , le développement de capteurs tactiles artificiels pour les prothèses intelligentes ou assistants robotisés, le développement des interfaces homme-machine pour l'interaction avec les réalités virtuelles ou des systèmes de télé-opération (télédiagnostic ou microchirurgie), ou encore le développement de tests d'évaluation de la sensibilité tactile lors d'un diagnostic. D'un point de vue biologique, la perception tactile humaine est reliée aux fibres des nerfs contenues dans la peau. Ainsi les stimuli mécaniques et thermiques provenant de l'interaction de l'homme et de son environnement produisent des impulsions électriques qui sont transportées par le système nerveux jusqu'au cerveau.

Les unités tactiles sont constituées d'une fibre afférente avec différentes terminaisons amyélininiques possibles les distinguant en disques Merkel, corpuscules de Meissner, de Ruffini et de Pacini [6, 7]. Chacune de ces terminaisons est associée à une population tactile, classée en différent types d'adaptation, sur la base de la taille des champs récepteurs et de la réponse à la stimulation soutenue : SA I, adaptation lente de type I ; FA I, adaptation rapide de type I ; FA II, adaptation

rapide de type II ; SA II, adaptation lente de type II. Les capacités de discerner les informations de la surface de l'objet sont liées à leur forme et à leur emplacement, qui leur confèrent des propriétés spécifiques de réponse et, en conséquence, différentes fonctions tactiles. En ce qui concerne les informations tactiles codées les SA I, réagissant entre 1 Hz et 16 Hz, sont responsables de la détection de la structure spatiale de l'objet, la texture et la forme ; les FA I, facilement excités entre 3 Hz et 40 Hz, donnent la perception du mouvement, fondamental pour le contrôle de l'adhérence ; les FA II, réagissant entre 40 à 500 Hz, transmettent une sensation des vibrations et les SA II, répondant de 100 Hz à 500 Hz, donnent la sensation de l'étirement de la peau [8].

L'étude d'un doigt se déplaçant sur une surface, comporte plusieurs difficultés liées aux caractéristiques du contact et aux mesures mêmes. Par exemple, il est impossible de mesurer et maintenir simultanément la fidélité du contact entre le doigt et la surface de l'objet. De plus, chaque doigt, chaque main possède ses propres propriétés mécaniques et densité de mécanorécepteurs spécifiques, et par conséquent, une sensibilité au toucher différente. Un autre problème majeur est dû à la difficulté d'analyser les vibrations induites par balayage, vibrations de très faibles amplitudes et il est donc difficile de les isoler du bruit sortant du dispositif expérimental.

Ces problèmes ont fait que la première étape du travail présenté a été la conception d'un nouveau dispositif expérimental, baptisé TriboTouch, développé pour reproduire le balayage d'une surface par un doigt dans des conditions de contact réalistes (vitesse de balayage, charge normale, rugosité de surface, etc.) et surtout, en évitant la production de bruit. Les forces de contact sont récupérées au moyen de deux capteurs de force triaxiaux, placés en dessous de l'échantillon de surface, tandis que les vibrations induites par le balayage sont mesurées avec un accéléromètre placé sur l'ongle. Le banc d'essai a été conçu pour garantir la reproductibilité des mesures et pour effectuer des mesures sans introduire de bruit parasite. En effet, le mouvement relatif entre le doigt et la surface est obtenu, sans aucune autre interface glissant grâce à un système à lames flexibles et un actionneur linéaire électromagnétique qui, à travers d'un contrôle de feed-back et d'un codeur TTL linéaire, permet d'imposer le déplacement désiré, évitant ainsi la présence d'interface de contact frottante autre que celle du doigt/surface.

Le TriboTouch permet de réaliser à la fois des mesures de la dynamique globale, avec un accéléromètre monté sur l'ongle du doigt afin de détecter les vibrations induites, et des mesures de la dynamique locales (au niveau de la zone de contact) employant un doigt en silicone. Notons que dans les deux cas, le doigt, principal point de mesure, est fixe, (le balayage de la surface étant permis par la translation de l'échantillon) ; permettant un meilleur contrôle de la force appliquée et de la vitesse de balayage. Le doigt modèle est réalisé en silicone RTV (Room Temperature Vulcanizing) qui permet de reproduire les empreintes digitales et la forme du doigt par moulage. Un levier en aluminium, qui représente l'os du doigt, permet de fixer le doigt sur la structure et ainsi rigidifie le doigt. Pour mesurer la vibration locale, une caméra rapide est utilisée pour enregistrer les mouvements du doigt modèle pendant le balayage sur la surface.

L'analyse présentée s'intéresse au comportement de l'index de la main droite, en contact avec différentes surfaces (rugueuses périodiques ou isotropes et issues de textiles), analysé pour différentes vitesses de balayage et valeurs de la charge appliquée. Des essais expérimentaux caractérisant les spectres de vibration à l'égard de la rugosité et de la vitesse de balayage sont développés en soulignant le rôle des empreintes digitales : La periode spatiale des empreintes discrimine la distribution de fréquence des spectres de vibration en confirmant le "double modèle de perception de rugosité" [5, 9, 10, 11, 12, 13, 14]. Ce modèle fait la distinction entre la perception des textures fines (période spatiale inférieure à 100 μm), mis en évidence par les vibrations, et les textures grossières (période spatiale plus grande que 200 μm), caractérisée par un "code spatial", perçue par les afférences SA I. Ces deux aspects jouent un rôle important pour les textures de transition, c'est à dire pour une taille caractéristique d'environ 100-200 μm.

En ce qui concerne les échantillons de rugosité périodique, les mesures effectuées montrent des pics de fréquence bien définies qui dépendent de la période spatiale des empreintes digitales et de la rugosité des échantillons. Comme prévu, les valeurs des pics sont fonction de la relation entre la rugosité de l'échantillon de surface, du doigt et la vitesse de balayage. Plus précisément, la valeur du pic de fréquence augmente linéairement avec l'augmentation de la vitesse de balayage. En ce qui concerne la longueur d'onde de la rugosité de l'échantillon, il est possible de distinguer trois comportements différents en fonction de la longueur d'onde des empreintes digitales :

- Zone I : la période spatiale de l'échantillon de surface est plus petite que celle des empreintes digitales ; la fréquence des vibrations induites dépend essentiellement de la période de rugosité de l'échantillon.
- Zone II : la période de l'échantillon de surface est comparable à celle des empreintes ; la fréquence des vibrations est fonction du rapport des périodes de l'échantillon et du doigt.
- Zone III : la période de la rugosité de la surface de l'échantillon est plus grande que celle des empreintes digitales ; la valeur du pic de fréquence dépend essentiellement de la période de la rugosité des empreintes digitales. Dans ce cas, les fréquences mesurées sont, pour le même sujet, presque constante pour toutes les rugosités des différents échantillons.

Le même comportement a été trouvé sur des sujets différents (tendances globales des spectres en fonction de la rugosité et la vitesse de balayage identiques), pourtant les valeurs des fréquences des pics changent en raison des caractéristiques des empreintes digitales des doigts qui sont par nature différentes. Ces résultats permettent de distinguer les deux mécanismes de perception différents de la rugosité de la surface en fonction de la longueur d'onde de la rugosité. Alors que dans les zones I et II, les spectres des vibrations induites par le balayage sont liées à la rugosité de la surface, dans la zone III, les spectres des vibrations induites ne donnent pas d'informations sur la surface, car ils sont fonction de la largeur des empreintes digitales.

L'amplitude des pics de fréquence augmente avec la vitesse de balayage et montre une dépendance non linéaire avec la charge normale appliquée. Les tests

montrent que, pour la même vitesse, l'amplitude des vibrations reste pratiquement constante pour des valeurs de force normale comprises entre 0,25 et 1 N et augmente pour des valeurs supérieures de la force. Ces résultats concordent avec les études neurophysiologiques affirmant que la reconnaissance tactile est indépendante des forces de contact entre 0,2 et 1 N [15] tandis que, pour des valeurs plus élevés, la charge normale appliquée influence la perception de la rugosité [16].

Des tests ont été effectués avec des échantillons de surface ayant une rugosité isotrope, c'est à dire sans direction préférentielle. Les mesures de vibrations induites provenant du balayage des différentes surfaces par le doigt montrent que, pour ce type de rugosité, les spectres de vibrations induites restent dans la gamme des fréquences d'activation des mécanorécepteurs. Les spectres de vibration montrent alors une large distribution de fréquences plutôt qu'un pic principal en fréquence, comme pour les surfaces à rugosités périodiques. Néanmoins, comme pour les surfaces à rugosités périodiques, à partir des spectres obtenus, il est possible d'observer que, en augmentant la vitesse de balayage, les fréquences et l'amplitude des vibrations induites augmentent. Ceci permet d'étendre l'effet de la vitesse de balayage à des surfaces non périodiques.

En fine, les spectres de vibration obtenus par le balayage du doigt sur des textiles montrent un comportement en fréquence qui est une combinaison des spectres obtenus avec des surfaces à rugosités périodiques et isotropes. En fait, des pics en fréquence bien définis, caractéristiques des surfaces avec rugosités périodiques, sont relevés ainsi qu'une distribution plus large en fréquences, caractéristique d'une rugosité isotrope. Ce comportement est dû à la structure même du textile : les pics en fréquence sont dus à la périodicité des empreintes digitales et aux périodes de la texture du tissu, tandis que la large distribution en fréquence est liée à la pilosité des fibres du tissu. Ces caractéristiques particulières des spectres de vibration induite, obtenues par le balayage du doigt sur des textiles, ouvrent un nouveau champ d'analyse pour relier les différentes composantes des spectres avec la perception de la qualité lorsqu'on touche un tissu. Les mesures développées avec le doigt modèle sont comparables au comportement global à l'égard de celles effectuées avec le doigt réel utilisé pour le moulage.

Un modèle numérique simple a été développé pour reproduire le comportement des vibrations induites lors du balayage de deux surfaces périodiques et les résultats sont comparés aux résultats expérimentaux. La correspondance de la distribution des fréquences de vibrations a mis en évidence le rôle clé des empreintes digitales dans les spectres de vibration et, en conséquence, pour la perception tactile. Un premier modèle éléments finis a été réalisé avec le code de PLASTD, développé au LaMCoS pour la simulation de problèmes de contact. Le balayage du doigt sur différentes surfaces de l'échantillon a été simulé numériquement pour reproduire les essais expérimentaux et analyser le comportement local de la zone de contact.

Les travaux de recherche de cette thèse ont montré la possibilité d'obtenir des données/index objectif pour la perception tactile, aux travers de l'analyse de spectres de vibrations induites, en accord avec les données neurophysiologiques

(subjectives) présentes dans la littérature. Ceci ouvre donc une large gamme de perspectives pour caractériser la perception tactile et, par conséquent, ce travail peut servir de base à la formalisation du lien entre la perception tactile, les vibrations induites et les propriétés de surface.

Mots-clé : Perception tactile, mécanorécepteurs, textiles, rugosité, vibrations induites, tribologie.

Contents

List of Figures

x

List of Tables

Introduction

Human tactile sensory perception is due to the nerve fibers contained in the skin. In fact, while the interactions between the environment and the humans consist of mechanical and thermal stimuli, brain codes are based on electrical impulses transported by the nervous system. The two code types are linked by the cutaneous sensory neurons that, activated by the physical stimulus (mechanical and/or thermal), respond producing an electrical signal sent to the brain.

Focusing the attention on the mechanical stimuli detection, when hand and object surface are in contact with a relative motion, the sliding between the two surfaces generate vibrations that propagate into the skin and cause a continuous change of the skin stress state. Four types of tactile sensors, named mechanoreceptors and located at different depths under the skin (dermis, epidermis), have to transduce the skin deformations throughout their discharge rate, into electrical impulses, allowing for the perception of object surface characteristics.

Thus, the induced vibrations [17] generated by the relative motion between surface and finger, under adequate applied force and scanning speed, allow for the perception of the surface features. Substantial changes, in the perception of surface properties, are introduced by the scanning parameters (like relative speed, contact load and motion direction) and by the skin properties. In fact, the skin is a multilayered structure, in which each layer has specific properties, in terms of anisotropy, elastic modulus, connectivity, hydration, innervations; in particular, the epidermis has specific ridge orientations, conferring unique characteristics (sensibility, compliance, friction) to the finger. So, in consequence, skin deformations capabilities determining stress strain field, influence the mechanoreceptor response and then the tactile perception. In addition to this, the mechanoreceptors have different sensitivity properties (range of frequency, discharge rate, directional sensitivity, etc . . .) related to their form. In consequence, when people need to know a specific characteristic about an object, chose to make the movement that is more appropriate for that property. For example, moving the hand back and forth across the surface it is possible to determine the texture information, while tapping with a finger it useful to characterize the object compliance and so on. . .

The open problem

The key of the human tactile sensing is contained in the skin frictional properties, in the biomechanics of skin and subcutaneous tissues and, consequently,

1

in the features of the vibrations induced by the finger/surface scanning. These issues that affect both the objects and the contact features allowing to understand the tactile perception mechanism.

With this purpose some steps have been performed in different research fields. For example, recent publications on virtual reality and augmented reality have highlighted the possibility of inducing the tactile sensation of surface undulations by exciting the finger nail with an appropriate vibration [18, 19]. On the other hand, tribological studies have investigated skin mechanical and frictional properties, highlighting the effects of skin natural production of sweat during the contact and finger scanning direction and inclination (with respect to the subject surface).

Great attention has been paid to the study of skin properties, both frictional and mechanical [1, 2], and of the finger position and normal load effects on friction [20, 21, 22]. On the contrary, the relationship between features of the vibrations induced by the scanning of the finger on the surface, the surface characteristics and the tactile perception constitutes a relative new research field. In fact, while it is accepted that vibrations activate the tactile afferents and are essential for the texture perception ([5]), it is still unknown how the surface characteristics are perceived and quantitatively distinguished through the friction induced vibrations and the consequent mechanoreceptors activation. In particular, investigating the relationship between the vibration spectra and the tactile perception could be possible to define objective indexes and reproducible stimuli of the perceived surface characteristics.

Thesis purpose and motivations

The aim of the project, which is the framework of the present thesis, is to approach the haptic sense directly investigating the vibrations induced by the finger/surface scanning, which are the direct cause of the tactile perception coded by the brain. Instead of focusing on each single feature of the contact pair (surface texture, material compliance, friction characteristics, etc.), the focus is moved directly into the induced vibrations, which are affected by the contact characteristic and already contain the information perceived by the brain. In such a way, the analysis keeps into account for the complexity of the phenomenon, which is affected by a large number of parameters that interact each other and by the signal perceived by the mechanoreceptors. In other words, to overcome the issue of neglecting the effect of a parameter or a combination of parameters (e.g. when accounting for the texture of the object surface only) the attention is focused on the consequence of the sliding contact, which is the direct element of activation of the human receptors, e. i. the induced vibrations. This thesis is a first step of a project that is aimed to the definition of a quantitative characterization of the link between contact features, induced vibrations and tactile perception. In particular the work object of the thesis can be divided into three main steps:

- First, the design and development of an innovative experimental test bench has been necessary, allowing for a reliable reproduction and measurement of the induced vibrations due to the scanning of a finger on different surfaces.
- Then, a first experimental campaign has been carried out to validate the set-up and to investigate the influence of some of the main factor of influence, like scanning speed and load, surface roughness and texture; the results have been validated by comparison with neurophysiologic studies in literature.
- Numerical models have been developed for reproducing the scanning phase and the induced vibrations, with the aim of performing a parametrical analysis and allowing for the comparison between global dynamics (measurements on the finger nail) and local dynamics (vibrations at the contact surface). The development of the models has been initiated during the thesis.

Starting from the obtained results, with the support of the new experimental test bench, the following perspectives of the project will be object of further investigations:

- While the presented results revealed the capability of recognizing the effect of the main parameters into the vibration spectra, the influence of several features of the contact has still to be investigated: material compliance, surface adhesion, texture adaptation, scanning direction, etc. The test bench will be used to dissociate the effect of each parameter from the others, under controlled conditions.
- The numerical analysis will be further developed for comparing the global and local dynamics, for understanding whether the global measurements are sufficient to characterize the local dynamics at the contact, which is perceived by the mechanoreceptors.
- Once the link between contact features and vibration spectra is obtained, a statistical analysis on a large number of human subjects has to be developed to investigate the link between the characteristics of the induced vibration spectra (objective data) and tactile perception (subjective data).

This work wants to contribute to the definition of objective indexes about the surface perception (softness, textile quality, perceived roughness, etc.) and, consequently, to a deeper understanding of the mechanisms of the tactile sense, that is important for manifold different applications like:

- textile quality quantification;
- ergonomics of everyday objects, which largely affects their commercial competitiveness;
- identification of surface imperfections;
- the design of tactile communication devices;
- the development of artificial tactile sensors for intelligent prostheses or robotic assistants;
- the development of human-machine interfaces for interaction with virtual realities or teleoperation systems, such as for telediagnosis or microsurgery;
- reproducing real perception (virtual reality);

    – increasing the human perception (augmented reality);

    – the development of tests for the evaluation of tactile sensibility during diagnosis or monitoring of process in rehabilitation.

Thesis overview

The investigation of the vibrations induced by a finger that moves on a surface involves different difficulties that are related to the contact characteristics and to the measurements themselves. When dealing with friction induced vibrations of relative low intensity, it is quite difficult to reproduce the phenomenon and to measure it without affecting the measurements with external noise coming from the experimental test-bench. In fact the reproduction of the sliding contact between two surfaces implies the relative motion between them, which is obtained by appropriate mechanisms having a more or less complicated kinematics and including several sliding surfaces (bearings, sliders, etc. . .). In such context, it results quite difficult to distinguish between the vibrations coming from the reproduced sliding and the parasitic noise coming from the other sliding contact pairs.

For this thesis, it has been decided to start the analysis considering a linear motion of the right hand index finger. In order to avoid undesired vibrations, a new experimental set-up, named TriboTouch, has been developed to provide the relative motion between the contact surface by means of a compliant system and to recover the contact forces (by means of two triaxial force transducers placed below the surface sample) and the induced vibrations (throughout a light accelerometer fixed on the finger nail).

The test bench has been designed to guarantee the measurement reproducibility and to perform measurements without introducing external noise. In fact, the relative motion between finger and surface is obtained without any other interface under sliding contact thanks to the afore mentioned compliant system and a linear voice coil actuator. Since the local dynamics, i.e. vibrations at the contact interface, cannot be investigated on the real finger, a silicone fake finger has been developed. Such fake finger allows to measure both the global dynamics, as for the real finger (mounting an accelerometer on the finger nail), and the local dynamics, by means of a fast camera. Indeed, creating a speckle image on the finger, at the contact zone, it is possible, with fast camera, to register the finger motions during the contact and throughout image cross-correlation technique to calculate the finger deformations fields.

A brief description of tactile perception mechanism and human fingers features is presented in the first chapter.

The second chapter contains the set-up development description. Once designed and constructed the TriboTouch test bench, a system validation to verify the parasitic noise magnitude and the measurement capabilities of the systems has been performed. The measurement methodology and the transducers choice have also been validated.

The experimental results obtained employing the TriboTouch set-up are presented in the third chapter. These measurements deal with the vibration spectrum characteristics as a function of the surface samples features (texture and hairiness), and of the scanning conditions (scanning speed and contact force). They show a good agreement with neurophysiologic studies in literature and allow to highlight the role of the fingerprints on the touch sense. The vibration spectra show different behaviors, with respect to the touched surface roughness properties, that largely depend from the relationship between the fingerprint period and the surface sample texture.

The global measurements of the induced vibrations on the finger nail serve as a reference for the reliability of the fake finger, too. Chapter 3 also contains the comparison between real and fake finger with respect to the measured induced vibration spectra and the measured friction coefficient.

In chapter four, the results obtained from a simplified numerical model, developed for reproducing the behavior of the induced vibrations when sliding two periodical surfaces, are presented and compared to the experimental ones. Therefore, a finite element model has been realized with the code PLASTD, developed at the LaMCoS for transient simulation of contact problems between deformable bodies, for simulating the scanning of the finger on the surface sample.

The numerical simulations allow for reproducing the experimental tests and investigating the local behavior at the contact surfaces. The numerical model can be employed for investigating the link between local and global dynamics.

At the end a concluding chapter gives a summary of the main results obtained by the presented analysis and the perspective of the project that serves as a base to the formalization of the link between tactile perception, induced vibrations and surface properties.

Chapter 1

Tactile sense in the literature

The sensory perceptions constitute several communication channels with the external world, each of them specialized in decoding specific information. For example, the sight furnishes information on object localization, but it is the touch sense that suggests information about the material. So, in general, it is an appropriate combination of the different senses that supplies the global information rather than a single isolated sense. On the other hand, the only way to perceive the physical properties of an object is to touch it. In fact, only during the contact, the human hand is able to detect the different object properties and characteristics, like material, geometric and thermal ones. Different recognized properties are linked to different hand motions. According to [6], it is possible to make distinction in:

- tactile sensing, in which there is contact between a stationary hand and an object, which may or not move. It provides some information about the surface of the object, like texture, compliance and thermal conductivity;
- active haptic sensing, where the hand moves on the surface object providing specific information about object properties;
- prehension, when the hand reaches to grasp an object;
- non-prehensile skilled movements, that involve each gesture made during or substituting a speech.

The specific movements made by the hand (active touch), or by the object (passive touch) active the somatosensory neurons that innervate the skin, providing the connection between touch and object properties perception. The somatosensory neurons have to transduce the physical stimulus into an electric one that is sent to the brain.

The cutaneous sensory neurons can be divided into three classes according to sensory modality [7, 23]: nociceptive units, thermoreceptive units and mechanoreceptive units. While the last two afferents take their name from the stimulus to which their are most sensitive, the nociceptive units are able to respond both to mechanical and thermal stimuli but from a very high threshold corresponding to a damaging level and thus to pain sensations [24]. Thermal information, in the range 5-45° C, are transducted from the termoreceptors that are divided into warm and cold receptors [25].

1.1   Mechanoreceptors

Focusing the attention on the touch sensation, it is possible to consider just the mechanorecetive units that are activated by the skin stress-state variation generated during the tactile sensing. In fact, due to the mechanical loads generated by the contact, the fingertip skin surface is deformed. At any instant of time, during the contact, there is a space-time variation of the stress-state that causes the mechanoreceptors to respond with an appropriate space-time variation of their discharge rate that transduces the mechanical stimulus (deformations and vibrations induced from the finger-surface scanning and propagating into the skin) into neural signals.

These tactile units are made by an afferent fiber and its unmyelinated ending that distinguishes them as Merkel disk, Meissner's corpuscles, Ruffini endings and Pacinian corpuscles. They are located at different depths in the skin, ranging from the epidermis (Meissner's corpuscles) to the subcutaneous fat layer below the dermis, corresponding to a maximal depth of about 3 mm (Figure 1.1).
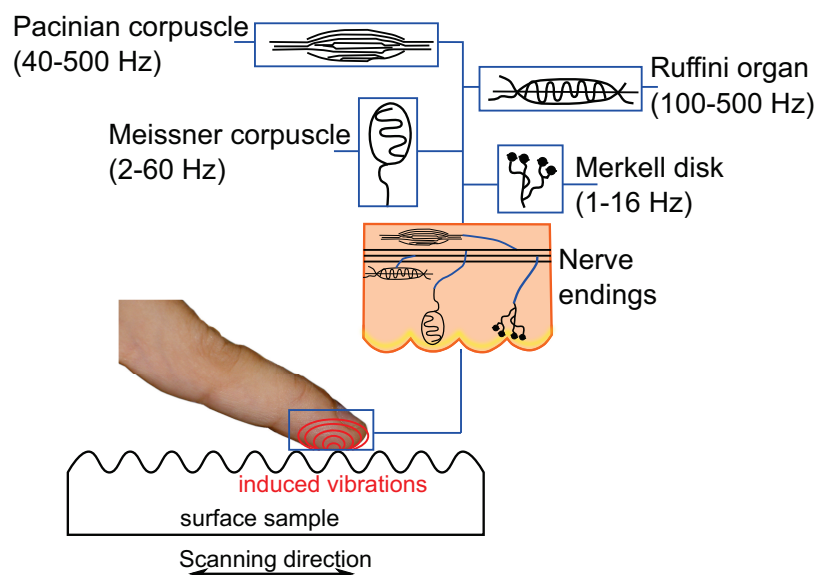
Figure 1.1: Schematic representation of the contact between the finger and the surface sample and of the mechanoreceptors.

The Meissner corpuscles have ovoid shape with axial dimensions of about 100x500 μm and have the long axis perpendicular to the skin surface. They have a peculiar shape that involves cell layers able to cushion and enfold the RA units endings, acting as a filter and thus protecting the afferent units from static skin deformation [26].

The Merkel cells are oval or rounded and have a diameter of about 10 μm.

The Ruffini corpuscles are spindle shaped, 500-1000 μm long, up to 200μm in diameter in the central area and 30-40μm near the poles, and their long axis typically runs parallel to the skin surface. The location in the dermis connective tissue gives them an high sensitivity to skin stretch.

The Pacinian corpuscles are multilayered and ellipsoidal in shape and their length spans from 0.3 to 1.5 mm along the long axis, and have a diameter that can varies from 0.2 to 0.7 mm. As happens for the Meissner structure, this multilayered form acts filtering and protecting the afferent, from very large stresses and strains.

As indicated in [26, 27], these endings are associated with four different tactile afferent populations, classified, on the basis of their receptive field size and their response to sustained stimulation, respectively in: the SA I (slowly adapting type I), the FA I (fast adapting type I, denoted as RA in the older literature), the FA II (fast adapting type II, denoted also as PC) and SA II (slowly adapting type II).

Their innervation density is non uniform but changes in function of the body sites and of the receptors type, conferring different sensitivity from a zone to another and between different stimuli, depending also to gender, age, health status, etc...

With respect to the hand, each population has a different presence percentage, but the overall density innervation rises from the hand palm to the finger and has a rapid increase for the finger base to the fingertip [7]. The higher presence corresponds to FAI and SAI units (mean values for the first population type are of 241 units/cm^2 at the fingertip and of 58 units/cm^2 at the palm).

The classification criteria are based on the hypothesis that the ending structure is linked to its sensory function and that its location corresponds to the maximum sensitivity area.

The first assumption has been demonstrated from the study of the receptive fields [7] while the second is confirmed from numerical models highlighting that the higher strain energy is concentrated at the tactile receptor locations [8]. FA I and SA I have a receptive field with a quite uniform sensitivity that covers an area of about 5-10 papillary ridges with some points of higher sensitivity corresponding to the nerve endings. For this reason they are able to recognize small spatial details. It has been shown [7] that these two afferent populations have well defined endings, similarly sensitive, located in a cluster like configuration that confers a quite uniform sensitivity to the whole receptive field region. The FA I units present higher sensitivity areas that are asymmetrical with respect to the papillary ridges due to their correspondence to the Meissner corpuscles located on both sides of the intermediate epidermal ridge. Completely different are the FA II and SA II receptive fields, that are characterized by a single well defined maximal sensitivity zone.

By means of microneurography, microstimulation [28] and electroencephalographic techniques [29] it is possible to investigate and characterize their physiological responses and affirm that:

– the SA I units, ending practically in the glabrous skin, densely distributed (1 per mm^2) react from about 2 Hz to 16 Hz, but are maximally sensitive to very low vibration frequencies ranging from about less than 2 Hz to 3 Hz. The information transmitted by them to the brain is a pressure [27]. They are sensitive to the local stress strain field and so to fine spatial details and are well able to code the curvature [30] without regard to normal

contact force [31] or contact area [32]. They have a linear response to skin deformations for indentations of at least 1500 μm. Their spatial resolution is minimally influenced by the scanning speed up to 80 mm/s [33] and forces ranging from 0.2 to 1 N [34]. All the afferent populations are sensitive to the normal load applied during the contact between the fingers and the object but in general their response is maximal along a preferential direction. The SA I have the greatest sensitivity for tangential force applied in the distal direction [35].

– The FA I units, located in the skin at a depth of about 0.5-0.7 mm (with a density of about 150 per mm^2), are easily excited between 3 Hz and 40 Hz, and produce the sensation of flutter [36] deformation and frequency vibration occurring during the increase and decrease of skin indentation [26]. They respond across their whole receptive field and are able to discriminate very fine spatial details, but provide critical feedback for precise control [34]. With respect to edges detection, their response starts to saturate at about 100μm and are insensitive for indentations up to 300-400μm [26]. They are most sensitive to tangential components of force applied in the radial and proximal directions [35].

– The FA II units are the largest in size and they are located in the deeper dermis layer, 1.5-2.0 mm. They are very sensitive to mechanical transients and vibrations of higher frequencies, reacting in a range of 40-500 Hz, with the highest sensitivity around 300 Hz. They are detectors of the acceleration vibration, conferring the perception of vibrations [27]. Their sensitivity is so high that they are able to respond to skin motion of 10 nm.

– The SA II units, characterized by an appreciable sensitivity to remote lateral stretching of the skin with a pronounced directionality (caused by the fact that their long axis is parallel to the skin surface), react from 100 Hz to 500 Hz, and produce the sensation of buzzing [37]. They contribute to the perception of object motion direction, force [38] and finger position [7].

Thus, it is possible to assert that the afferent units form and location confer them specific properties and tactile functions.

With respect to the tactile information coded, the SA I are responsible for the detection of object spatial structure and form; the FA I give the perception of the motion (fundamental for grip control); the FA II transmit vibrations sensation and the SA II give the skin stretch sensation.

Naturally, even if this distinction between the receptors capabilities, based on their most significant features, is useful to characterize, explain and analyze specific aspects of the tactile perception, it is necessary to consider that the complete information coming for the touch sense is given by the sum of the signals generated by all the different tactile afferent units.

Substantial changes in the perception of surface properties are also introduced by the movement direction. In fact, the mechanoreceptors have a directional different sensitivity related to their form and their receptive field size and to the asymmetric strains fields generated by the ridge orientations. Directional different sensitivity is also due to the skin properties. In this sense, two aspects have to

be considered: the first is that the skin is anysotropic, implying great differences between a direction and another; the second is that the skin is not homogeneous but starting from the external layer until the bone there are several skin layers with proper mechanical characteristics. In addition to this, viscoelasticity has significant effect on tactile perception, as confirmed by the fact that somebody is more sensitive to tangential forces than to normal forces on his forearms, but the opposite is true on his fingerpads [39].

1.2 Skin frictional properties

As previously said, skin frictional properties and biomechanics of skin and subcutaneous tissues, which are excited by the vibrations induced from the scanning of the finger on a surface, are fundamental for the human tactile sensing. For example, the skin on the hand volar surface, bending along the hand flexure lines, ensures the object grasp security, and papillary ridges, on the palm and on area interested by grasping, serve as friction pads [40]. The frictional properties are influenced by hydration, lipid film, surface structure, subject age, anatomic site and gender, which characterize the physiochemical and mechanical properties of the skin [41].

Skin is divided into epidermis (external layer) and dermis. The epidermis provides a protection for loss of hydration and bacteria and contains free nerve endings. It is divided into five layers: stratum corneum, stratum lucidum, stratum granulosum, stratum spinosum, and stratum germinativum. In particular, the stratum corneum is linked to hydration (as suggested from [41]). Age influences skin elasticity and affects the dermis structure. The dermis is divided into papillary and reticular layers and contains both blood vessels and capillaries network, collagen, elastin (conferring elasticity) and reticular fibers that create a support structure. A third layer consists of fatty tissue, where are located the Pacinian corpuscles, and it is not considered as a part of the skin but as a link between the dermis and the muscles.

The papillary folds, connecting epidermis and dermis, create the fingerprint structure. When the finger is in contact with a surface, sweat appears along the ridges. This makes the finger softer (more compliant) and increases friction [6].

In the specific case of the epidermis, there is a characteristic pattern due to the presence of intersecting lines that form the skin micro-relief. They are oriented along the direction of elastic tension proper of each body site and change, for the same person, also in function of aging. These surface patterns are peculiar to each individual as well as, referring to the finger, the fingerprints generated by the ridges configuration.

The hypothesis asserted by Wang at all. [42] is that the fingerpad skin exhibits marked anisotropy and substantial hysteretic losses under local cyclical loading, in addition to stiffening and time-dependent effects. These effects are significant under the large local deformations resulting from lateral traction loads. Under these considerations it is possible to obtain a non linear force-strain curve and

elastic modulus significantly dependent on the direction of the deformation relative to the orientation of the ridges. In order to have an idea of the Young moduli magnitude, it is possible to consider about 3.61 MPa stretching and 1.36 MPa shearing along the ridges, and 1.54 MPa stretching and 0.96 MPa shearing across the ridges [42]. The skin is stiffer along the ridges than across them, implying that the stiffness difference is related to the ridges direction. Naturally, there is a great variance of Young's moduli from a person to another, due to the different thickness of the skin layers for each subject. The skin micro-geometry may generate distributed stress fields across the ridge grooves, contributing to the directionality of the responses of receptors such as the Merkel discs and Meissner corpuscles, which are structurally associated to the papillary ridges. In fact, as previously introduced, the response of individual afferents is dependent on the direction of skin stretch or on the direction of stimulus movement. The activation of mechanoreceptors also depends on the direction of relative sliding motion [43], due both to non uniform distribution of mechanoreceptors in the skin and to shape of the fingertip surface [34], as well as the different reaction rates (frequency range and stimuli characteristics) [30, 31, 32, 33, 15].

Moreover, the human skin has viscoelastic properties that generate a dependence of friction behavior on the load, contact area and elastic modulus. Skin friction is mainly determined by adhesion, implying that the friction coefficient decreases with the increase of the contact load (because the skin relief deformations are mainly elastic, and increasing the load, these deformations rise until the relief is completely deformed and the contact area approximates to the contact of a large single relief [44, 4, 20]) and increases when the Young modulus decreases (the skin becomes softer), like happens with the hydration (the stratum corneum becomes softer, because of the water presence, conferring higher smoothness to skin surface and so increasing the contact area). The presence of water and lipidic film, at the contact, acts also to reduce the stress strain, reducing the force necessary to brake the junctions create between the two bodies in the contact zone [45]. Specifically, the presence of a thin lubricant film due to the presence of lipids, between the finger and the surface, reduces the friction coefficient, while for a larger moisturization the friction coefficient starts to increase [44].

Adhesion could occur both in solid-solid contact and liquid involved contact. Two clean solid surfaces tend to create strong bond, whereas contaminated or boundary film covered surfaces tend to yield weak bonds. The adhesive junctions of asperities on solid-solid contact are caused by interatomic and intermolecular force of attractions. Generally, the adhesion can be chemical or physical. The former includes covalent bonds, ionic or electrostatic bonds, metallic bonds, and hydrogen bonds; the physical interaction involves the Van Der Waals bonds [46].

The adhesion is generally proportional to the normal force, because the applied normal force increases the real contact area promoting the bonds. On the other hand, the real contact area also increases as a result of interatomic attraction. Nevertheless, the effective contact area does not increase linearly with the load and, when the surfaces in contact are distorted, can differ sensibly for the theoretical contact area.

This skin frictional behavior, causing a decrease of the friction coefficient when the contact force increases, highlights that the skin/surface contact does not adhere to the Amonton's law [47, 48].

Indeed, Amonton's law postulates the independence of friction coefficient from the scanning speed between the two bodies in contact, while skin friction coefficient tends to decrease increasing the scanning speed [49, 50].

The skin frictional behavior is a complex phenomenon because it involves several different aspects like the non homogeneity of the skin elasticity (Young modulus for the forearm E=10^5-10^7 kPa); the anisotropy of the skin microtopography (arithmetic mean of roughness R_a=0.4-50μm) and the skin flexibility that allows to conform the skin contact area to the touched one, implying that higher friction coefficient corresponds to smoother surfaces because it corresponds to larger contact area [51, 52, 53].

In addition to this, due to the finger and fingerprint structure (asymmetrical) and the nail presence (that causes a further stiffness) the friction coefficient is not the same for different scanning directions. It is higher when the surface is moved along the line of the finger with the versus from the palm to the fingertip than in the opposite direction and for large contact angles [54]. Realistic values of finger friction coefficient, scanning on a rigid plate with a contact angle of 30°, are between 2.5 and 0.4 for a contact force varying from 0.5 to 7 N.

A predictive model of skin behavior as a function of the normal load is given by the Wolfram theory [55, 56], for a sliding surface on a distorting one (developed on the basis of Hertz contact model to take into account the adhesion that mainly affects the skin friction), where the friction coefficient is expressed as:

$$\{\mu\} \propto S(\frac{K}{E})^{\frac{2}{3}}N^{-\frac{1}{3}} \tag{1.1}$$

N is the applied load, E is Young's modulus of the skin, K is a colligative term including average dimension of adhesive contacts, their number, and frequency per unit areas, and S is the shear strength of the adhesive contacts.

Experimental studies, very consistent with the adhesion model, show little variation in the load power value, related to the experimental conditions and the body site where the skin is analyzed. Specifically, Wolfram theory suggests that μ is proportional to $N^{-0.33}$ while e.g. Sivamani et all. [57] found out a dependence on $N^{-0.32}$ for middle finger hairy skin and Koudine at all. [44] on $N^{-0.28}$ for forearm skin.

Nevertheless, there is not a well defined protocol defining univocally the concept of skin dryness. In consequence, the friction results can differ on the base of the measurements conditions.

Even if it is difficult to ensure the repeatability in this type of measurements, there are, in literature, several studies allowing for the quantification of skin friction coefficient under different contact conditions, because it gives information about both the skin status and the touched surface features. In consequence, the study of the skin friction is crucial for several research fields, such as physiology, textile industry, skin care products and ergonomics.

1.3 Object properties perception

Several biomechanical and neurophysiologic experiments have been developed to characterize human capabilities to perceive object characteristics, making distinction between different properties. According with Klatzky [58] object properties discrimination can be divided into two major classes: material (e.g., texture, compliance and thermal characteristics) and geometry (like dimensions and form). Weight perception is based on density and dimension valuations and so it is a special case that requires both features.

When people need to know a specific characteristic about an object, they chose to make the movement that is more appropriate for that property. In fact, for example, moving the hand back and forth across the surface it is possible to determine the texture information, while tapping with a finger is useful to characterize the object compliance.

Obviously, each movement requires different execution times, necessary to well code the desired information and, in general, the contour follow operation corresponds to the longer time [59].

Determining surface compliance requires both tactile information (meaning that they are provided by the mechanoreceptors) and kinesthetic one (regards the position, motion and force sensations provided by the sensory neurons located near articulations and muscles) depending on the surface stiffness. If the surface is soft, at constant force, the spatial distribution of pressure in the fingertip contact area is related to the object compliance and the SA I units discharge rate is well able to code this information [60]. On the other hand, for rigid surfaces, kinesthetic information are required as well, because their discrimination is more complex and less accurate that the soft ones.

Surface curvature discrimination seems to be basilar for object shape representation [30]. In addition, object surface curvature influences the responses of the mechanoreceptors and there is a strong interaction between the surface curvature and the direction of fingertip force. Changes in curvature may influence afferents's preferred force direction, while similarly the effect of curvature on afferent's response may depend on the direction of the applied force. Generally, the object curvatures are of the same orders of the fingertip one, and only relatively gentle curvatures (0 and $80.6 m^{-1}$) affect the mechanorecptor responses. Further increases in curvature have progressively smaller effects on the responses. As happens for each contact between hand and object, signals originated from tactile afferents distributed over the entire terminal phalanx can also contribute to encode magnitude and direction of fingertip forces.

When hand moves on a bar or on a texture with well defined lines, it is necessary to take into account that the line orientation sensitivity is not the same in all directions. Specifically, it is less accurate when the line or the bar is obliquely oriented with respect to the finger scanning direction. On the other hand, it is possible to say that bar longitudinal disposition helps to overestimate line length, like it happens in visual illusions.

Some perception differences are related to the hand sensitivity features.

With respect to edge sensitivity, when an object is moved on the skin, a deformation gradient is created within the highly sensitive area of the receptive fields exciting FA I and SA I units, taking into account that the spatial acuity becomes significantly lower from the index finger to the ring one [33]. So, generally, people perceive roughness as greatest with the ring fingertip, followed by middle and index one and can discriminate 0.06 micron high grating by Pacinian fibers. In addition, pressure sensitivity on the palm and fingers of the left hand of right handed subjects is higher than that of the right hand, and the contrary happens for left-handed subjects. With respect to vibrotactile sensitivity , for vibrations falling in the range 70-480 Hz, the left index finger is more sensitive than the right index finger [61].

During object manipulation people apply, throughout the fingertip, a time varying force in controlled direction changing their mechanoreceptors responses. In fact, if a tangential force is applied in the distal or proximal direction in addition to the normal force, the activation of SA I, SA II and FA I units depends on the direction of the fingertip, showing higher responses for the tangential force. Their activation depends as well from the force application point: at the forearm, the sensitivity to tangential force is higher with respect to the normal one; while the opposite happens in the fingerpad because of its larger stiffness to tangential force components [39].

The dependence on the application point is caused by fingertip anisotropic mechanical properties and spatial relationship between the afferent units receptive field center and stimulus site [62, 63].

1.3.1   Texture perception

Among the different surface characteristics, particular attention has been dedicated to the study of the texture perception, highlighting that texture perception depends from spatial and vibrational cues. Specifically, neurophysiologic studies showed that the perception mechanism of roughness is based on the "duplex model of tactile roughness perception" [5, 10, 11, 12, 13, 64]. This model makes distinction between the perception of fine textures (spatial period is smaller than 100 μm), perceived by the induced vibrations, and the coarse ones (spatial period is larger than 200 μm), characterized by a "single spatial intensive code", mediated by SA I afferents. Both the aspects play an important role for transition textures, meaning a characteristic size of about 100-200 μm. In other words, tactile characterization of fine texture is related to the power of vibrations induced by the dynamic contact with the skin and it is perceived by Pacinian afferents. On the other hand, the coarse textures are transformed into a spatial code generated by the firing variation of the SA I afferents.

In the same research field, there are, also, several studies that support, experimentally, the duplex model of roughness tactile perception [65, 66, 67, 68, 69, 70].

When both the hand and the object are in stationary contact (meaning that there is not a relative movement), no vibrations are generated at the finger surface interface and the discrimination of relatively smooth surfaces is practically

impossible while coarse surfaces are still perceived even if smoother; the capability to discriminate changes in material properties, related to their thermal properties, remains [58].

Moreover, it has been showed that applying vibrations perpendicular to the contact surface, the surface roughness is perceived as rougher than the same surface without applied vibrations, meaning that these vibrations are able to change the surface perception [71]. This increase of roughness perception rises with the augmentation of the applied vibration amplitude.

Furthermore, this perception feature opens an interesting research problem to reproduce the whole tactile sensations applying appropriate vibrations to the fingers [18, 72, 73]. Some steps have been done in this direction to build tactile devices like more comfortable and practical prothesis and to confer human tactile capabilities to robots.

With respect to the tactile afferent units, in static contact, only SA I slow adapting units are activated in a continuous way, and, throughout the skin deformation detection, they give information about the surface spatial characteristics, while fast adapting (FA) mechanoreceptors are activated at the beginning of a contact. In dynamic contact, the slow adapting (SA) units' activation occurs and the fast adapting units are activated by the induced vibrations characterizing the relationship between the spatial characteristics of the finger and of the object surface. The fast adapting sensory units are sensitive to a phenomenon called vibrotactile adaptation. This means that when a vibration is applied for a long time, depending on the intensity, the mechanoreceptors sensitivity threshold can change or be inhibited. With respect to the texture perception, vibrotactile adaptation regards only the finer surfaces underling that fine and coarse texture are processed throughout different mechanisms.

The existence of a texture perception mechanism transition zone, where there is a change from a vibrational code to a spatial one and vice versa, is highlighted by the fact that if any vibration occurs, meaning that there is not relative motion between the surface and the finger, textures with size following in the range 200-100 μm are perceived as equally rough, meaning that the only spatial code is not sufficient to distinguish them well [65].

Additional information comes from experiments on indirect touch. In this case, the hand is stationary and a probe with a texture pattern is moved on the skin. In consequence, SA I units feel only the probe geometry while the vibrations code the texture. This is confirmed by the fact that, in direct touch, the adaptation to the imposed vibrations is significant only for fine textures, while in indirect touch both fine and rough textures are affected by this phenomenon [67].

Thus, indirect touch experiments help to investigate the duplex perception mechanism, isolating the vibrational code. To highlight this possibility, some experiments have been developed, comparing direct and indirect touch results, for the perception of textures with characteristic size bigger than 200 μm when vibration adaptation occurs. In direct touch, the spatial code supplies the lost of the vibrotactile one and the texture is well perceived. In indirect touch, the spatial code is eliminated by the probe and the vibrotactile code is reduced by the

adaptation. In consequence, the perception is completely degraded [67].

So direct and indirect touch differ for the neural mechanism of tactile perception. In indirect touch (when probes are employed) all texture information have to pass only through vibrations. In direct touch, the subject touching the texture has all texture information directly. This causes some dissimilarities in texture roughness, hardness and stickiness sensation. They are similar but not identical. Indeed, the scanning mode influences vibration, compliance and friction evaluation. Specifically, perceived roughness increases with vibration power, thus it is influenced both by force and scanning speed because of their capabilities to change vibration intensity. In direct touch, the spatial code integrates the vibrotactile one, so that contained variations of the vibration power, corresponding to scanning values normally employed, have not significant effects on the roughness perception. Perceived hardness increases when the texture compliance decrease [67]. In these experiments, hardness is evaluated applying force against the probe. Thus, proprioceptive information, coming from SA II units, seems to be important for evaluating the applied force and so for the hardness perception. Perceived stickiness increases in accord with friction between finger and texture. In direct touch, it is related to the ratio between the force applied in the normal direction, with respect to the contact surface, and the force applied in the direction tangential to the scanning one. In general the normal force is constant suggesting that the stickiness perception is linked to the tangential force variations. In this case, an important role is played by the SA II units, sensitive to skin stretch. In indirect touch, stickiness information comes from the proprioceptive codification of normal and tangential force. Both in direct and indirect touch, further information about stickiness can come from the vibrations generated by the skin sliding on a sticky surface [67, 74].

In conclusion, it is possible to assert that relative motion between a surface and a finger under adequate applied force and scanning speed allows for a complete perception of the surface texture.

Neurophysiologic investigations show that the tactile pattern recognition is independent of contact forces ranging from 0.2 to 1 N [15].

For larger force values, it has been demonstrated that the normal load applied from the fingertip on the object surface influences the perceived roughness [16]. Higher applied forces correspond to larger perceived roughness. This is due both to the vibration magnitude increase and to the change of the contrasts in the roughness pattern in contact: increasing the contact force, the finger deformations rise modifying the contact area and the finger pattern.

For the same contact force, the roughness perception in active (stationary surface and moving hand) and passive (stationary hand and moving surface) touch is the same. Equal are, as well, the changes, in the roughness perception, due to applied force and groove width. So active and passive touch are completely equivalent with respect to the roughness estimation [75].

In addition to these factors, a fundamental role, in the texture perception, is played by the fingerprints that, substantially, determine the different sensation among different subjects for the same touched surface, acting as a filter of the

vibrations induced by the scanning of the fingertip on the surface [43, 76].

Fingerprints allow both for creating a finger stress strain field in which the points at higher stress correspond to the mechanoreceptors location and to spatially modulate the interfacial stress field between skin and object surface [43]. The ridge effects are important for the duplex mechanism model for different reasons. First of all, stress concentration is useful for an appropriate activation of the SA I units; on the other hand, the deformation field modulation amplifies the vibration induced by the texture scanning in the subcutaneous tissues, thus activating the FA II units.

More complex and less investigated is the tactile perception of fabrics. In fact, in these cases, it is not sufficient to consider hand, skin and contact features only, but it is required great attention to those of the fabrics. Fabrics can confer completely different sensations depending on the scanning force, speed and direction [77, 78, 79]. For example, they appear rougher if scanned along a versus opposite to the fibers direction and/or against the hairiness direction. Also, they can completely deform on the base of the contact load. So, it is still not clear which are the most significant parameters characterizing the fabric and allowing to predict the fabric tactile sensation.

1.4   Concluding remarks

The literature dealing with tactile perception is mainly focused on physiological analysis of mechanoreceptors and neurophysiological and psychophysical studies of the perceived surface properties.

Nevertheless, considering the main role of the induced vibrations in the tactile perception, the possibility to predict the object tactile perception, starting from its surface features, seems to be strongly linked to the features of the vibrations induced by the friction. For this reason a newer research direction, aimed to link the vibration spectra with tactile perception, is approached in some recent publications. By characterizing both the relationship between the single object surface feature and the vibration spectra (accounting also for the scanning conditions), and the link between this relationship and the given tactile sensation, it would be possible to define objective indexes allowing for a quantitative characterization of the tactile perception.

In this context, a first approach to the analysis of the link between the friction induced vibration spectra, scanning parameters and surface features is presented in this thesis.

Chapter 2

The TriboTouch set-up

The study of a finger that moves on a surface involves different difficulties that are related to the contact pair characteristics and to the measurements themselves. The aim is the measurement of the vibrations induced by the scanning, which are very low in magnitude; consequently it is very complicated to isolate them from the vibration noise coming from the experimental set-up and to detect them without any significant alteration. In addition to this, the impossibility of measuring and maintaining the fidelity of the local contact features (local means at the contact region) between fingertip skin and object surface, implies the choice of measuring the global dynamic response of the finger during the object scanning, relatively far away from the contact zone. Then, measurements of the local dynamics can be performed on a fake finger and correlated with the global measurements on the real one.

For these reasons a new experimental set-up, named TriboTouch, has been developed to recover the contact forces and the vibrations induced by the sliding contact between both real and fake finger and sample surfaces. The test bench has been designed to guarantee the measurement reproducibility and, due to the low amplitude of the vibrations of interest, to perform measurements without introducing external noise. The relative motion between finger and surface is obtained, without any other interface under sliding contact, by a compliant displacement system and a voice coil linear actuator.

2.1   Method and transducer validation

The first approach to the investigation of the induced vibration spectra consisted in preliminary measurements of the global vibration detected on the finger, with an appropriate accelerometer, to verify if effectively it is possible to detect the friction induced vibrations generated by a finger scanning on a surface [80]. For this purpose, a first experimental set-up, made of an aluminum surface sample translated by a hydraulic table which allows linear alternative motion, has been employed to analyze the behavior of the right hand finger during the scanning phase. Two mono-axial force transducers (detecting the normal force) are placed below the surface sample for monitoring the global contact force. In such a

way, only tests with constant normal force during scanning and with comparable value of the force impressed by the subject, have been retained for the analysis. Because of the low amplitude of the vibrations of interest, two accelerometers, monitoring the sample and the table vibrations during tests, are used to detect the presence of undesired noise that could modify the signal measured on the finger. A low mass accelerometer is applied on the finger nail to measure the vibration induced induced by the scanning with the test surface (Figure 2.1).

In order to have a better control of the applied normal load (given by the pressure applied by the subject) and scanning speed, the finger is maintained fixed and the roughness sample is moved at a constant speed.

The two blocks shown in Figure 2.1 at the sides of the roughness sample are used with the purpose to create a base for the finger at the same level of the surface sample before and after the surface sample useful for the measurement. In this way, the transducers begin to measure when the finger/surface scanning is in stationary conditions (the scanning speed and load have reached a constant value). For this analysis, nine surface samples with periodical roughness, ranging from 0.64 μm to 5.2 μm (verified by a laser profilometer), and oriented along the normal direction with the respect to the friction (scanning) one, have been used (Table 2.1 and Figure 2.1).

Roughness sample	Roughness Ra μm	Wavelength mm
R_1	0.64	0.3
R_2	1	0.15
R_3	1.4	0.78
R_4	1.9	0.66
R_5	2.5	0.87
R_6	3.3	1.10
R_7	3.7	1.40
R_8	4.5	1.71
R_9	5.2	2.17

Table 2.1: Roughness and wavelength values of the samples used for the measurements. Ra is the arithmetic mean of the variations to the average. The samples length is always 60mm.

Speed samples	Speed values mm/s
v_1	10
v_2	20
v_3	30
v_4	40
v_5	50

Table 2.2: Values of scanning speed used for the measurements.

<center>(a)</center>
<center>(b)</center>

1 Accelerometer   4 Control accelerometer
2 Surface sample   5 Control accelerometer
3 Force transducers 6 Finger supports
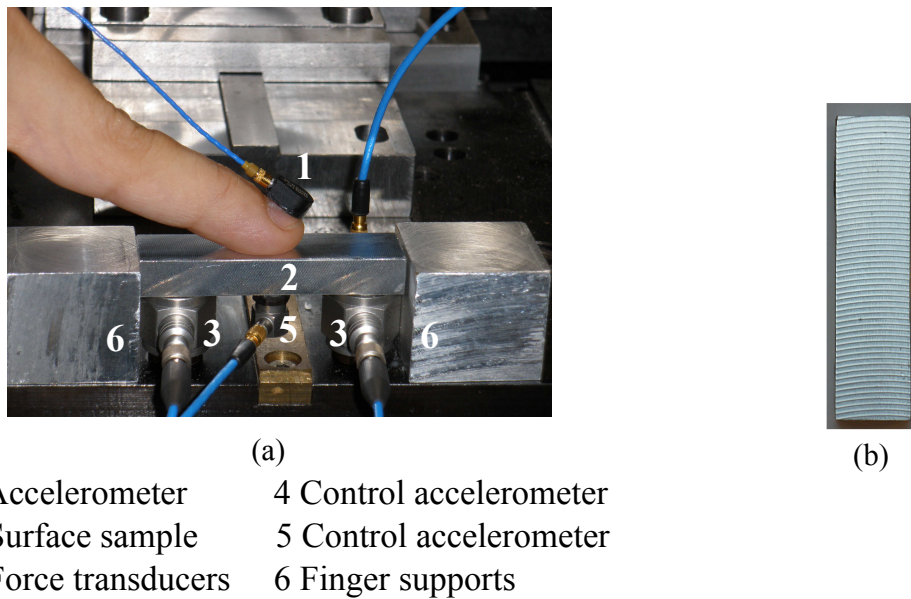
Figure 2.1: (a)Experimental set-up. The roughness sample is translated, while the finger is maintained fixed. (b) Example of the employed surface samples with periodical roughness.

The aluminum samples roughness is obtained by milling the surfaces with different milling cutters. Large values of the cutter radii have been chosen to minimize the curvature of the roughness ridges.

The chosen roughness values represent a good range to analyze human tactile perception, because they cover both surfaces perceived practically smooth, and others with a well defined roughness. For example, with respect to the objects of everyday life, Ra=0.64μm is the roughness of an aluminum can, and Ra=5.2μm is a type of bottle cork.

Five scanning speeds have been used, from 10 mm/s to 50 mm/s, and are chosen to cover the range of the scanning speed that is usually employed by people judging a surface [81, 45, 82, 14].

During the scanning, the normal applied load is maintained at about 0.5 N. The small value of the contact force and the frequency range of interest requires force transducers with a very high sensitivity and resolution. A light accelerometer (0.8 g) but with high sensitivity (100 mV/(mm/s^2)) has been used to avoid a significant influence on the measurements (Figure 2.1).

A preliminary test is performed with the sample fixed and with the scanning directly performed by the subject, which moves his finger to investigate the surface. In fact, in the everyday life, when someone touches a surface, no controlled speed movement system is employed. This preliminary test is used as a reference to verify if the selected scanning speeds are compatible with the real one.

Figure 2.2 shows the FFT of the acceleration measured on the finger during the free scanning. The FFT spectrum shows no significant vibrations over 300 Hz; larger vibrations can be observed between 10 and 300 Hz, with a main peak around 50 Hz.
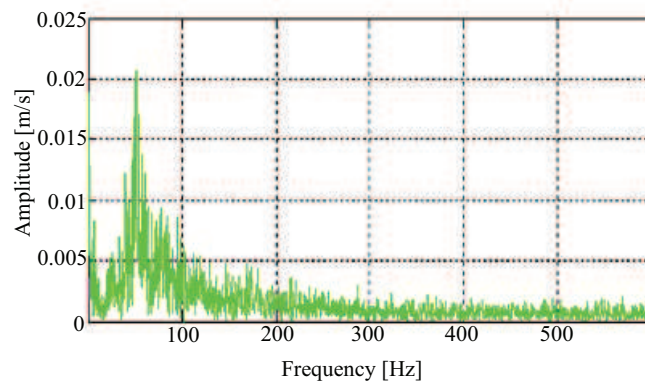
Figure 2.2: Example of the acceleration FFT behavior during the finger free scanning on the roughness sample R5.
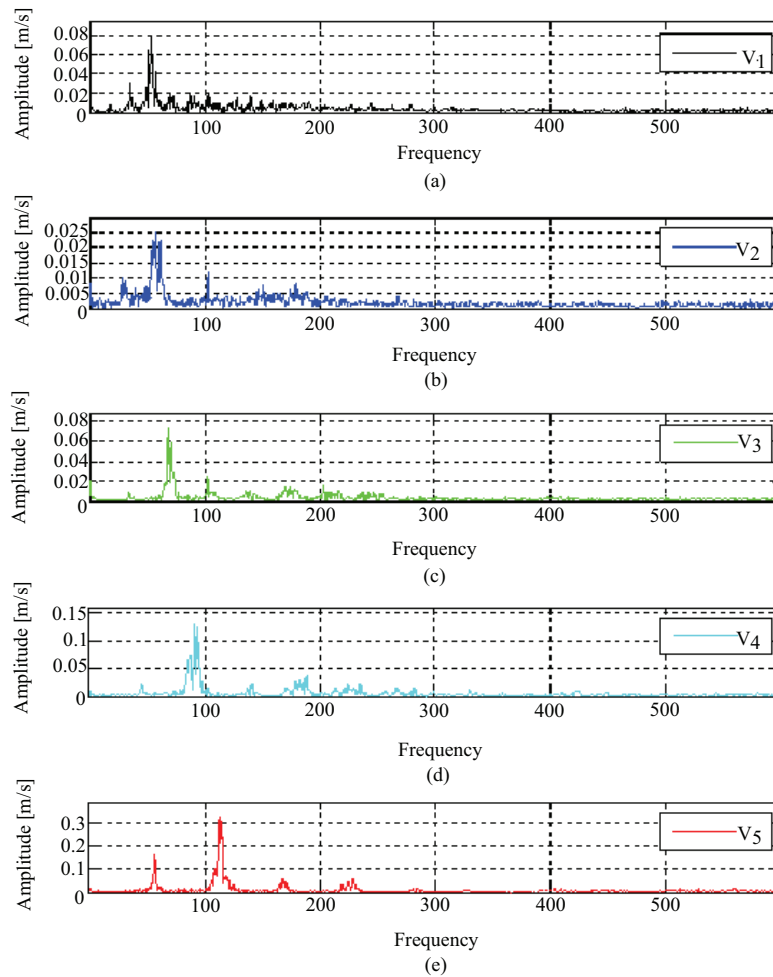
Figure 2.3: FFT of the signals obtained by the accelerometer for scanning on the R5 roughness sample for different speed. v_1=10mm/s; v_2=20mm/s; v_3=30mm/s; v_4=40mm/s; v_5=50mm/s.

Figure 2.3 shows the FFT of the acceleration measured on the finger for different scanning speeds on the same roughness sample (R5). Increasing the scanning

speed from v1 (10 mm/s) to v5 (50 mm/s) the distribution of the frequency spectra cover larger values. In particular, the main peak of vibration shifts from 40 Hz for the V1 speed up to 120 Hz for the V5 speed. Moreover, the amplitude rises with the speed from 0.008 mm/s to 0.3 mm/s.

The same behavior can be found for another volunteer (i.e. a different finger), as shown in Figure 2.4. Depending on the normal force applied by the subject, the skin characteristics (for example the fingerprints) and the finger ones, there are some differences related to the frequency of the acceleration main peaks and to their magnitude; nevertheless, the same behavior in the acceleration spectra is obtained: for the same surface sample, there is an increasing of the frequencies and magnitude of the acceleration peaks with respect to the increase of the scanning speed.
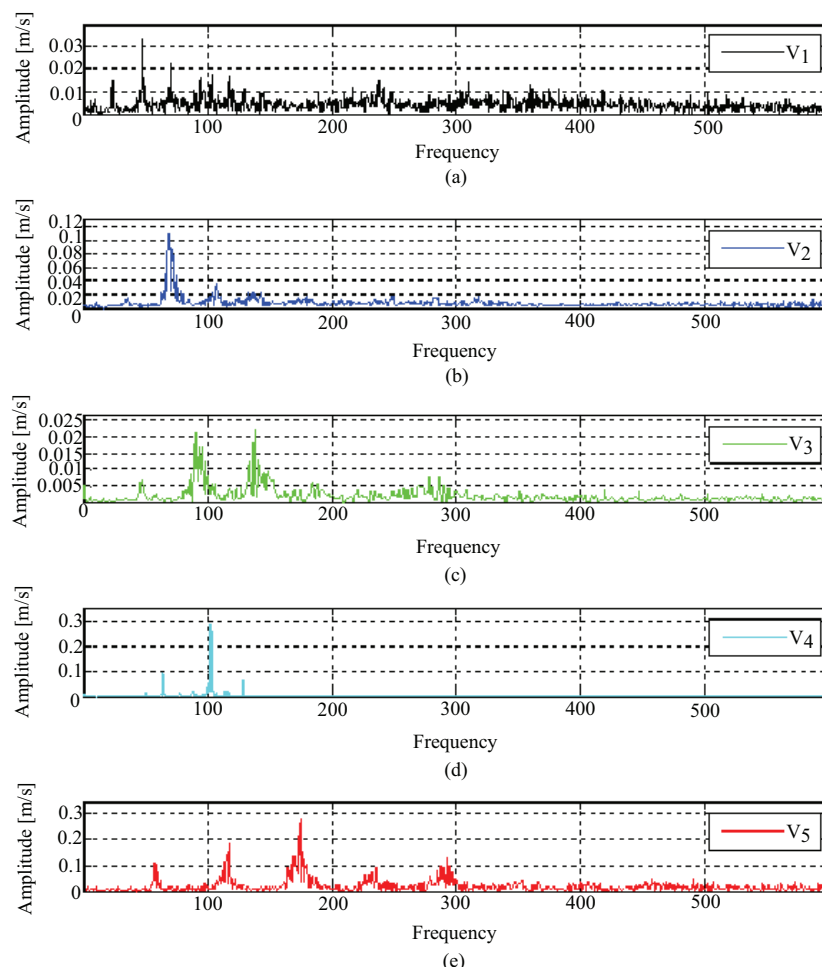
Figure 2.4: Example of the acceleration FFT magnitude referred to another subject, for different speeds and for the R5 roughness sample. v_1=10mm/s; v_2=20mm/s; v_3=30mm/s; v_4=40mm/s; v_5=50mm/s.

The free scanning measurements (Figure 2.2) are comparable to the measurements made, for the same roughness, at a speed ranging from 10 mm/s to 30 mm/s when the surface sample is moving rather than the finger itself. This

means that the natural scanning speed used by the subject for testing the surface falls in this range and the tests on this set-up, with the controlled translation of the sample surface, are significant.

Each surface sample is investigated, under each scanning speed, with the right hand index finger of four subjects, two females and two males. All the experiments take place at the same temperature 24°C and in the same environmental conditions. The skin is untreated, meaning that no moisturizers are employed, but, but the finger skin and the surface sample are cleaned up using alcohol, before each measurement.

In order to be sure that the presence of the accelerometer on the nail is not invasive for the results, the same measurements have been performed replacing it with a laser vibrometer. The measured speed has been derived to obtain a comparable acceleration.

The comparison between the two signals, as shown in Figure 2.5, confirms that the choice of the accelerometer type is proper for the considered measurements and that its presence does not affect the results significantly. The same vibration frequency and peak amplitude have been obtained.
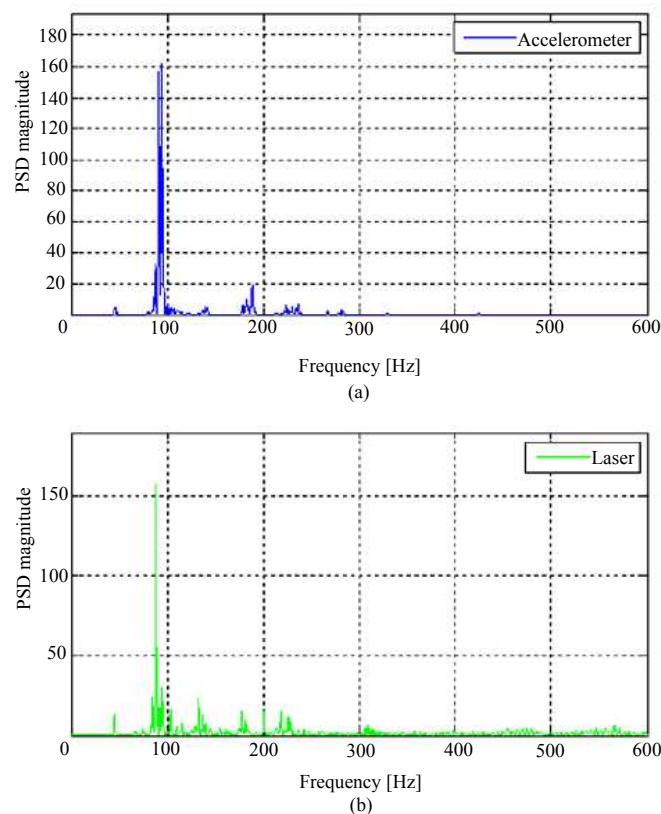
Figure 2.5: Power spectral density of the signals obtained from the accelerometer (a) and the laser vibrometer (b). The signal corresponds to a scanning speed v4 (40 mm/s) and a roughness R5.

A main step in the definition of the test methodology is the choice of the kinematics for the relative motion between the fingerpad and the sample surface.

It is well known that skin biomechanics and superficial characteristics (e.g. anisotropy, micro-relief, fine wrinkles) change in function of age, race, gender, individual health status and of the different body sites. The directional stiffness variance due to the skin stretching is larger than the one generated by shearing the skin, implying that stiffness directionality occurs locally. As highlighted in the previous chapter, a single direction movement is not sufficient to well activate all the mechanoreceptors types. In fact, generally, people does not judge a surface just scanning on it in one direction only, but performing movement in all directions.

Nevertheless, it is really difficult to analyze complex movements of the finger on a surface under well defined values of the scanning parameters. Thus it is more constructive to begin investigating the phenomenon with a linear movement of the scanning in the direction of the finger line which is considered the main one.

For this reason the analysis performed on this thesis has been focused on linear movements of the finger with respect to the sample surface. During the tests, the angle between the finger and the surface sample is maintained at about $25°$.

The main direction used by a subject when scanning a surface is the one on the line of the finger bones, perpendicular to the fingerprints direction of the fingerpad. A comparison of the acceleration signals obtained from two opposite scanning versus is presented in Figure 2.6. The first (scanning) direction is the one on which the surface sample moves. It is along the line of the finger with the versus from the palm to the fingertip (from left to right, with respect to the Figure 2.1). The second direction is the opposite one (from right to left). In both cases the periodic roughness of the sample is perpendicular to the scanning direction.

From Figure 2.6, it is possible to see that the frequency distribution of the acceleration spectra is similar, with a large value of the vibrations around the peak at about 200 Hz.

Nevertheless, the second direction of scanning implies the compression of the finger causing a phenomenon of sprag slip and consequent increase of the acceleration magnitude. This is due to the increase of the contact force generated by the compression and deformation of the skin (Figure 2.6). In fact the skin deformations are not the same in the two scanning directions because of the natural behavior of the finger that is compressed by the tangential component of the contact force and it tends to "sprag" on the surface sample.

Then, for the second scanning direction, a sprag-slip and stick-slip behavior of the contact vibrations occur when increasing the applied force, which is usually avoided by human subjects during the surface scanning, by controlling the normal force applied to the fingerpad.

For this reasons the linear scanning direction along the line of the finger with the versus from the palm to the fingertip has been retained for the tests, for reproducing the touching phase under controlled conditions.

From these first preliminary tests, it is possible to assert that:
– the free scanning measurements performed by the human subject are well comparable to the measurements made, for the same roughness, on the

used set-up at a speed ranging from 10 mm/s to 30 mm/s when the sample is moved and the finger is fixed. The performed measurements are thus significant. (Figure 2.2 and Figure 2.3);

– for the same contact surface with periodic roughness, a speed increase corresponds to an acceleration peak displacement toward higher values of frequency and to higher value of the acceleration magnitude;

– the results taken from the different volunteers, except for the frequency and magnitude of the acceleration peaks, present similar behavior with respect to the variation of the control parameters;

– in all the measurements the acceleration peaks are distributed between 2 and 500 Hz, corresponding to the physiological data of the mechanoreceptors sensitivity range;

– the results and their reproducibility allow for the validation of the measurement methodology and transducers capabilities.
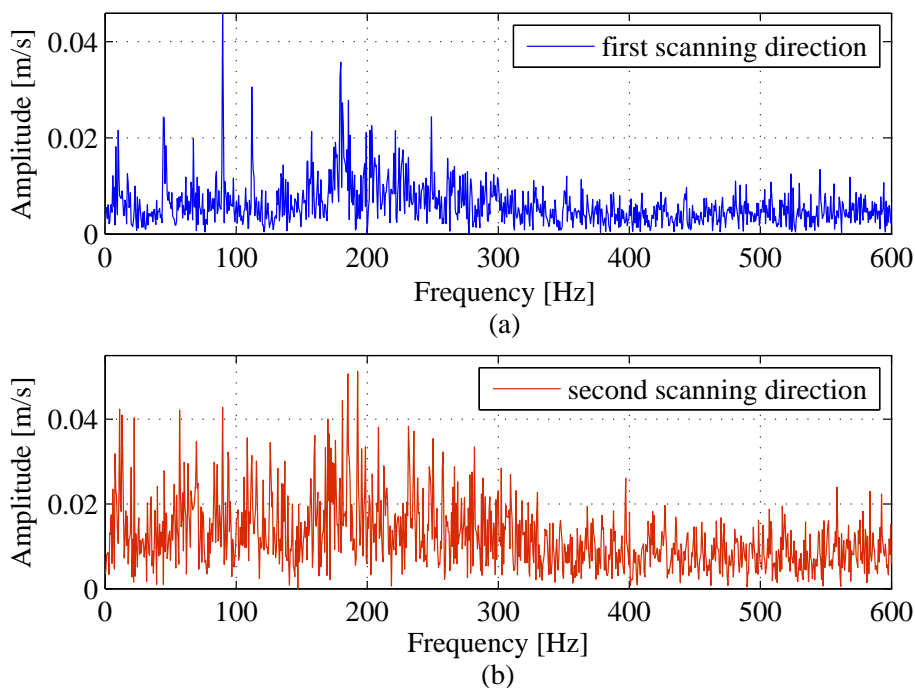
Figure 2.6: Example of the acceleration FFT magnitude for backward and forward scanning movements. (a) First scanning direction, (b) Second scanning direction. The scanning speed is v5 (50 mm/s) and the roughness sample is R9.

These preliminary tests allowed also to highlight some main features of the measured friction induced vibrations like their magnitude and range of frequency, which are fundamental for the development of the new experimental test bench. The low value of the vibration amplitude implies the definition of a dedicated displacement system to isolate the contact from the parasite vibration noise coming out from the experimental set-up and to detect them without significant alteration. Moreover, the desired test bench has to allow for measurements of both

global and local dynamics on real and fake fingers [83]. Another requirement for the new experimental set-up is the absence of acoustic noise, in order to perform measurement of the friction noise with microphones. On the basis of these considerations, the design, validation and development of the new test bench, named TriboTouch, is presented in the next sections.

2.2   Experimental test bench

The test bench TriboTouch has been designed to recover the contact forces and the induced vibrations guaranteeing measurement reproducibility and, due to the low amplitude of the vibrations of interest, to perform measurements without introducing external noise. For these reasons, the relative motion between finger and surface is obtained without any other interface under sliding contact by a compliant system and a linear voice coil actuator [84].

(A)   (B)

(a) Surface sample;   (d) Linear voice coil actuator;
(b) Compliant mechanisms;   (e) Force transducers;
(c) Flexible joint;

(C)

Figure 2.7: Front (A) and side (B) view of the experimental set-up (scale 1:8), and a scheme of the compliant system (C)

The designed experimental set-up (Figure 2.7) is made of a surface sample (a) linked to a rigid plate made in steel. It is translated by a compliant mechanism (b) which allows linear motion of the sample without any other sliding contact surface. Specifically, the compliant guide is a mechanism consisting of rigid links connected each other by a flexure hinge (c).

For the system stability, two compliant mechanisms nominally identical are placed parallel and slightly tilted the one toward the other, as shown in Figure 2.7. Each element is constituted by a double parallelogram system which allows for a linea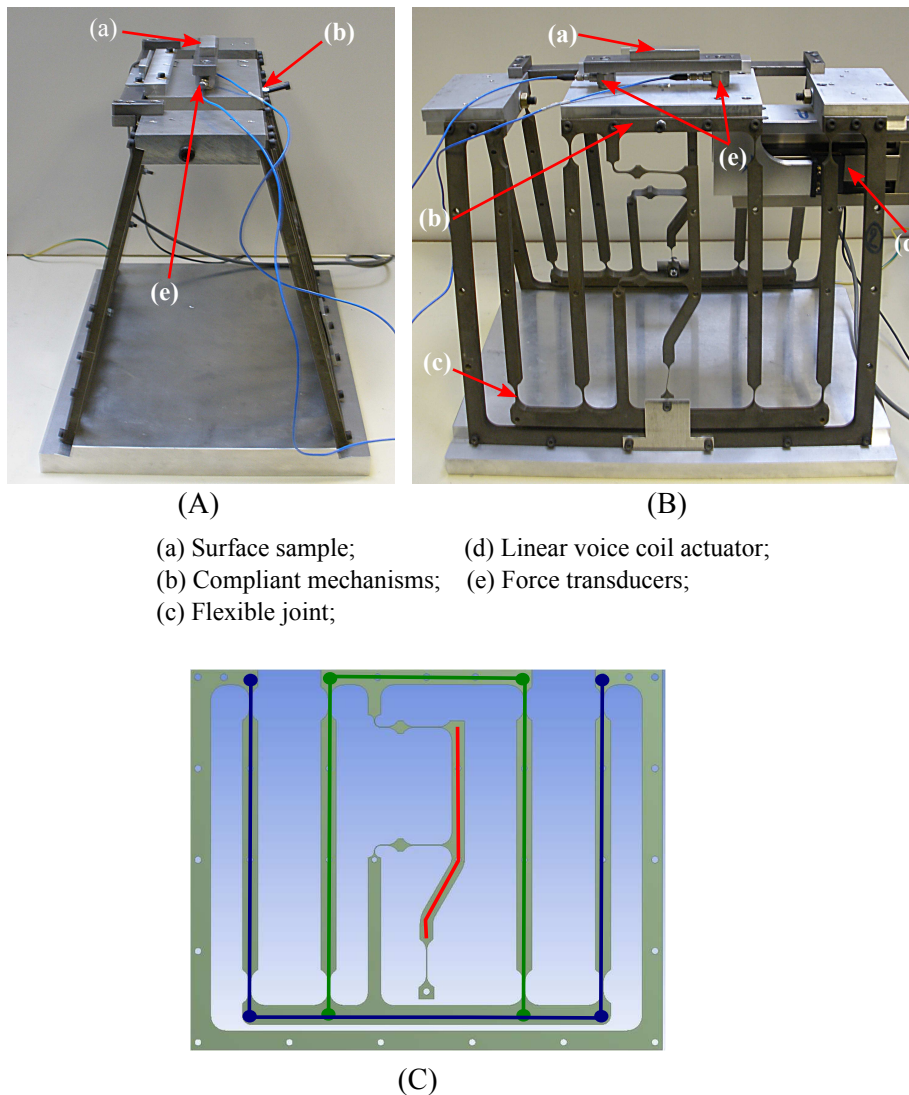r translation of the upper rigid segment where the surface sample lies (a). In fact, while the lower horizontal segment of the first parallelogram performs a circular trajectory, the vertical displacement is recovered by the trajectory of the upper basis of the second parallelogram. The same deformation for the two parallelograms, necessary for having an horizontal trajectory of the upper segment, is guaranteed by the central levier that connects the two horizontal segments. The flexible hinges (c) approximate pin joints between the rigid segments of the double parallelogram and have been dimensioned to allow for a linear displacement of the surface sample (upper segment) of 100 mm. The horizontal translation of the sample is obtained by a linear voice coil actuator (d) which, through a feedback control system and a TTL linear encoder, allows for imposing the desired scanning speed with a displacement resolution of 0.5 μm. The fingertip, which is the main point of measurement, is fixed while the scanning of the surface is allowed by the upper segment translation.

Two mono-axial force transducers (e), detecting the normal force, are placed below the sample for monitoring the global contact force. In this way, only tests with constant normal force and with comparable value of the force impressed by the subject have been retained for the analysis. In fact it is practically impossible to maintain the normal force perfectly constant during the surface scanning. To have a better control of the applied normal force (given by the pressure applied by the subject) and of the scanning speed, the finger is maintained fixed and the roughness sample is moved at a constant speed. This solution is also due to the possible employment of the experimental set up for local measurements of the induced vibrations on a fake finger (Figure 2.12) by image cross correlation techniques.

The applied normal force varies between the subjects in function of the gender, and the age [20], and generally falls in the range 0.2-1 N.

The accelerometer, used in the preliminary tests, is mounted on the finger nail to measure the finger vibration induced by the scanning with the test surface (Figure 2.8).

To account for the different point of measurement with respect to the fingertip surface (excited by the sliding contact), tests have been performed to obtain the finger transfer function by exciting the fingertip contact surface with a shaker and measuring the response with the accelerometer on the finger nail. The results show high reproducibility for the same subject and similar trend of the curves for different subjects.

The calculated spectra of the measured vibrations have been then treated by

the measured transfer function in order to obtain spectra representatives of the local excitation (vibration) at the contact.
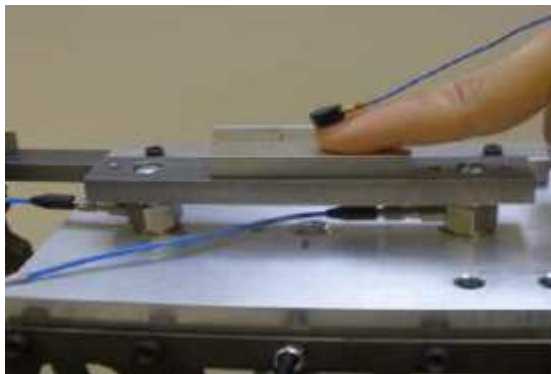
Figure 2.8: Experimental set up configuration used for the measurement.

Figure 2.9 shows that in the frequency range of interest, corresponding to the mechanoreceptors activation range, the finger transfer function is almost flat, except for an initial peak. As confirmed from the coherence function, the transfer function is reliable for frequencies larger than 15 Hz. The lost of coherence under 15 Hz is due to involuntary movements of the finger and the arm during the measurements. In order to account for this aspect the first part of the spectra, under 15 Hz, has not been considered for the analysis of the presented tests.
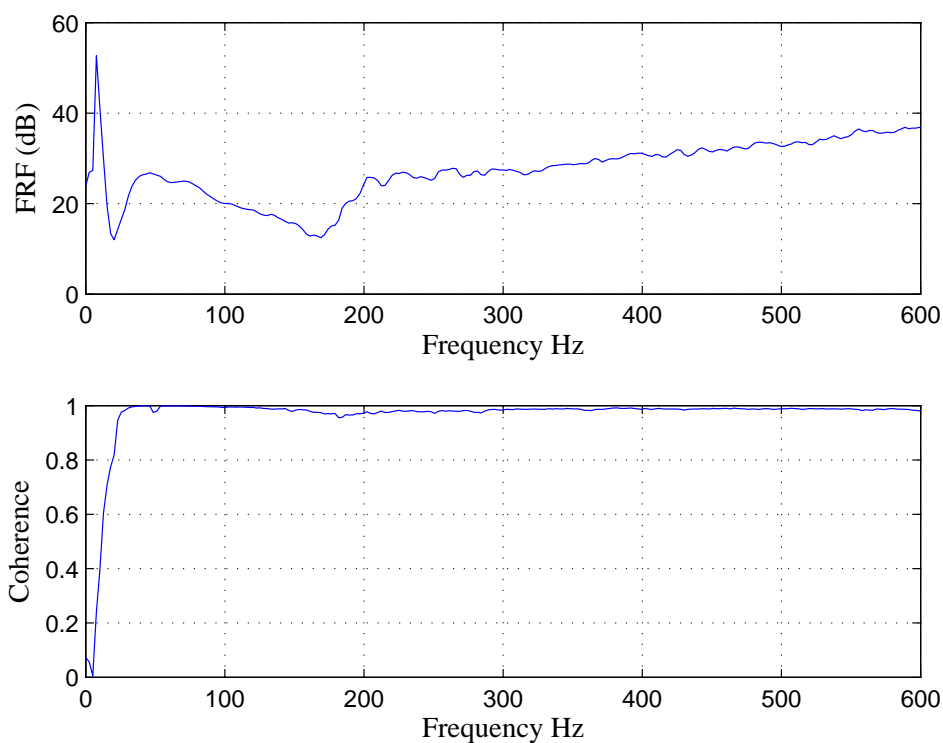
Figure 2.9: Example of the measured finger transfer function.

2.2.1 Compliant system design

By definition, compliant systems transfer motion, force, or energy gaining their mobility from the deflection of flexible members rather than from movable joints. The system presented here is machined by Wire Electric Discharge Machining (EDM) technique from a brute plate of martensitic stainless steel (X30Cr13). More specifically, the construction is developed in two steps: the shaping of the whole system obtained by EDM; and the refining of flexible joints to the wished dimensions using the same machining technique. Consequently, the maximum system dimensions (in this case 372x300 mm) are limited by the maximum working dimensions of the EDM machine.

The flexure hinge, that is a thin member providing the relative motion between two adjacent rigid members through flexing, is obtained machining a blank piece of material, meaning that it does not require any sliding surface and, in such a way, there is not friction loss, wear, or noise coming out from the joint motion [85]. On the other side, a compliant mechanism is very sensitive to fatigue and overloads, and because of the plasticization risk and the necessity to contain the structure dimensions the maximum displacement is limited. The most employed flexure hinges configurations are the circular, the corner filled, the parabolic and elliptical, each one having specific properties that make it more suitable for a specific application. Considering the hinge geometry, the simplest are the circular and the corner filled ones (Figure 2.10). In cases like this, where there are dimensions limits of the structure and a high deflection angle to reach in order to perform the wanted maximum displacement, corner filleted flexure hinges, with respect to circular ones, allow for reducing the system dimensions [86].
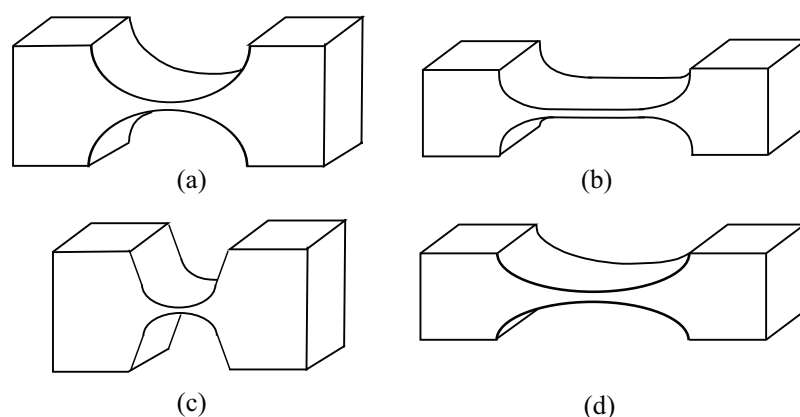
Figure 2.10: Circular hinge (a), corner filleted hinge (b), parabolic hinge (c), elliptic hinge (d).

Employing flexible joints the simplest way to obtain the motion of a rigid horizontal segment is to build a table with four of them (green line in Figure 2.7 c), i.e. a parallelogram. The table is constituted by a base (fixed block) and an upper mobile block linked by two identical arms with a hinge at each extremity. The

parameter describing the relationship between the rigid part of the arm and the hinge is:

$$\xi = 2\frac{l_c}{l} \tag{2.1}$$

where l_c is the length of the hinge strength part (Figure 2.11) and l is the whole arm length. ξ varies between 0 and 1 representing respectively an arm without hinge and an arm without rigid part.
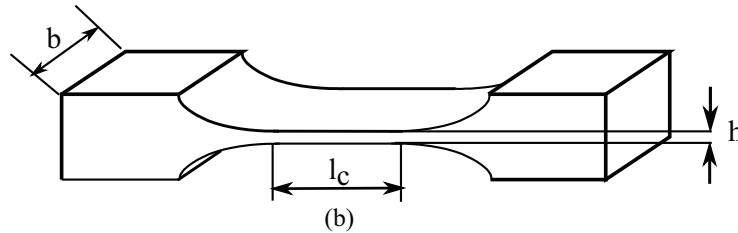
Figure 2.11: Corner filleted hinge geometry.

If a force is applied to the mobile part, it moves causing a quasi identic arms deformation. Considering the case in which the force $\overline{P}$ is applied at a distance $l/2$ from the basis, at each arm extremities there is a force of

$$P = \frac{\overline{P}}{2} \tag{2.2}$$

and a torque of

$$M = \frac{Pl}{2} \tag{2.3}$$

The torque distribution is symmetrical with respect to the point at $l/2$ where it is null. In this force and couple configuration, the lower half arm displacement (f_l) is the half of the global one (f)

$$f_l = \frac{f}{2} \tag{2.4}$$

Considering the lower hinge, linking the fix base with the arm, there are a force P and a torque M_h

$$M_h = \frac{Pl(1-\xi)}{2} \tag{2.5}$$

that allows for calculating the displacement and the rotation of this hinge as:

$$f_h = \frac{P}{KfP} + \frac{Pl(1-\xi)}{2K_{fM}} \tag{2.6}$$

$$\alpha_h = \frac{P}{K_{\alpha P}} + \frac{Pl(1-\xi)}{2K_{\alpha M}} \tag{2.7}$$

31

where K_{fM} is the stiffness generated by the admissible couple applied to hinge extremity and the given displacement:

$$K_{fM} = \frac{M}{f} \tag{2.8}$$

and $K_{\alpha M}$ is the stiffness generated by the admissible couple applied to hinge extremity and the given rotation:

$$K_{\alpha M} = \frac{M}{\alpha} \tag{2.9}$$

While the linear stiffness opposite to the motion is

$$K = \frac{bh^3 E}{\xi(3 - 3\xi + \xi^2)l^3} \tag{2.10}$$

where E is the material young modulus. The corner filleted hinge admissible displacement is

$$f_{adm} = \frac{\xi(3 - 3\xi + \xi^2)l^2\sigma_{adm}}{3Eh} \tag{2.11}$$

where σ_{adm} is the material fatigue limit stress for 10^7 cycles.

Once fixed the material, the desired displacement and the dimensions limits, this equations allows to calculate the hinge dimensions (ξ). In general, several iterations of this process are needed to optimize the system dimensions reducing costs and improving performances. The ideal dimensions combination is the one that allows for maximizing the hinge thickness (to make easier the fabrication process), the maximum applied load, the stiffness to the vertical motion, and to minimize the stiffness to the horizontal displacement. Obviously, it is not possible to obtain all of these points but it is possible to follow the optimization criteria that is more appropriate for the desired application.

With regard to the kinematics, the horizontal motion of the horizontal segment of one single table (approximated by a parallelogram) is not perfectly linear. In fact the trajectory of the horizontal segment is circular with respect to the fixed segment; moreover, due to the complex joints motion, the rotation is not pure, and the rotation center of the joint does not remain fixed during the motion. Consequently, the height of the final position of the upper segment of the parallelogram is less than the starting one. This lost implies undesired variations of the contact force and can cause misalignment of the mobile part of the voice coil actuator. To avoid this effect, it is possible to use a second table (double parallelogram) as shown in blue in Figure 2.7 (c). In fact, the double parallelogram allows to perform the desired horizontal displacement without any vertical motion, because the two identical tables are placed in opposition erasing the final vertical displacement. Because of the joint unperfect symmetry due to the fabrication process and the experimental test bench asymmetry, to obtain the desired displacement avoiding vertical displacement of the upper segment, i.e. the same hinges deflection angle for the two parallelograms which constitute the compliant

system, a lever (red in Figure 2.7 c), connecting the two horizontal segments with the frame, has to be introduced in the central part of the system. Moreover, introducing the second parallelogram, the final displacement of the sample surface is the sum of the horizontal displacements of the two parallelograms, allowing for reducing the dimension of the flexible hinge and increasing the joint precision.

The wire electro discharge machining is able to fabric pieces of high precision with electrically conductive materials even on hard ones. To avoid that the small forces generated during the process cause a degradation of the finished surface, the ratio between the length and the thickness of the hinge has to be less than 60 and restriction on b/h ratio preserves the EDM wires (the wire serves as the electrode and the electrical discharges actually cut the workpiece). The resolution is about 0.1 μm, the precision of 5μm and typical value of finished surface roughness is of 0.18 μm.

For this specific application, the compliant system and its hinges have been dimensioned starting from the total dimension of the workpiece (limited by the machine dimensions) and the desired final linear displacement of the surface sample (100 mm). In order to obtain such excursion of the tangential displacement, accounting for the whole system dimension limits, the flexible joints length is, depending on the joint position, 6 mm (parallelograms joints) or 20 mm (lever joints). After the preliminary dimensioning of the joints by the equation 2.11, a finite element model of the system (presented in section 2.3.1) has been developed to verify the respect of the material fatigue limit stress during the maximum deflection of the hinges

2.2.2 Finger model

In addition to the measurements developed on the real finger, the TriboTouch allows to perform the same tests involving a fake finger (Figure 2.12). In this way it is possible to analyze both the global vibrations (on the finger nail using the accelerometer) and the local ones (at the contact zone using a fast camera and the image cross-correlation technique), avoiding the need to analyze all the surface samples with the real finger. The fake finger is made of RTV silicone. The fingertip shape and the fingerprints are reproduced by molding technique. An aluminum lever, representing the finger bones, fixes the finger on the set-up structure and confers stiffness to the finger.

This configuration is the result of an optimization process started with a very simplified model, (Figure 2.13a) made of an aluminum thin plate arm representing the finger and an aluminum frame holding the fingerprint mold. The fake finger model has been changed step by step, trying to reproduce as best as possible the finger behavior, avoiding bucking phenomena, stick slip and sprag slip behavior, natural frequencies falling in the frequency range of interest.

In fact, the finger model has to reproduce as much as possible finger compliance, stiffness and dynamic behavior, but if in the real finger these characteristics are conferred from multi layers with very different properties, from the epidermis to the bone, it is not trivial to approximate its behavior with a finger model

made of aluminum and isotropic silicone material.

Figure 2.12: Tribotouch with the finger model (scale 1:4).

Since the first prototype, fingerprints are conferred throughout molding technique employing silicone. In order to have the positive fingerprints, the molding process is realized in two steps: at first the real finger transfers fingerprints on a dentistry paste, and later on, liquid silicone is dripped into the dentistry paste mold to reach the shape during the hardening process.

The first and second prototypes (Figure 2.13a-b) showed sprag-slip and stick-slip phenomena. For these configurations, the accelerometer is mounted in the aluminum frame hole, and a thin steel plate links the finger model to the holding structure, throughout screws and hepossidic glue (Figure 2.12).

To avoid these undesired phenomena, a third version of the finger model has been developed, by changing the angle of attack, the thickness of the thin plate and the mass on the fingerpad. This solution solved the previous undesired phenomena but involved a low system natural frequency in the range of interest, not observed in the real finger.

Several different blades have been tested for the link with the structure, (aluminum, steel, teflon, sandwiched blades) but the damping and the displacement of the resonant frequency to higher frequency was not sufficient to exclude them

from the interest frequency range. Another improvement comes from the changing of the angle between the finger model and the structure. In fact, the first model is perpendicular, the second has an angle of 45° while the third and the fourth model have an angle of 30° that augments the system stability and approaches the real angle of attack used by human subjects when testing surfaces. With the thin plate model of the fake finger, it was not possible to avoid the resonant frequency in the range between 2 and 500 Hz; consequently, the prototype was changed, switching to the entire molding of a half finger with an internal aluminum lever conferring stiffness (Figure 2.13 (d)).

For this last model, mounted with the block at 30°, the angle of attack and the finger position has been chosen for being representative of the real scanning process by the human subject. For each configuration several tests for the development of the fake finger have been carried out. The final experimental validation of the fake finger by comparison between vibration spectra of the real and fake finger is presented in section 2.3.2.
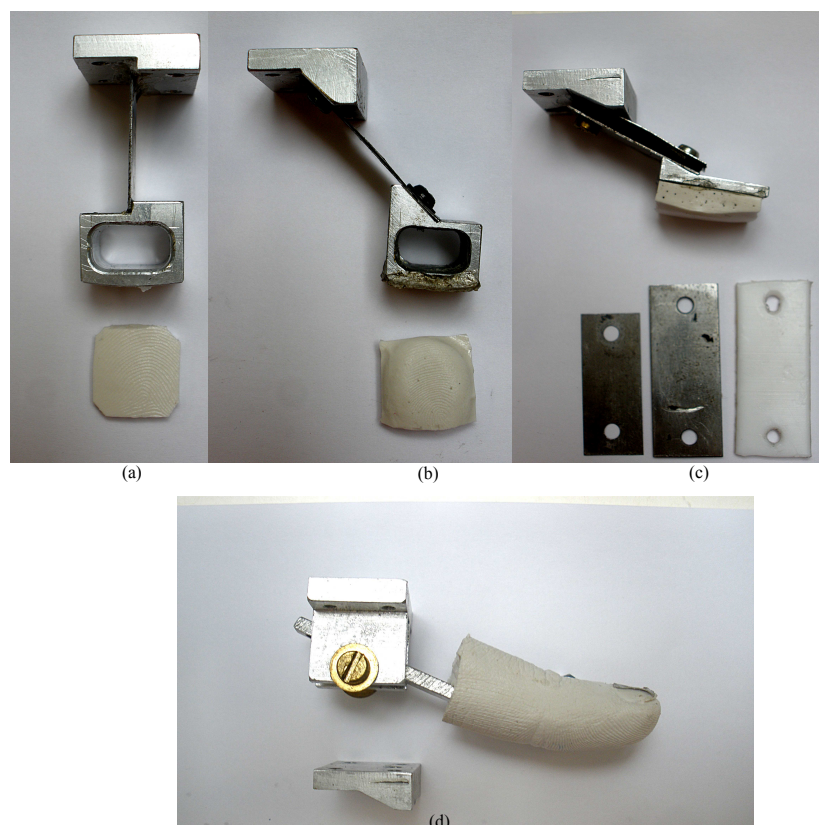

(a) (b) (c)

(d)

Figure 2.13: Finger models.

2.3 Test bench validation

To ensure the capabilities of the designed set-up to perform the desired measurements, both numerical and experimental validations were carried out.

2.3.1 Finite element method validation

Once the preliminary dimensioning of the joint hinges of the compliant system were stated, a validation by FEM calculation has been performed by the commercial code ANSYS. The finite element analysis (based on a model with 245747 nodes and an hexahedral mesh) permits to validate of the global stiffness of the system, to ensure the planarity of the sample displacement and to evaluate of the stresses distribution at the flexible joints which has to be lower than the material stress limit.
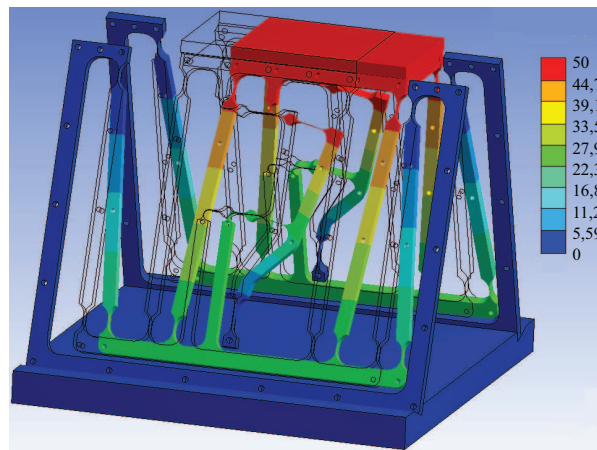
Figure 2.14: FEM simulation of the system displacement.

Figure 2.14 shows the compliant mechanism configuration when a tangential force of 4 N is applied and the maximum displacement is obtained.

The compliant mechanism is able to reach a maximum displacement of 100 mm creating an angle between the base and the mobile part of 20°. Taken the equilibrium position as a reference, the motion can be divided into two parts: a positive course of 50 mm and a negative one of the same length (corresponding to the direction in Figure 2.14, that is the one used for the measurements). This classification is useful for the discussion of the numerical simulation results because the results show a non perfect symmetry of the system response with respect to the equilibrium position. This non symmetric behavior is due to the presence of the central lever and to its fixation mechanism to the horizontal segments of the double parallelogram, which is asymmetric.

Specifically, the force required to reach the maximum displacement, the stiffness and the non planarity are not the same for the two directions, as shown in Figure 2.15. The non-planarity of the sample displacements is due to slight errors in the deflection of the hinges that cannot be approximated to perfect pin joints because of their non negligible length, which was necessary to reach the desired final displacements of the surface sample. Nevertheless, the non planarity of the sample displacements (less than 10μm for a displacement of 50 mm and less than 0.12 mm for a displacement of 100 mm) remains negligible for this application and the force required to reach the maximum displacement is furnished by the linear actuator without problems.
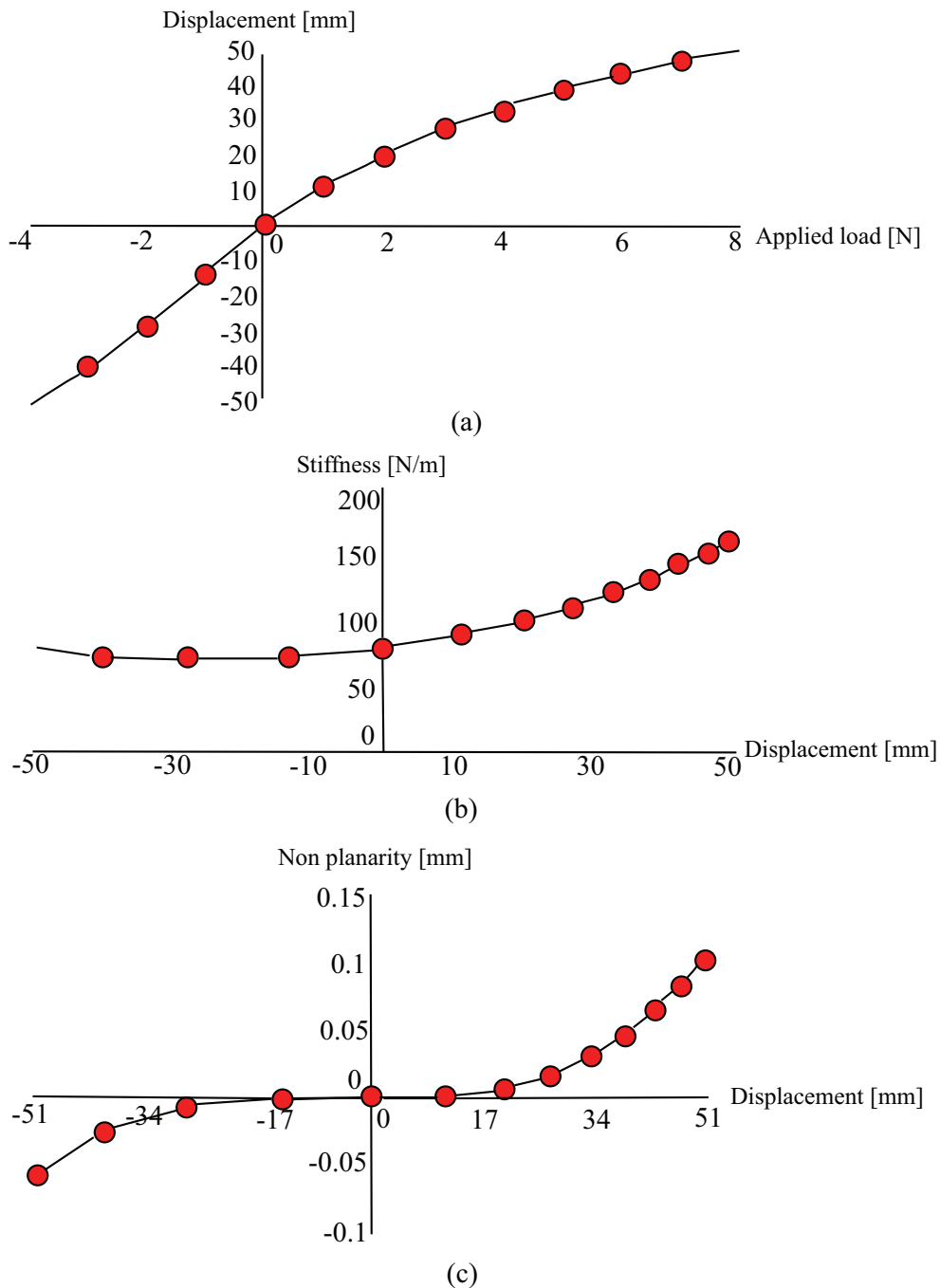
Figure 2.15: Relationship between the required force and obtained displacement (a), stiffness behavior respect to the displacement (b) and non planarity as a displacement function (c).

An important aspect of the numerical simulation is the analysis of the joint stress to verify if in the most solicited parts of the system the stress is lower than the material stress limit.

Because of the system structure and kinematic, the most solicited joints are the ones linking the central lever to rest of the system (Figure 2.16) and the ones linking the central lever to the basement (Figure 2.17). From Figure 2.16 and Figure 2.17 it is possible to say that the stress distribution values are always lower than the material stress limit, that is of about 850 MPa.
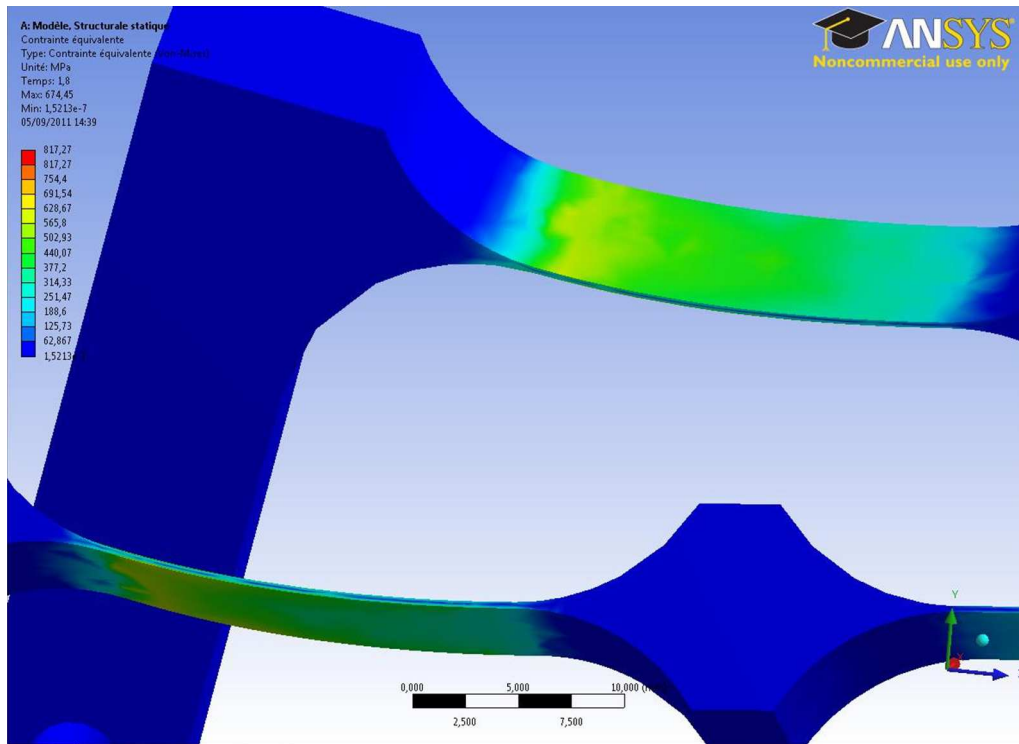
Figure 2.16: Stress distribution at the joints linking the central lever with the compliant system.
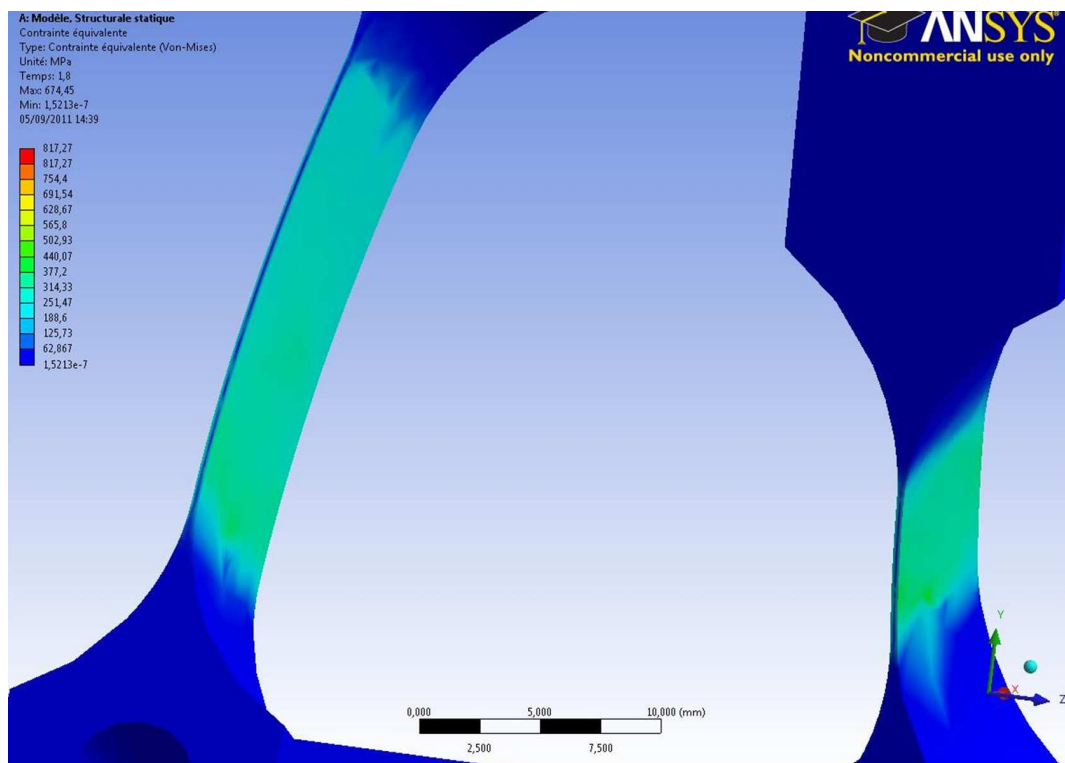
Figure 2.17: Stress distribution at the joint linking the central lever with the compliant system basement.

2.3.2 Experimental validation

To validate the set-up and the measurement methodology it was decided to perform several tests employing samples with a periodical roughness both to confirm the possibility to detect the desired vibrations and to quantify the noise generated by the set-up. These tests involve the same surface samples described in the previous paragraph (2.1), with roughness groves perpendicular to the scanning direction in order to have vibration spectra features easily identifiable and that can be linked to the surface sample and fingerprints' roughness [83], [84]) (chapter 3). In these conditions the vibrations coming from the scanning of the finger on the surface sample can be identified and distinguished by eventual external noise.

In order to verify the negligible value of the parasite noise coming from the set-up, the measurements of the acceleration with and without scanning between the fingertip and the surface sample are compared. Specifically, in Figure 2.18a, the red line shows the vibration detected on the finger while it follows the sample without a relative motion between the two surfaces (fingertip and sample) in contact and thus without the vibrations induced by finger scanning, but with the set-up fully functioning; the blue line shows the vibrations induced by friction when the finger stays fixed and the sample is moving, which is the configuration used for the tests. The first acceleration peak at 1.1 seconds is due to the start of the sample horizontal displacement. The parasitic noise coming from the functioning of the set-up is found to be negligible with respect to the friction induced vibrations measured when scanning the surface, as confirmed from the two signal FFTs (Fast Fourier Transform) shown in Figure 2.18b. The spectrum due to the vibration of interest (blue) is considerably higher than the one of the parasitic noise (red).

The measurements performed on periodical roughness samples show well defined frequency peaks that depends on the period of the roughness sample. As expected, the frequency peak values are a function of the relationship between the surface sample roughness, the fingertip roughness and the scanning speed.

Figure 2.19 shows the FFTs of the acceleration measured on the finger for six different scanning speeds on the same roughness sample (R2) divided by the finger transfer function [83]. Increasing the scanning speed from 10 mm/s to 60 mm/s, the peaks on the frequency spectra cover larger values and their amplitude rises. The same behavior can be found for all the surface samples and for different subjects, confirming that the designed experimental set-up is suitable for measuring and investigating the vibrations induced from the finger surface scanning.

As mentioned before, it is not possible to perform the vibration measurement directly at the contact zone between the fingertip and the surface sample, because the presence of local transducers would modify the contact and the measured vibrations. For this reason the accelerometer detecting the vibrations is mounted on the finger nail; to account for the different point of measurement with respect to the position of the mechanoreceptors (the fingertip surface),the obtained FFTs

have been weighted by the finger transfer function (see 2.2).

(a)

(b)
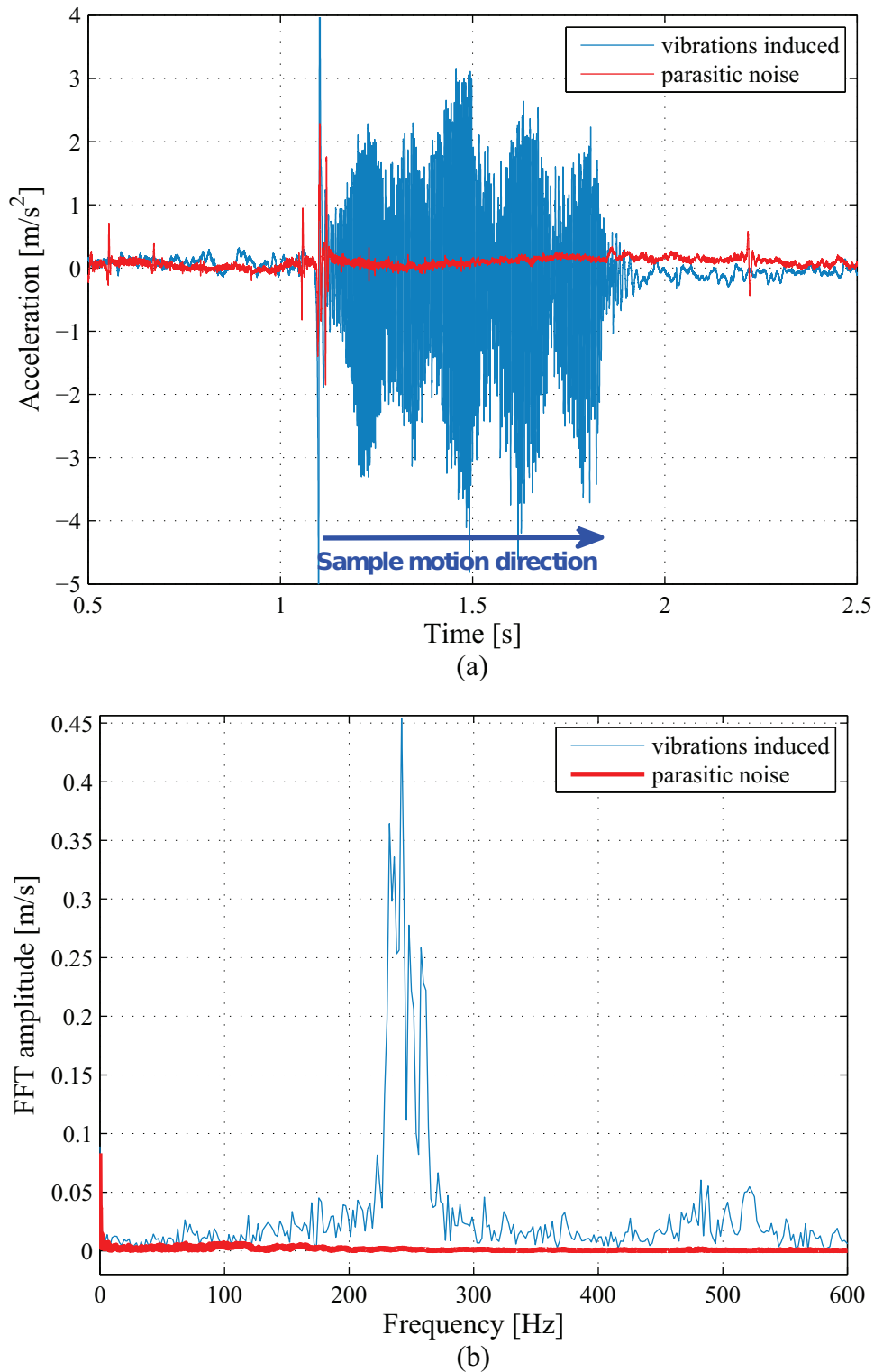
Figure 2.18: An example of the comparison between the acquired acceleration signal of the vibrations induced by the fingertip/surface scanning and the parasite noise from the set-up functioning (a) and their FFTs (b).

40
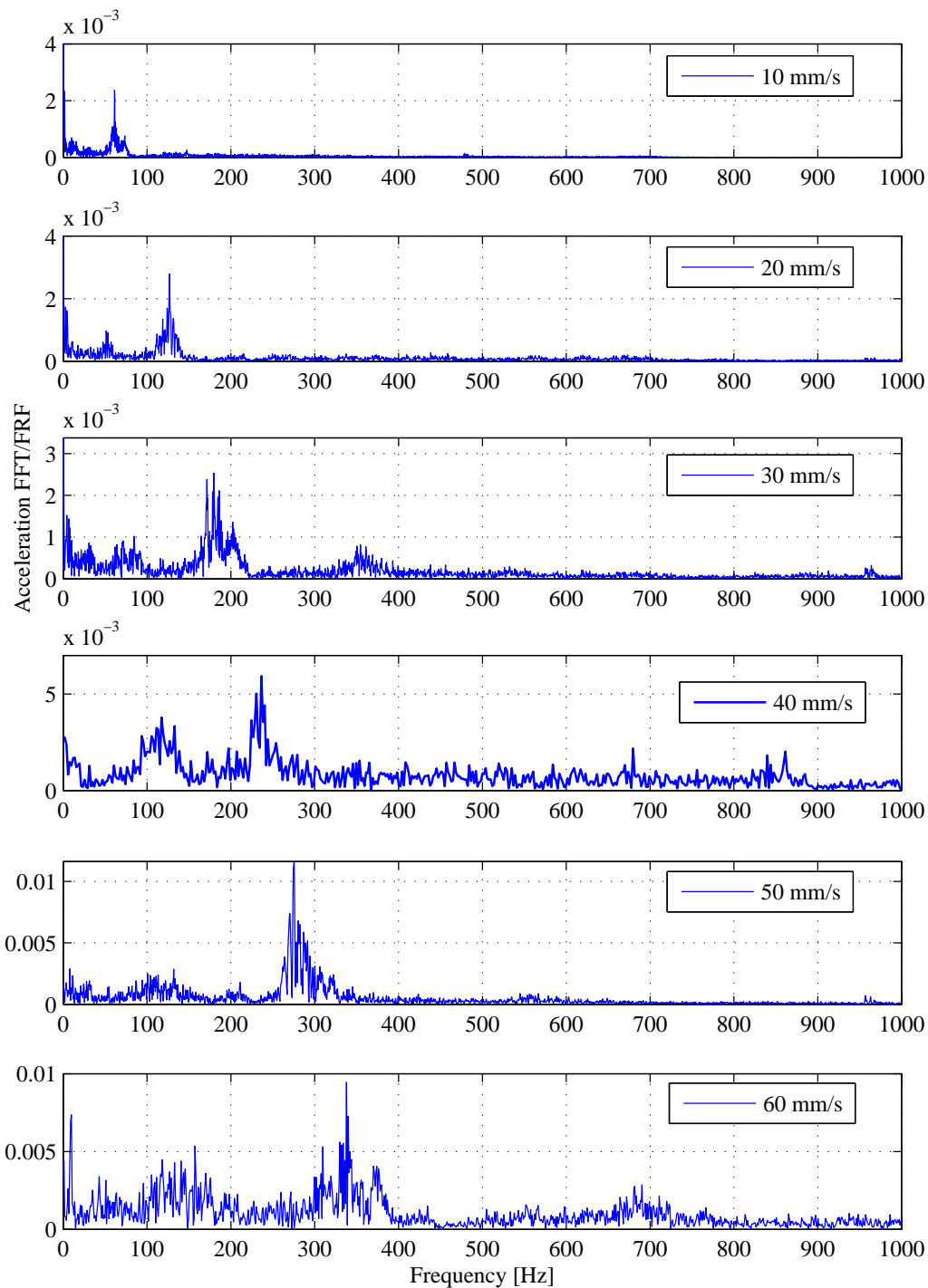
Figure 2.19: Acceleration FFTs of the signals obtained from the accelerometer, at different speed and for R2 roughness sample (roughness wavelength 0.15 mm), divided by the finger transfer function.

Finger model

To validate the representativeness of the measurements obtained by the fake finger, the same tests, performed with real finger have been carried out with the fake one. As shown in Figure 2.20 from the comparison between the vibrations FFTs coming out from the scanning of the real finger and the fake one, on the same

41

sample (roughness wavelength 0.15 mm and mean roughness 1 μm) for different scanning speeds, the vibration spectra show a good agreement of the results.
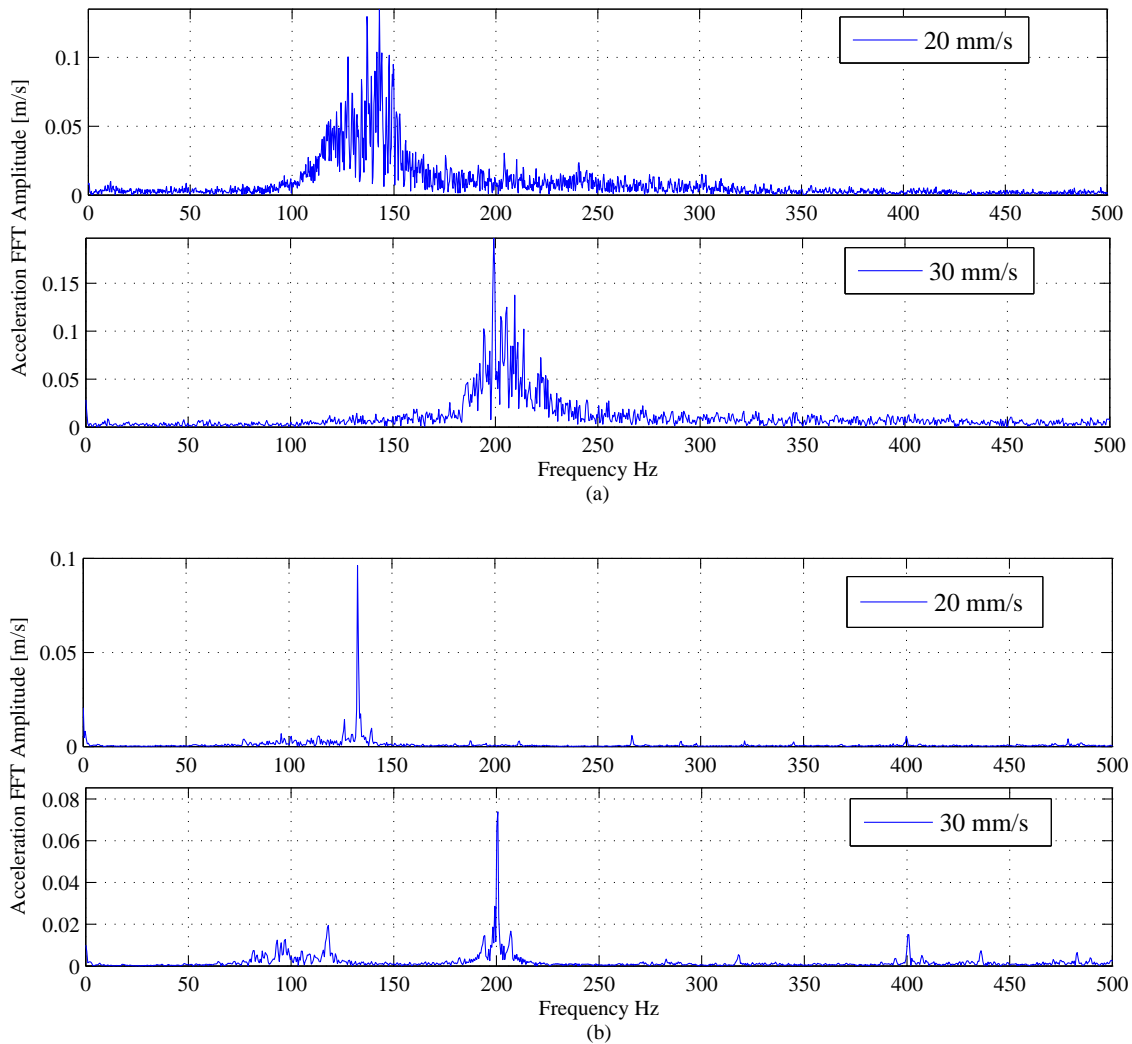
Figure 2.20: Comparison between the acceleration FFTs obtained, on the same surface sample with periodical roughness, scanning with the real finger used for the molding (a) and the fake one (b). The sample roughness wavelength 0.3 mm.

The fake finger shows, compared to the real one, more clear spectra with well defined peaks. This behavior is probably due to the different structure between the two fingers. In fact, the real finger is a multilayered structure while the silicone fake finger is homogeneous. In addition, each epidermis and dermis layer has different mechanical properties that seem confer a lower damping to the fingertip with respect to the fake one.

The agreement between the dynamic behavior of the real and the fake finger is confirmed also from the similar values of the friction coefficient. In fact, as explained in 3.7, to reduce the silicone adhesion (highlighted from preliminary tests) it has been decided to exploit the polymer permeability treating the finger model with lubricant oil (vaseline) obtaining friction coefficient values comparable to the real finger ones.

2.4 Friction coefficient

The designed apparatus has been developed taking into account the possibility to quantify the friction coefficient characterizing each measurement, which can furnish additional information about the touched surface.

At a first step, two monoaxial force transducers (Figure 2.7b), monitoring the normal forces at the connection between surface sample and support, have been employed for this purpose.

In this case, only the normal component of the contact force is measured directly; to calculate the friction coefficient it is necessary to recover the tangential force by geometrical considerations and the equilibrium equations of the surface sample.

With respect to Figure 2.21 and Figure 2.8, the global contact force between the fingertip and the sample surface can be decomposed into the normal component, N, along the direction normal to the sample surface and the friction one, T, and which acts along the direction tangential to the sample surface, opposite to the motion direction. The global friction coefficient μ is defined as the ratio between T and N.
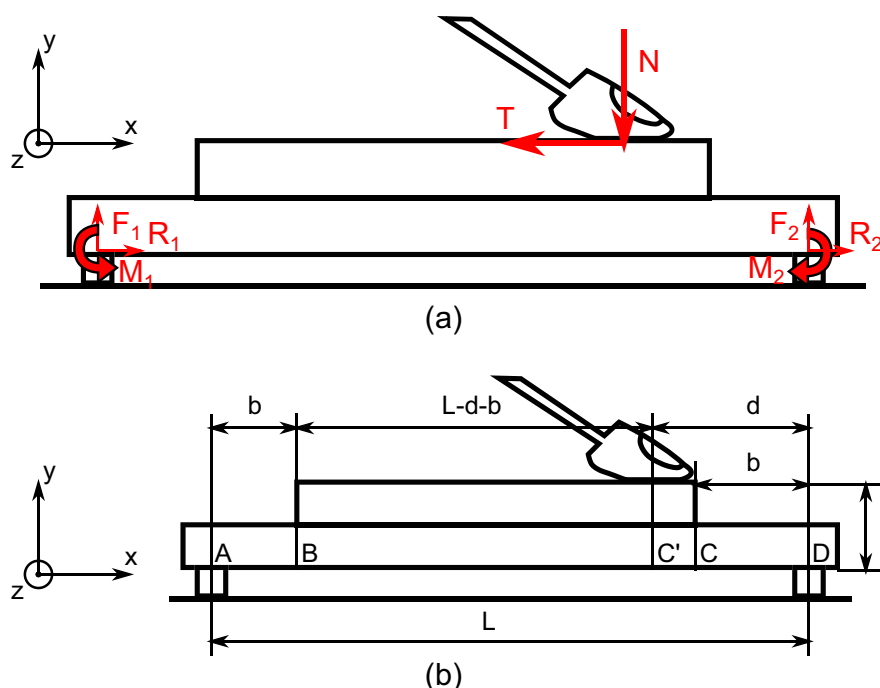
Figure 2.21: (a)Scheme of the mechanical actions for the friction coefficient computation, (b) geometric parameters.

The surface sample is fixed at the two force transducers that connect it to the linear guide (Figure 2.7). If the finger motion lies in the same vertical plane of the two points of connection the problem can be reduced to a planar one and, at each point, three reaction components have to be accounted for: F_1 and F_2, which are the force components measured by the force transducers; R_1 and R_2, along the tangential direction; and the two moments M_1 and M_2 (Figure 2.21). Considering

the structure as a clamped beam, it is possible to obtain the equilibrium equations:

$$T = R_1 + R_2 \tag{2.12}$$

representing the force equilibrium along the x axis;

$$N = F_1 + F_2 \tag{2.13}$$

representing the force equilibrium along the y axis;

$$N(d - L) + \mu Nh + F_2 L - M_2 + M_1 = F_1 + F_2 = 0 \tag{2.14}$$

representing the moment equilibrium at the point A. Only the last two equations are useful for this application, and in particular the second one furnishes the desired friction coefficient:

$$\mu = \frac{M_2 - M_1 - F_2 L + (F_1 + F_2)(L - d)}{(F_1 + F_2)h} \tag{2.15}$$

While F_1, F_2, L, and h are directly measured during the scanning of the fingertip on the sample surface, M_1 and M_2 are unknown. They can be calculated as a function of the normal force N, the dimensions of the structure, and the finger position, considering the hyperstatic problem shown in Figure 2.22, where the friction force T gives the moment M_T at the line between the two points of connection with the frame:

$$M_T = Th = \mu Nh \tag{2.16}$$
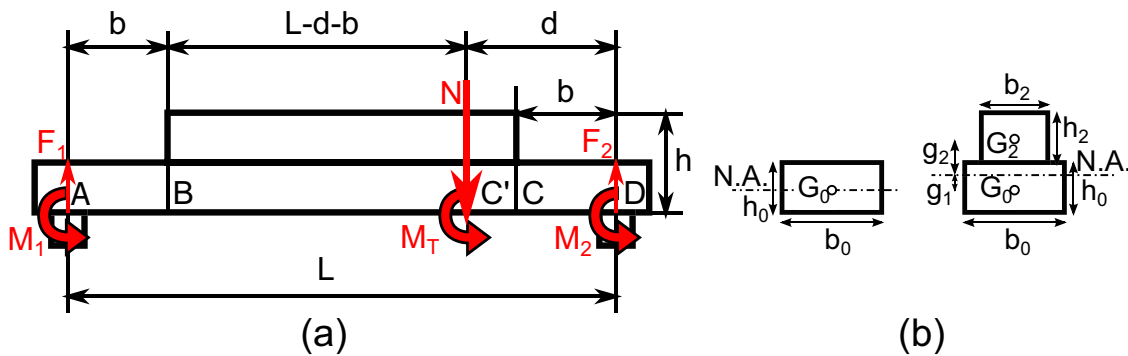
Figure 2.22: (a)Hyperstatic problem for the calculus of the flexion component as a function of known parameters, (b) Cross sections of the different beam elements.

The displacement of the sample is driven by a trapezoidal function of the actuator speed. The parameter d contains the information about the fingertip position, which is calculated as

$$d = p_0 + vt \tag{2.17}$$

where, p_0 is the initial distance of the fingertip from the force transducer when the sample reaches the constant value of the actuator speed, v is the actuator speed and t is the time.

The differential equations giving the shear (V) and the bending moment (M) as a function of the slope (y′), the deflection (y), the Young modulus (E), and the inertia moment (I) is:

$$V = \frac{dM}{dx}, M = EI\frac{dy'}{dx} \simeq EI\frac{d(\frac{dy}{dx})}{dx} = \frac{d^2y}{d^2x} \tag{2.18}$$

It can be used to determine the shear and bending moment diagrams and the equations of the elastic curve for each beam element subject to a given set of loading. Through successive integration, these equations are used to determine the slope and deflection functions of a segment of beam. The integration constants can be determined enforcing boundary and/or continuity conditions of the beam segment. Boundary conditions are imposed at the points of support for the structure and continuity conditions at the points common to two adjacent beam segments.

Specifically, in this case (Figure 2.22), there are four beam elements to consider: AB, BC′, C′C, and CD. The following boundary and continuity conditions are assumed:

Boundary conditions   Continuity Conditions

$$y'_{AB}(A) = 0, y'_{CD}(D) = 0 \qquad y'_{AB}(B) = y'_{BC'}(B), y'_{BC'}(C') = y'_{CC'}(C'), y'_{C'C}(C) = y'_{CD}(C)$$

$$y_{AB}(A) = 0, y_{CD}(D) = 0 \qquad y_{AB}(B) = y_{BC'}(B), y_{BC'}(C') = y_{CC'}(C'), y_{C'C}(C) = y_{CD}(C) \tag{2.19}$$

Integrating the equations on each beam element and introducing the boundary and continuity conditions, it is possible to obtain the equations of M_1 and F_1 in function of N, μ, and the geometric components;

$$\begin{aligned} M_1 = \frac{N}{(L + 2b(\alpha - 1))(-2b - L)^2 + 2b(4b^2 - 6bL + 3L^2\alpha}&\{[(4b^5(\alpha - 1)^2 + \\ - 2b^4(\alpha - 1)^2(4d + L + 4H\mu) + 2bL(\alpha - 1)&(-d^3 + dL^2 - 3dH^2\mu + HL^2\mu) + \\ + dL^2(-d^2 + 2HL\mu + d(L - 3H\mu)) - b^2 L(\alpha - 1)&(-6d^2 + 3d(L - 4H\mu) + \\ + L(L + 3H\mu)) + 2b^3(\alpha - 1)(-2d^2 + 3dL(\alpha - 1)& - 4dLH\mu + \\ + L(L + 3H(\alpha - 1)\mu)))]\} \end{aligned} \tag{2.20}$$

$$\begin{aligned} M_1 = \frac{1}{(L + 2b(\alpha - 1))(-2b - L)^2 + 2b(4b^2 - 6bL + 3L^2\alpha)}&\{(N(4b(\alpha - 1) + \\ + 6bL(\alpha - 1)(d + H\mu) - 3b^2(\alpha - 1)(2d + L + 2H\mu) + d(-2d^2 + 6HL\mu + \\ + 3d(L - 2H\mu))))\} \end{aligned} \tag{2.21}$$

Then, M_2 and F_2 can be calculated from the equilibrium equations and, finally, the friction coefficient can be calculated as a function of the measured forces F_1 and F_2:

$$\begin{aligned} \mu = \frac{1}{(6hN((p_0 + vt)((p_0 + vt) - L) + b^2(\alpha - 1) + b(L - L\alpha)))}&\{(F_2 L^3 - (p_0 + vt) - L)^2 \\ + (2(p_0 + vt) + L)N + 4b^3(2F_2 - N)(\alpha - 1) + 6bL(F_2 L + ((p_0 + vt) - L)N)(\alpha - 1) \\ - 3b^2(4F_2 L + 2(p_0 + vt)N - 3LN)(\alpha - 1)\} \end{aligned} \tag{2.22}$$

where α is the ratio between the inertia momentum I_o, of the AB element beam cross section, and I_1, of the BC element beam cross section, as shown in Figure 2.22b.

Figure 2.23-a shows an example of the force components detected and the calculated friction coefficient. During the first phase of the test (Phase I) there is no contact between fingertip and sample. At time t=2.6s the fingertip is put in contact with the surface sample (Phase II). During the Phase III the normal force is maintained constant and the sample moves to make the fingertip scan the surface. In this phase the contact moves from one transducer position to the other, so that F_1 increases as the motion takes place and the opposite happens for F_2; their sum, N, remains constant during the measure.

Figure 2.23-b shows the friction coefficient calculated, as reported above, during the surface scanning of the fingertip skin on a steel sample (Phase III) [2], [21].
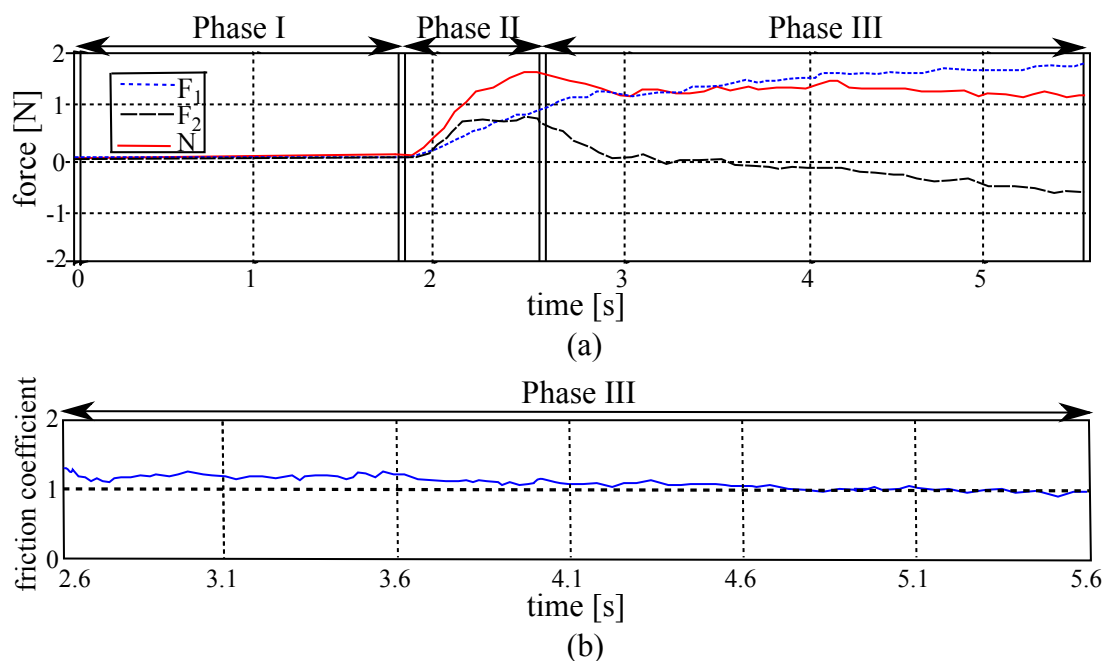
Figure 2.23: (a) Example of the measured normal load components F_1, F_2, and the resulting normal load N. During the Phase I the measurement begins but there is no contact between the finger and the surface sample; In Phase II the contact between the fingertip and the surface sample engages; In Phase III the scanning of the contact surface takes place and the contact point moves between the two force transducers. (b) An example of the calculated friction coefficient between the fingertip skin and a steel sample during Phase III.

Figure 2.24 shows the dependence of the friction coefficient with respect to the scanning speed and the contact load.

Figure 2.24a shows the friction coefficient mean value, averaged on the scanning time, as a function of the scanning speed for a normal contact force of 0.5 N. As expected by the literature [1], the friction coefficient decreases with the increase of the scanning speed. In fact, during the scanning, phenomena like natural skin hydration and production of cutaneous lipid film take place, reducing the friction coefficient.

Figure 2.24b is an example of the friction coefficient behavior with respect to the normal load. The decrease of the friction coefficient with the increasing of normal load suggests the effect of the adhesion mechanism.
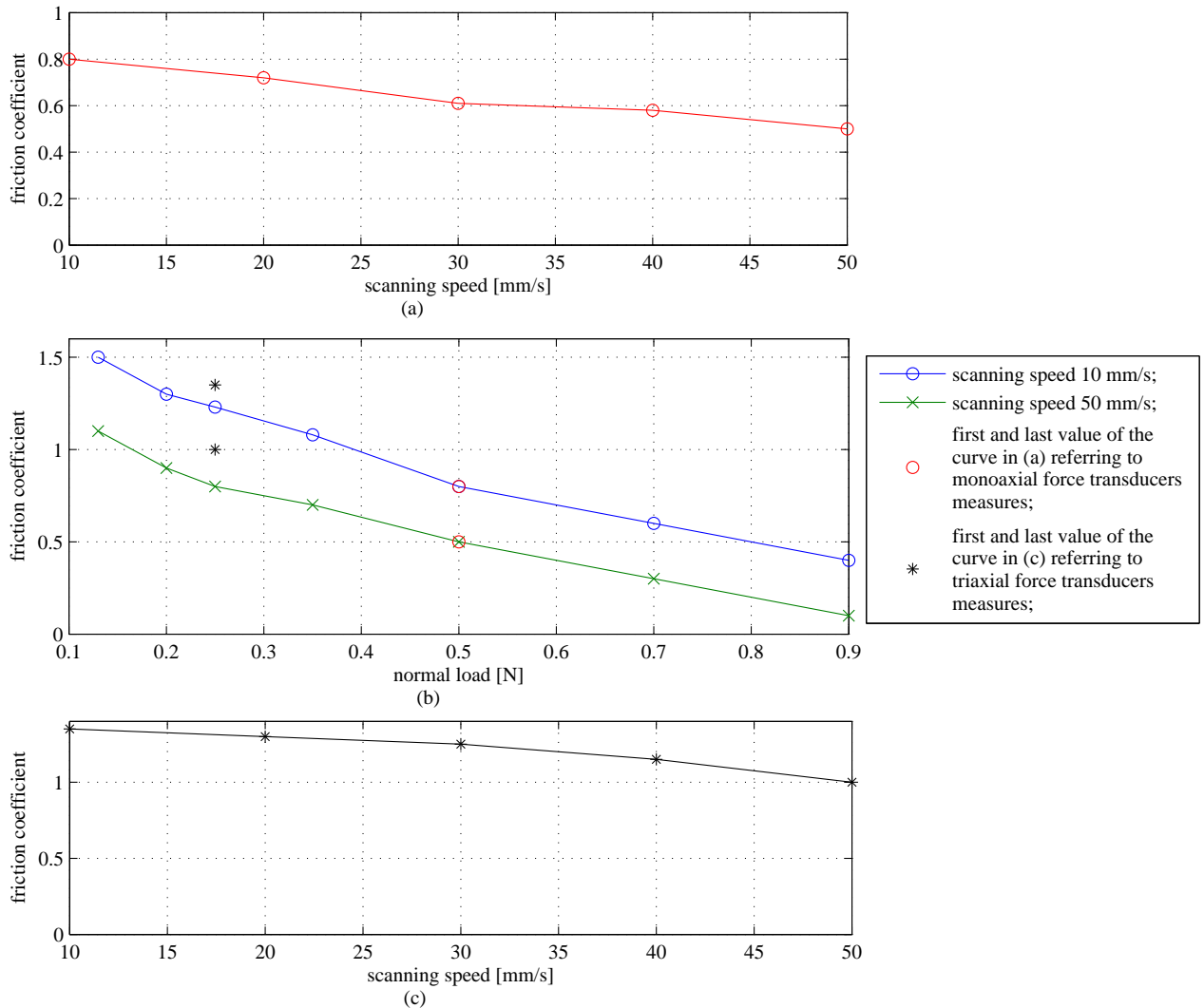
Figure 2.24: (a) Friction coefficient between the fingertip and a steel surface sample with respect to the scanning speed employing monoaxial force transducers. (b) Friction coefficient between the fingertip and a steel surface sample with respect to the normal load for the extremal scanning speeds (10 mm/s and 50 mm/s) employed during the measurements with monoaxial force transducers.(c) Friction coefficient between the fingertip and a steel surface sample with respect to the scanning speed employing triaxial force transducers. The used surface sample is the same for all the measurements.

Neglecting the moments M_1 and M_2, i.e. solving the equivalent iso-static problem and considering the connection with the transducers as pin joint, there is a relative error up to 30% in the calculation of the friction coefficient.

A fundamental parameter of this method is the height h, which increases the friction force moment. In fact, if this parameter is too small, the moment becomes negligible in the calculus, and the friction coefficient estimation is not well approximated. An experimental analysis has been developed for different values of h, and the results on the friction coefficients are acceptable for values up to 50 mm. So, when interested to the friction coefficient quantification, a steel block with a height of 50 mm is placed between the force transducers and the surface sample (Figure 2.25). In order to verify all the hypotheses, measurements of the friction coefficient have been performed with a triaxial force

transducer along a smaller displacement (about 30 mm for avoiding the torque on the transducer). The relative error with respect to the measurements obtained accounting for M_1 and M_2 was found to be less than 20%. Nevertheless, the use of a single triaxial force transducer implies a small scanning distance while the surface samples length varies between 60 and 100 mm.

Figure 2.25: Monoaxial force trasducers configuration for the friction measurements (scale 1:3).

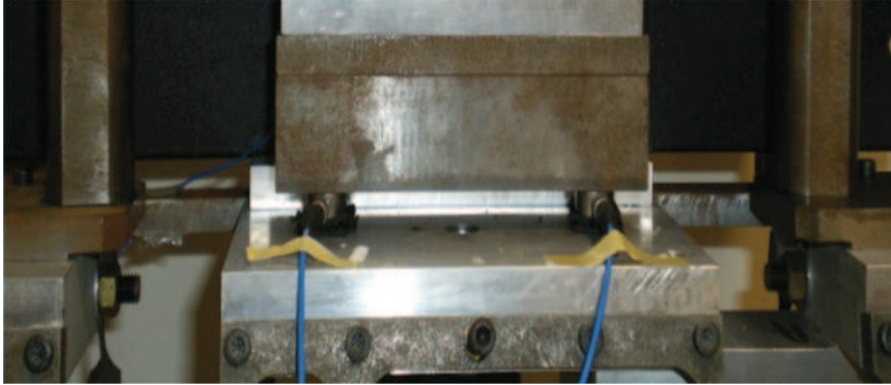On the other hand, with respect to monoaxial force transducers results, the friction coefficient computation involves the estimation of the finger position starting from the actuator position and the assumption of a punctual contact between finger and surface sample. Indeed, the friction coefficient is calculated in the second actuator motion phase, when it reaches a constant speed. In consequence it is necessary to determine the finger position at the initial frame of this motion at constant speed, on the base of the actuator motion low. The length of the contact segment is comparable with the total surface length (100 mm), introducing an error in the finger position estimation. Furthermore, the contact between the finger and the surface involves an area that depends on the skin deformations and so, from the contact load, while the position d introduced in the formula is the medium point of contact between fingertip and sample.

For these reasons, the two monoaxial force transducers have been replaced with two triaxial force transducers (Figure 2.12). They allow for measuring directly both the normal and tangential forces at the connection between surface sample and support and the friction coefficient is calculated directly as the ratio between the two force components at each instant of the scanning time.

In Figure 2.24 (c) there is an example, for a surface sample with periodical roughness, of the friction coefficient behavior with respect to the scanning speed, while the normal force is maintained at 0.25 N.

The comparison between Figure 2.24 (b) and Figure 2.24 (c) highlights how the two friction coefficient estimations are comparable for the smaller scanning speed (10 mm/s) (the relative error is about 10%) and differ as the the scanning speed increases (the relative error is about 20%). This behavior could be explained considering that, for first method, the constant speed hypothesis becomes less appropriate with the increasing of the scanning speed reached by the actuator because the acceleration and deceleration phases increase and, in consequence, the estimation of the finger position is less precise.

2.5 Concluding remarks

An experimental set-up has been designed to reproduce the scanning of the finger on a surface sample and to measure the induced vibrations. The set-up allows for reducing parasitic noise and for reproducing the scanning with realistic values of the contact parameters (normal force, scanning speed, contact with real finger, everyday objects' surface roughness). A numerical and experimental validation of the set-up has been carried out showing the possibility to recover the global vibration spectra and the macroscopic friction coefficient between finger and surface. The test bench permits to analyze the local contact vibrations by means of a fake finger and of the cross correlation technique. In this thesis, the presented set-up has been used for the analysis of the linear scanning of the finger on rigid surface samples and on textiles, along the direction of the finger (perpendicular to the fingerprints). Nevertheless, the test bench can be used for the reproduction of the sliding along different directions, for analyzing the effect of the sliding direction on the induced vibrations and, consequently, on the perception.

Chapter 3

Experimental analysis of the relationship between contact properties and induced vibrations

When a finger moves to scan the surface of an object (haptic sensing), the sliding contact generates vibrations that propagate in the finger skin activating the receptors (mechanoreceptors) located in the skin, allowing the brain to identify objects and perceive information about their properties. Thus, the information about the surface of the object is transmitted through vibrations induced by the sliding between the skin and the object scanned by the fingertip. The mechanoreceptors transduce the stress state cues into electrical impulses that are conveyed to the brain.

In this context, it is necessary to perform appropriate experiments to find out the frequency characteristics of the contact, looking for how the tactile sense is connected to the measured frequency spectra to a better understanding of the tactile perception mechanism. While the correlation between surface roughness and tactile sensation has already been approached in literature, the vibration spectra induced by the finger/surface scanning, which are the direct cause for the mechanoreceptor activation, have received less attention.

In this chapter, frequency analysis of signals characterizing the surface scanning is carried out (using the TriboTouch experimental set-up previously described) to investigate the vibration spectra measured on the finger and to highlight the changes shown in the vibration spectra as a function of the contact parameters such as scanning speed, contact load, surface roughness and surface texture. To identify the main features of the frequency distribution of the measured spectra, measurements on surface samples with periodical and isotropic roughness, and on textiles have been performed; the global dynamics has been acquired by detecting the contact force (with two force transducers placed below the surface sample) and the induced vibrations (with a low mass accelerometer applied on the finger nail).

3.1 Materials and method

For the present analysis, as previously explained, the behavior of the right hand finger has been investigated, and to have comparable measurement conditions, the finger is maintained fixed and the roughness sample is moved at a constant speed by the linear

voice coil actuator (Figure 2.7 and Figure 2.8). In this way, it is possible to have measurements with an almost constant contact force.

The surface samples consist of:

– seventeen aluminium alloy samples with periodical roughness obtained by milling (Figure 2.1 (b)). The sample length varies between 60 mm and 100 mm and the depth between 13 and 2 mm. The height is 8 mm. Varying the mill diameter it is possible to obtain periodical roughness with different mean roughness and spatial period. The samples have Ra ranging from 0.64 to 5.2 μm and roughness wavelength varying between 0.15 and 2.17 mm;

– ten steel samples with isotropic roughness obtained by sandblasting. Different mean roughness are related to variations of sandblasting pressure, distance and grains dimensions. The samples have a mean roughness varying between 0.4 and 5 μm;

– twenty-one fabric samples, that differ each other for material, texture and hairiness.

The roughness parameters of the rigid surface samples have been verified by a laser profilometer, while the fabric features have been observed by a microscope.

The considered scanning speeds are 10 mm/s, 20 mm/s, 30 mm/s, 40 mm/s and 50 mm/s both for measurements involving the fake finger and the real one.

Each surface sample has been investigated, at each scanning speed, for different subjects.

All the experiments took place at the same temperature 24°C and in the same environmental conditions.

For the real finger, the skin was untreated, meaning that no moisturizers were employed. The finger and the surface were cleaned with alcohol before starting the measurements. The accelerometer, detecting the induced vibrations is attached to the finger nail, by means of wax. The finger is put in contact with the surface sample and then the sample starts to move. The direction is the one on the line of the finger bones, perpendicular to the fingerprint direction.

In case of measurements with the fake finger, the experimental tests are preceded by lubricant oil bath which confers, to the silicone polymer, friction characteristics close to the real finger ones. A thin aluminium plate is attached to the silicone reproducing the finger nail and then, the accelerometer is mounted on the thin plate. The finger is put in contact with the sample and the contact force can be regulated by means of the two screws on the set-up upper part (Figure 2.12). Also in this case, after the contact, the linear voice coil starts to perform the desired displacement allowing for the finger/surface scanning.

In both cases, the contact force are detected from the triaxial force transducers placed below the surface sample.

3.2 Surface texture and fiction induced vibrations spectra

The first tests have been performed on aluminium surface samples with periodical roughness (Ra ranging from 0.64 to 5.2 μm and roughness wavelength varying between 0.15 and 2.17 mm) oriented along the transverse direction with respect to the scanning one (chapter 2 and Figure 1.1).

For a periodic roughness, as expected, the vibration frequency can be found as a function of the scanning speed and of the roughness spatial period.
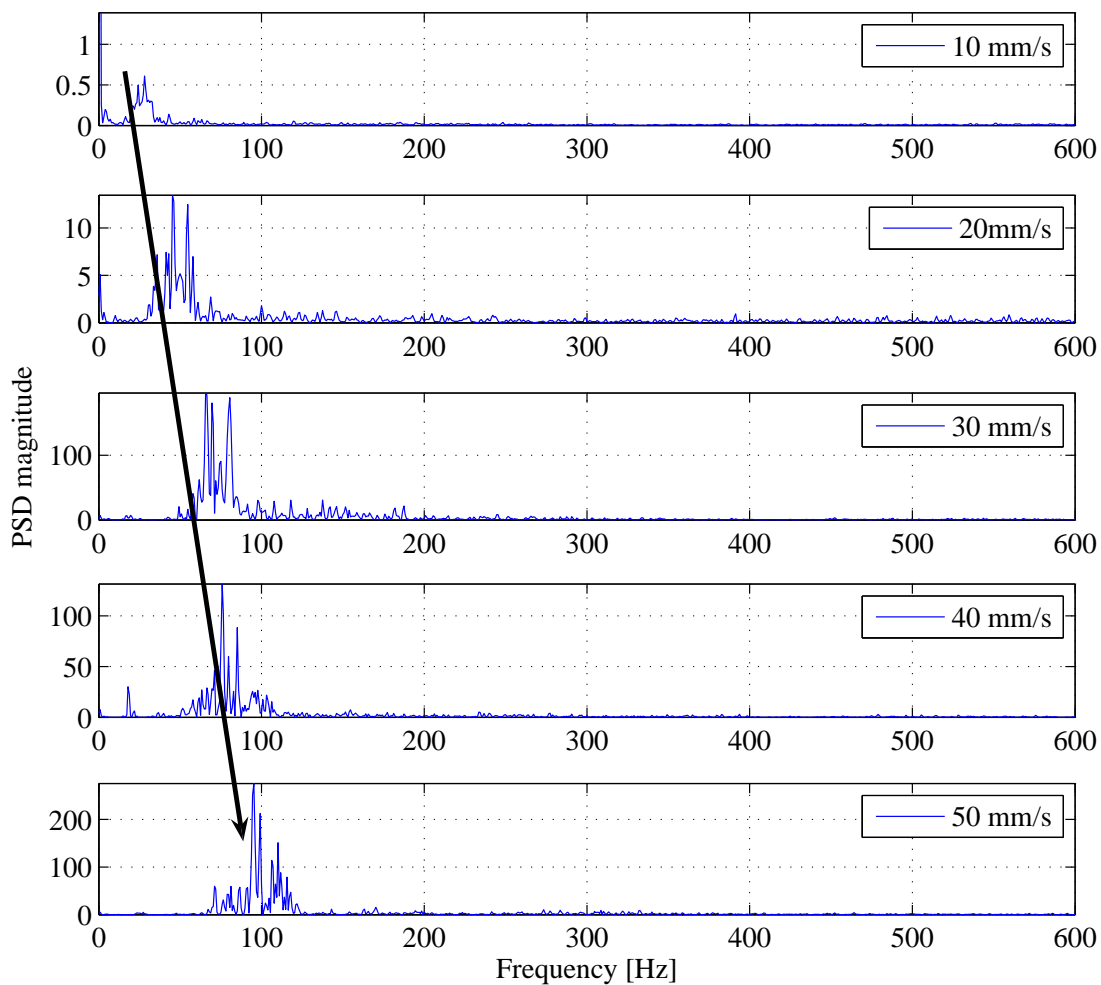
Figure 3.1: Example of the acceleration PSD for the signals obtained from the accelerometer employing a surface sample with periodical roughness. This sample has a roughness wavelength of 1.7 mm and a roughness mean value of 4.5 μm.

Figure 3.1 shows the Power Spectral Density (PSD) of the acceleration measured on the finger for different scanning speeds on the same roughness sample (R8). Increasing the scanning speed from v_1 (10 mm/s) to v_5 (50 mm/s), the distribution on the frequency spectra covers larger values. The same behavior can be found for different subjects (chapter 2) with some differences related to the frequency of the acceleration main peaks and to their magnitude, depending on the normal force applied from the subject, the skin characteristics and the finger ones (as discussed in the next paragraphs).

Considering roughness wavelengths and scanning speeds of everyday life touched objects, the frequency peaks of the measured vibration spectra, obtained from periodical roughness samples, stay in the frequency range expected from the literature that deals with the perception range of the mechanoreptors [2-500Hz].

The change of the spectrum characteristics in function of the driving parameters are described in the next sections. The test performed on periodic surfaces allows to understand the influence of different parameters on spectra. A second interesting step in this study is the investigation of the vibration spectra in the opposite limit case, i.e. without any periodic surface texture. To this aim, tests have been performed with surface samples having isotropic roughness, i.e. without any preferential direction.

Figure 3.2: Example of the acceleration PSD magnitude for the signals obtained from the accelerometer employing an isotropic surface sample with Ra 0.6 μm.
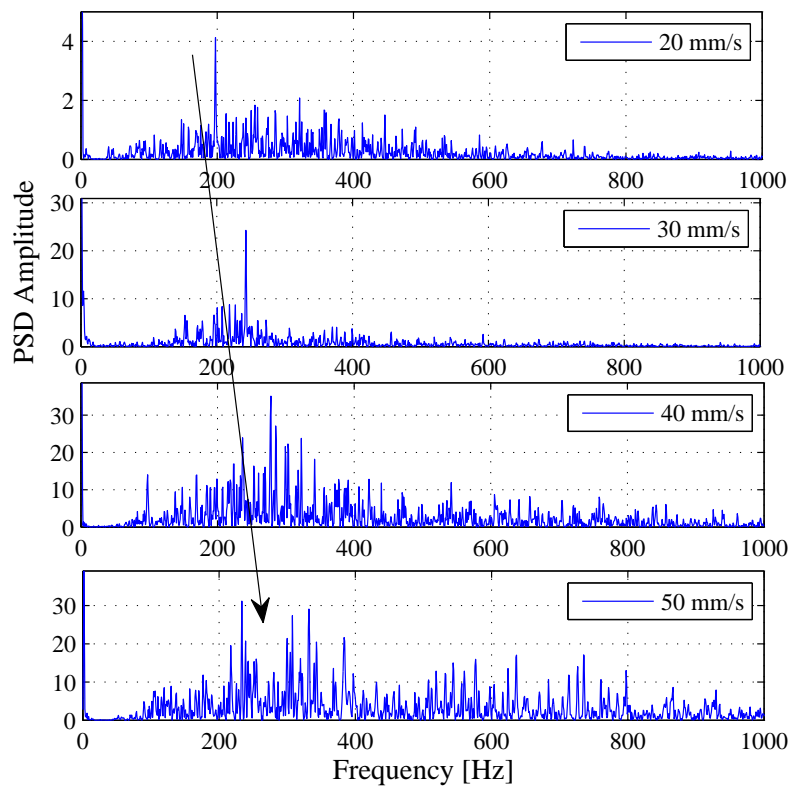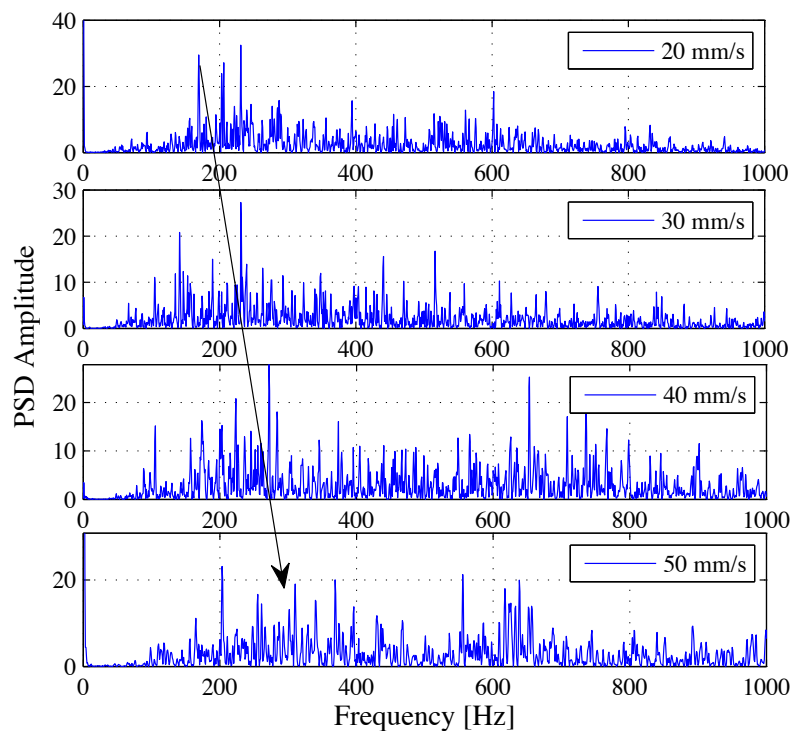

Figure 3.3: Example of the acceleration PSD magnitude for the signals obtained from the accelerometer employing an isotropic surface sample with Ra 1.6 μm.

Measurements of induced vibrations coming from the scanning between fingertip and isotropic roughness (Figure 3.2 and Figure 3.3) show as well that the induced vibration spectra cover the activation frequency range of the mechanoreceptors. In this case, the vibration spectra do not show a mean frequency peak, like for periodic roughness, because of the non periodicity of the employed surfaces. Nevertheless, like for the periodic roughness surfaces, from the obtained spectra it is possible to observe that, increasing the scanning speed, both the frequencies and the amplitudes of the induced vibrations increase.

The large frequency distribution characterizing the spectrum corresponding to isotropic roughness samples is limited by a maximal and a minimum frequency related respectively to the smaller sign impressed on the sample from the sand used for the sandblasting process and to fingerprint period.

3.3   Scanning speed and friction induced vibrations spectra

When dealing with samples that have periodic surface roughness, a well-defined peak in its vibration spectrum is measured [80]. The vibration frequency is a function of the scanning speed and of the relationship between the roughness spatial period (width) of the surface samples and of the fingerprint.

An experimental campaign has been developed with different subjects (different fingerprints) on periodic surface samples with different roughness spatial period. Each measurement has been repeated at different scanning speeds.

With respect to the effects of the scanning speed on the spectra obtained from the vibrations induced by the scanning on a surface with periodic roughness, Figure 3.4 shows the frequency peaks as a function of the speed for each roughness width for two different subjects: subject 1, a female 27 years old (fingerprint wavelength 0.45 mm) and subject 2, a male 32 years old (fingerprint wavelength 0.67 mm), respectively. The results are well reproducible and it can be asserted that the frequency peak value increases linearly with the increase of the scanning speed.

The frequency peaks can be linked to the theoretical frequency calculated as the ratio of the scanning speed and the roughness spatial period. To show this behavior, in Figure 3.5 there is the superposition of the vibration frequencies measured experimentally for the subject 2 (fingerprint wavelength 0.45 mm) when scanning the samples with roughness spatial period equal to 1.4 mm (stars) and 0.3 mm (circles), and the curve representing the frequencies calculated analytically as a ratio of the scanning speed and the roughness spatial periods. When the wavelength of the surface roughness (0.3 mm) is much smaller than the fingerprints wavelength (0.45 mm), the measured frequencies correspond to the analytical frequencies calculated with the surface roughness wavelength. On the contrary, when the surface roughness (1.4 mm) is much larger than the fingerprint spatial period (0.45 mm) the measured frequencies correspond to the analytical frequencies calculated considering the fingerprint period. The frequency of the scanning induced vibrations is related to the smaller roughness spatial period.

To investigate this phenomenon, the next section presents the vibration frequency peak as a function of the roughness period.
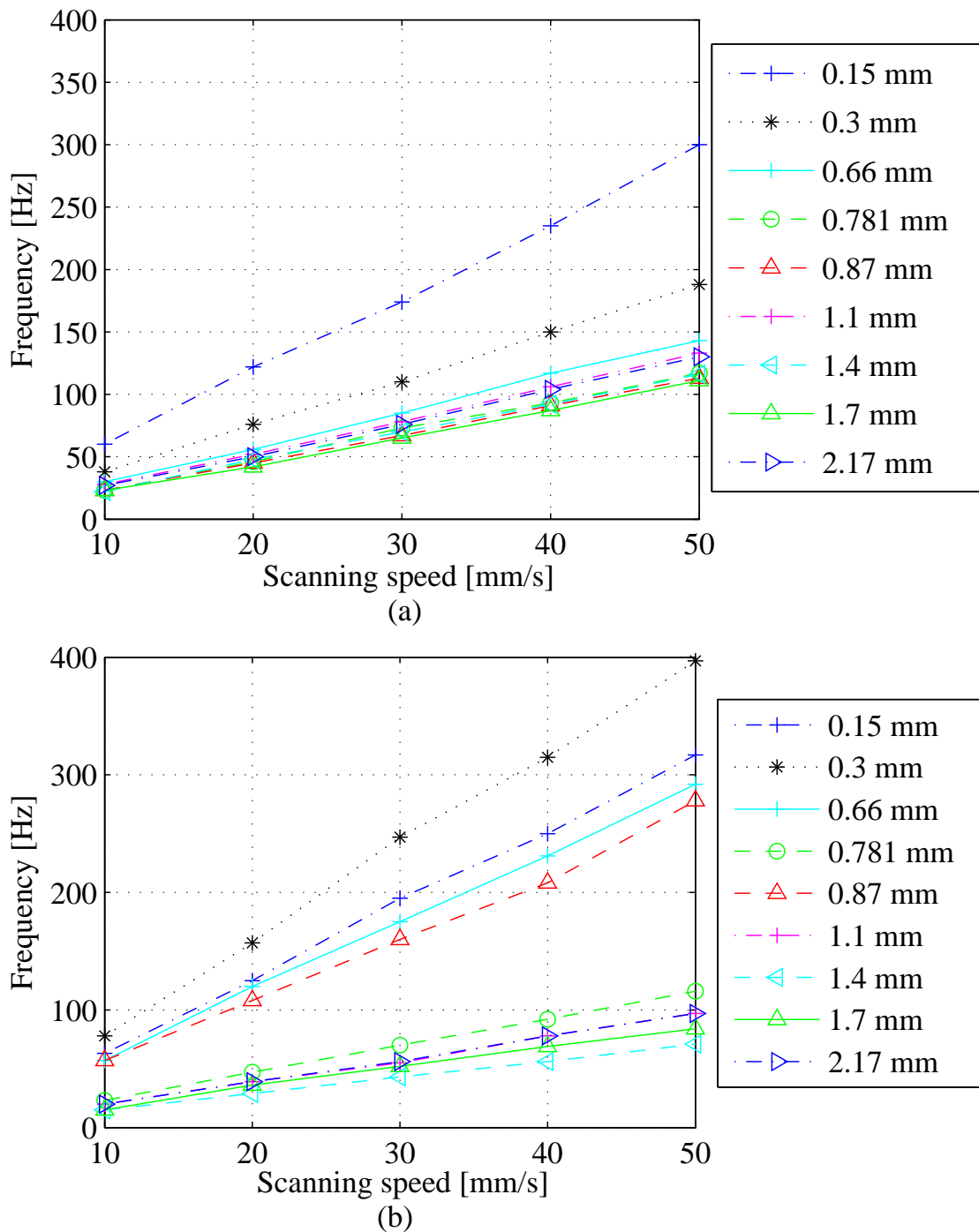
Figure 3.4: Relationship between the frequency main peaks and the scanning speed for different roughness samples: (a) subject 1, (b) subject 2.
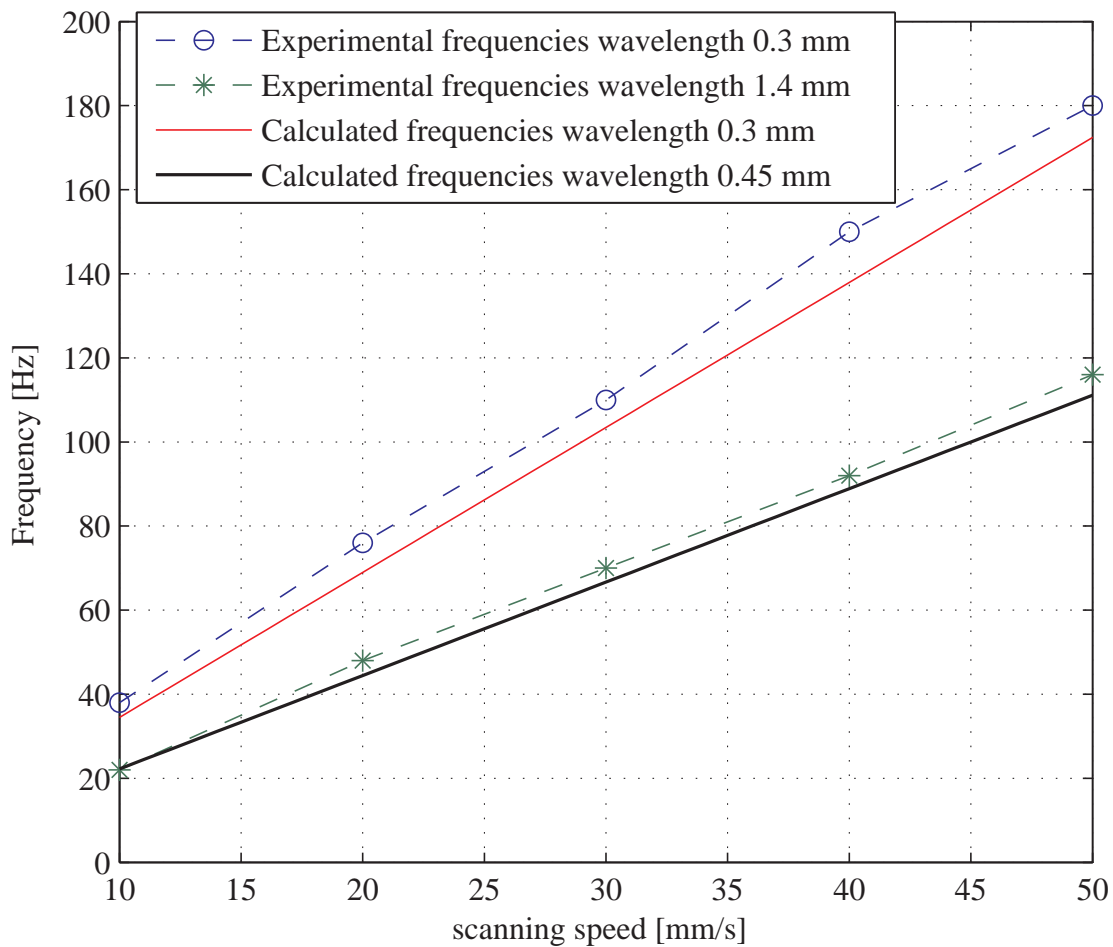
Figure 3.5: Comparison between experimental and analytical frequencies.

3.4   Surface roughness spatial period and friction induced vibrations spectra

With respect to the effects of the roughness spatial period on the spectra obtained from the vibrations induced by the scanning on a surface with periodic roughness, Figure 3.6 shows the frequency of main peak of the induced vibrations as a function of the sample roughness width, at each scanning speed, for the two subjects.

Figure 3.6 shows a non-linear dependence of the frequency peak with respect to the roughness width of the sample, which is due to the presence of the fingertip roughness. From the trend of the induced vibration peaks it is possible to distinguish three different zones in function of the fingerprint wavelength:

– ZONE I: the surface sample wavelength is smaller than the fingerprint one, and the frequency peak value depends primarily on the roughness wavelength of the sample. The same frequencies of the scanning induced vibrations were measured for the two subjects at each scanning speed.

– ZONE II: the surface sample wavelength is comparable with the fingerprint one, and the frequency peak is function of the ratio between the periods of the sample and of the fingerprint. Roughness samples having period equal to a multiple of

the fingertip roughness semi-period show higher frequencies [14]. This behavior is due to the excitation mechanism provided by the sliding between the two quasi-sinusoidal surfaces.

  – ZONE III: the surface sample wavelength is larger than the fingerprint one, and the frequency peak value depends primarily on the roughness period of the fingerprints. In ZONE III the measured frequencies are, for the same subject, almost constant for all the sample roughness. The vibration frequency is different for the two subjects, because of the different fingerprint period.

Figure 3.6: Relationship between the frequency main peaks and the roughness spatial period for different scanning speed: (a) subject 1; (b) subject 2.
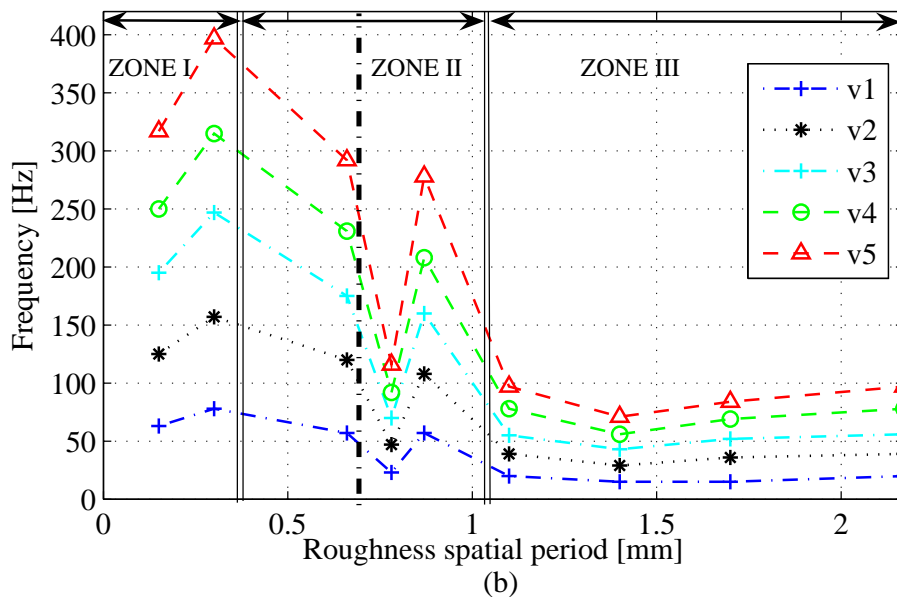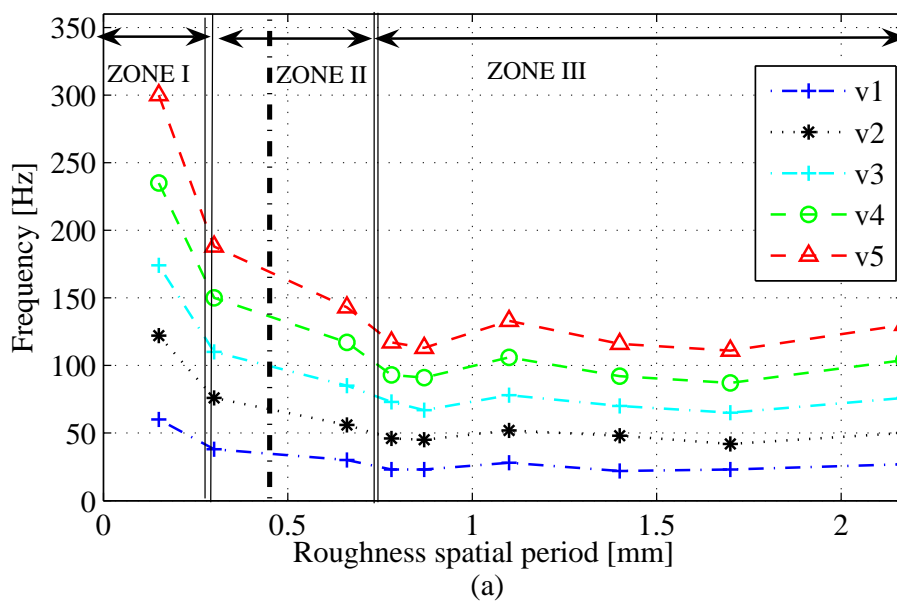
The same behavior was found for other subjects; nevertheless, even if the global trend of the spectra in function of roughness and scanning speed is the same, the values of the frequency peak and the slope of the curves shown in Figure 3.4 and in Figure 3.6 change because of the different finger and fingerprint characteristics, as shown in Figure 3.4(b) and Figure 3.6(b).

The presented results highlight two different perception mechanisms of the surface roughness as a function of the roughness period: while in ZONE I and ZONE II the spectra of the scanning induced vibrations are affected by the surface roughness, in ZONE III the spectra of the induced vibrations do not give information about the surface, because they are only function of the fingerprints width. During tests with samples in ZONE III subjects asserted to perceive the roughness sample as a spatial distribution of the contact pressure between the fingertip and the sample surface, but they could not perceive any difference on the local vibrations. On the contrary, when scanning surface samples of ZONE I and ZONE II, subjects could not perceive any information about the pressure spatial distribution, but they perceived the different roughness of the samples by the sensation of local vibrations at the fingertip/sample interface. These results agree with the duplex model of tactile perception highlighted by psychophysical and neurophysiologic studies [5, 10, 64], and described above.

Two different perception mechanisms are highlighted as a function of the surface texture and the vibration spectra: when the spatial period of the surface texture is smaller or comparable to the fingerprint one, it is perceived thanks to the vibrations induced by the finger scanning; when the texture roughness period is larger than the fingerprint one, it is perceived as a quasi-static pressure distribution on the fingertip surface. These results and the agreement with psychophysical and neurophysiologic analysis, reported in literature, show that the characteristics of the vibration spectra can result in important quantitative information (i.e. objective indexes) able to characterize qualitative features of the tactile perception, highlighting the possibility to develop further analysis focused on the objective characterization of tactile properties.

3.5   The effect of normal load on the induced vibration amplitude

Neurophysiologic and psychophysical studies assert that people can discriminate forms and textures of everyday objects with a high resolution, and that the tactile pattern recognition is independent of contact forces ranging from 0.2 to 1 N [15]. On the contrary, for higher force values, the normal load applied from the fingertip on the object surface influences the perceived roughness [11]; higher applied forces correspond to higher perceived roughness. This different behavior was attributed to both to the vibration magnitude increase and to the change of the contrasts in the roughness pattern in contact. In fact, increasing force, finger deformations rise modifying the contact area and the finger pattern.

In order to experimentally analyze and quantify the induced vibration frequency spectra with the normal load, tests involving the fake finger have been developed by scanning on a periodic roughness sample (wavelength 0.3 mm and mean roughness 11 μm) at three different scanning speeds (10 mm/s, 20 mm/s and 30 mm/s) for different loads, ranging from 0.1 to 1.8 N.

The choice of using the fake finger for this analysis is due to the fact that it assures

a perfectly constant contact force and allows for a slight force variation, thanks to the two screws permitting the vertical displacements of the fake finger support (Figure 2.12). Having a perfect constant load is not possible with the real finger because of involuntary movements of the finger and the hand of the subject. Nevertheless, some tests have been done employing the real finger as well, to verify the results obtained with the fake one and to get a reference curve.

Figure 3.7 collects the amplitude of the acceleration peaks in the FFT spectra, obtained at each scanning speed as a function of the contact load. The surface sample used for this analysis is the periodic one, with roughness width equal to 0.3 mm. The values corresponding to the fake finger measurements, indicated by markers, are joined by a line, the color of which indicates the relative scanning speed (blue line corresponds to 10 mm/s, the black line to 20 mm/s and the red line to 30 mm/s). The measurements on the real finger confirm the behavior obtained on the fake finger and are reported, on the same figure, by a marker in the same color of the corresponding fake finger test parameters. Even if the trend is the same obtained with the fake finger, the measurements made with the real finger show a less regular trend, which is due probably to the difficulty to have perfectly constant load.
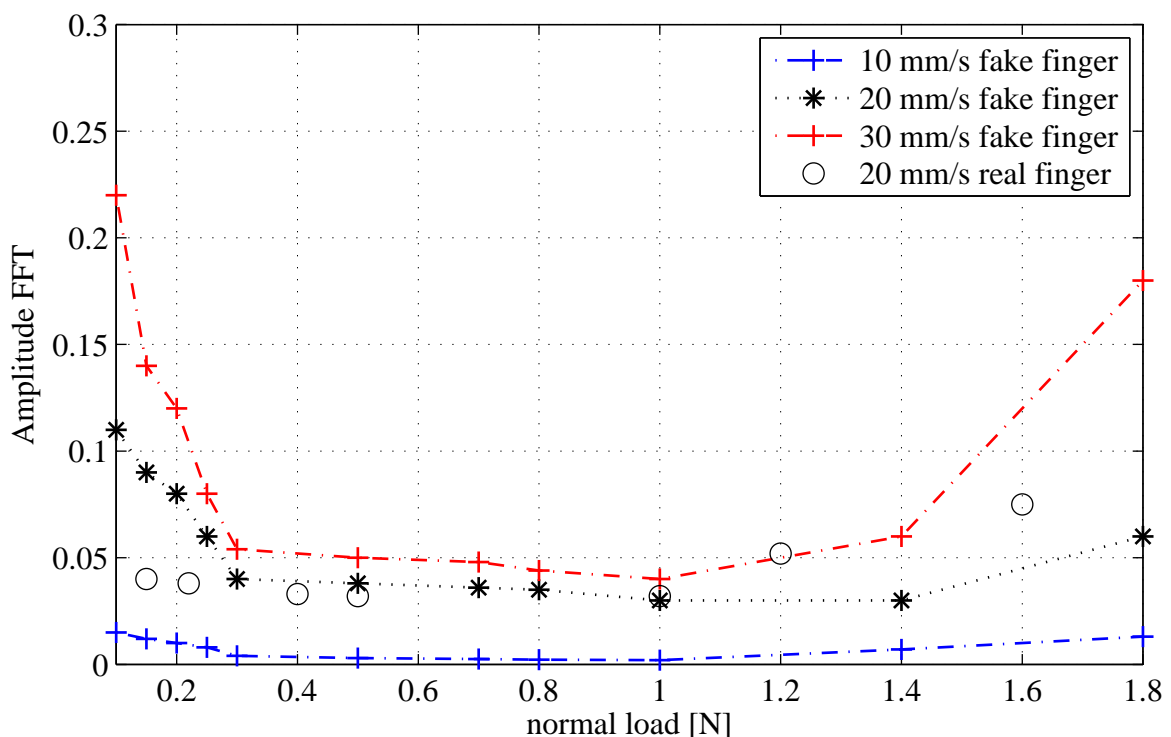
Figure 3.7: Relationship between the acceleration FFT magnitude and the normal applied load during the scanning. The surface sample has a roughness wavelength of 0.3 mm.

The obtained results agree with the neurophysiologic and psychophysical analysis [15, 11] presented in the literature: when the contact load is between 0.2N and 1N, the amplitude of the induced vibrations is almost constant for the same scanning speed; for larger values of the contact load the induced vibration amplitude increases affecting the roughness perception.

3.6   Friction induced vibration from the finger/fabric scanning

The quantification and the investigation of the perceived quality of a fabric are fundamental issues in textile industry. For this reason a particular focus is given to the scanning between finger and textiles. The analysis of the vibration spectra obtained when scanning textiles is more delicate because of the complexity of the surface roughness (texture and wire features), the non isotropic behavior of the material, and the compliance of the material that cannot be supposed rigid.

Figure 3.9 shows the spectra obtained scanning with the fingertip on a textile for two different values of the scanning speed; the frequency behavior is a combination of the two characteristic spectra described previously for periodic and isotropic surfaces. In fact, there are both a well defined frequency peak, characterizing surfaces with periodical roughness Figure 3.1 and Figure 2.3, and a larger frequency distribution, characteristic of the isotropic roughness surfaces Figure 3.2. These two components are always present in the spectrum obtained scanning on a fabric sample, but their contribution in the spectra depends on the structure of the textile (Figure 3.8). Specifically, the well defined frequency peak can be related to the periodicity of the fabric texture, while the larger frequency distribution is related to the roughness of the wires composing the texture. For the tissue showed in Figure 3.8 the texture width periodicity is 2.2 mm, which is greater than the fingerprint width and so, as expected, the frequency peak of the induced vibrations is the one calculated for the fingerprint width (Figure 3.4). Like for the periodical and random roughness surfaces, it is possible to observe that, increasing the scanning speed, the amplitude of the vibration increases and the induced vibrations move to higher frequencies.

Figure 3.8: Fabric texture. The texture period is 2.2 mm.
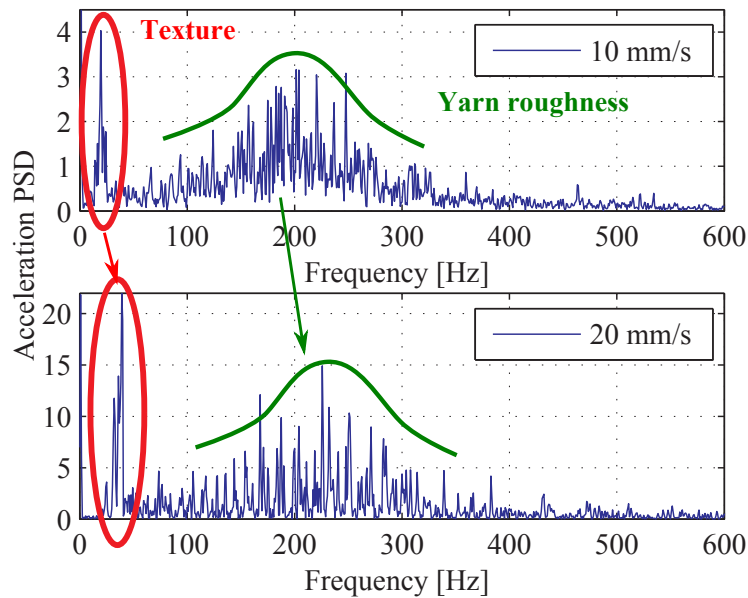
Figure 3.9: Example of the acceleration PSD for the signals obtained by the accelerometer employing the tissue sample in Figure 3.8.

I order to better understand the influence of the textile texture on the frequency distribution of the induced vibrations, some examples of fabrics are reported in the following figures. Figure 3.10 shows a fabric without a well defined periodic texture, which is constituted by long wires oriented without a preferential direction. The resulting spectrum of the induced vibrations is characterized by a large frequency distribution given by the yarns that provide an isotropic like roughness of the surface. In Figure 3.11 it is possible to recover as well the frequency peak due to the roughness of fingerprints; nevertheless, in this case this peak is not well distinguished from the rest of the spectrum, like for the scanning of periodic surfaces. In fact, the spectrum obtained from the scanning on the textile in Figure 3.10 shows comparable magnitudes for the frequency spectra given by the fingerprints period and the frequency distribution due to the yarn fabric.
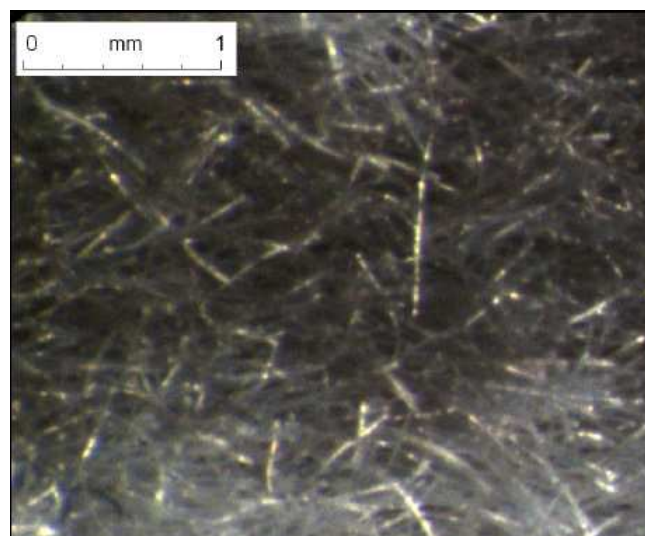
Figure 3.10: Example of fabric with a high hairiness and without a well defined texture.
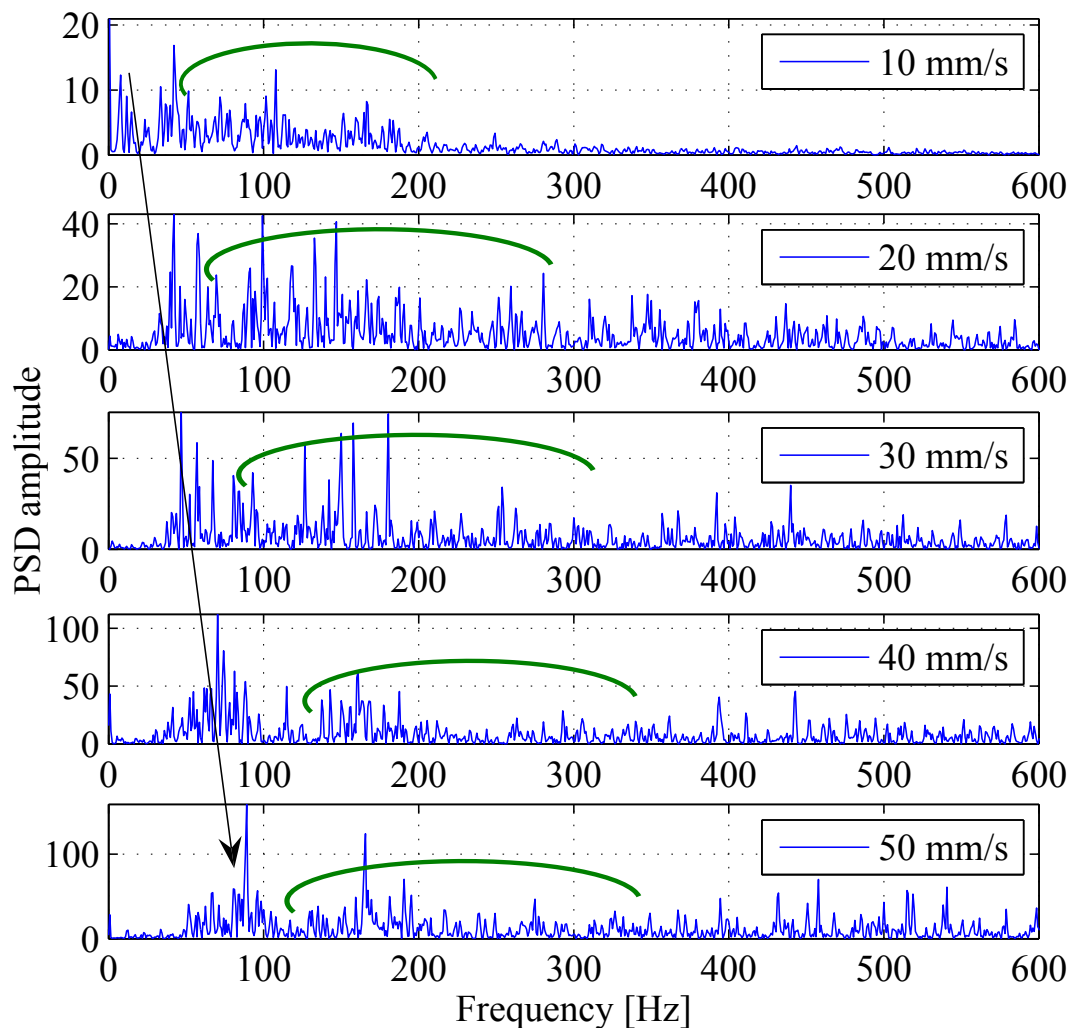
Figure 3.11: The acceleration PSD magnitude for the signals obtained from the accelerometer employing the tissue sample in Figure 3.10. The black arrow represents the position of the peak corresponding to the fingerprint period while the green curve covers the frequency distribution given by the yarn roughness.

Figure 3.12 and Figure 3.13 represent fabrics with a well defined and regular texture and with an high yarn compactness. The texture of these fabrics are characterized by two fundamental periods that are visible in the corresponding vibration spectra: each spectrum presents three main vibration peaks corresponding to the fingerprints period and the two texture periods (Figure 3.14 and Figure 3.15).

A different behavior of the amplitude of the peaks can be observed as a function of the scanning speed: while the peak amplitude due to the finer texture period (higher frequency) dominates for higher speeds, the amplitude of the vibrations due to the larger period (lower frequency) dominates for low scanning speeds. This different behavior could be ascribed to the accommodation of the textile fibers occurring during the scanning and changing the contact pattern. The frequency peak due to the fingerprints, which in this case are stiffer than the scanned surface, stays in the spectrum for all the scanning speeds. For these fabrics, the wires are rewound on themselves conferring a small yarn roughness to the fabrics as confirmed from low magnitude of the spectra frequency dis-

tribution, with respect to the frequency peak magnitude given by the fingerprints and texture periods.
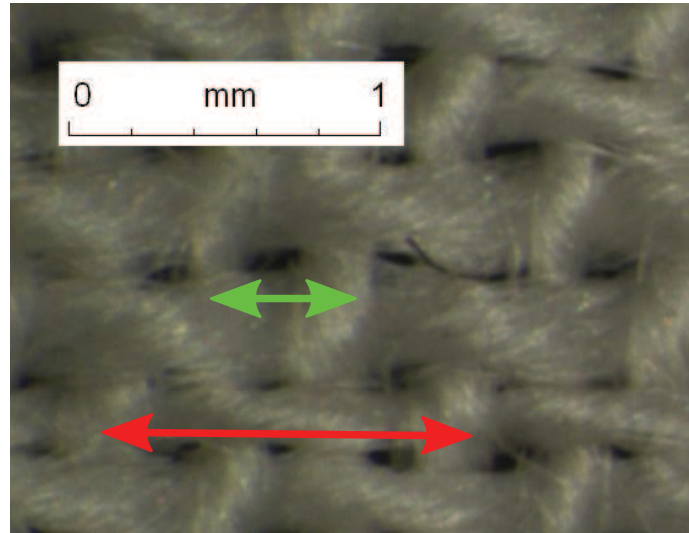
Figure 3.12: Example of fabric texture with two texture periods (highlighted by the red and the green arrows), one of 1 mm and the other of 0.42 mm width.
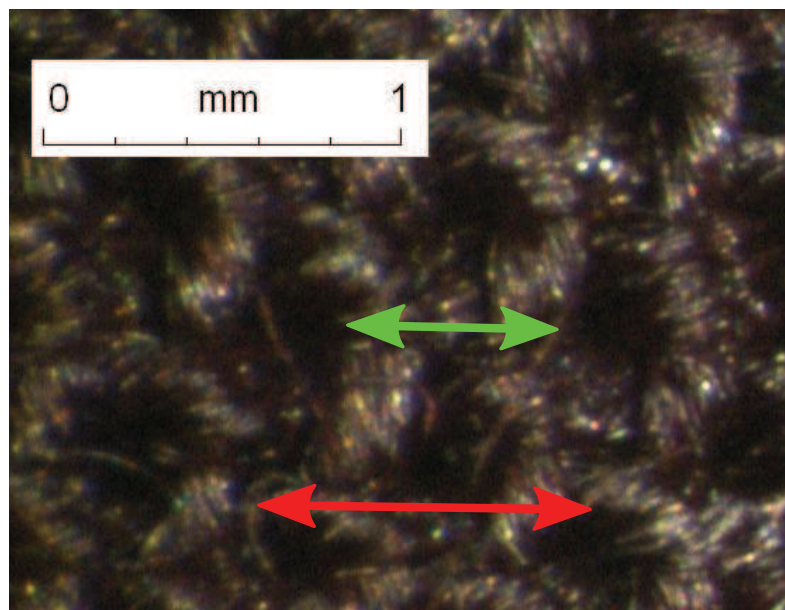
Figure 3.13: Second example of fabric texture with two roughness periods (highlighted by the red and the green arrows), one of 0.87 mm and the other of 0.5 mm.

The comparison of Figure 3.11, Figure 3.14 and Figure 3.15 suggest the possibility to distinguish the contribution of the yarn roughness and the texture periods in the vibration spectra form. It seems that, when the yarn roughness is dominant with respect to the texture periods, its contribution in the vibration spectra is larger and comparable in magnitude to the one given by the fingerprints period. On the contrary, its contribution on the vibration spectra is quite lower in Figure 3.14 and Figure 3.15 where the texture periods are dominant with respect to the yarn roughness. The shown features of the induced

vibration spectra, when scanning a textile, open a new interest domain of investigation to link the two components of the spectra with the quality perception when touching a textile.

Further investigations and statistical companions are needed to relate the spectra characteristics with the quality perception of a textile. In particular, the influence of the relative amplitude and position in frequency of the two spectrum contributions, and the influence of the textile accommodation on the scanning, need to be investigated.
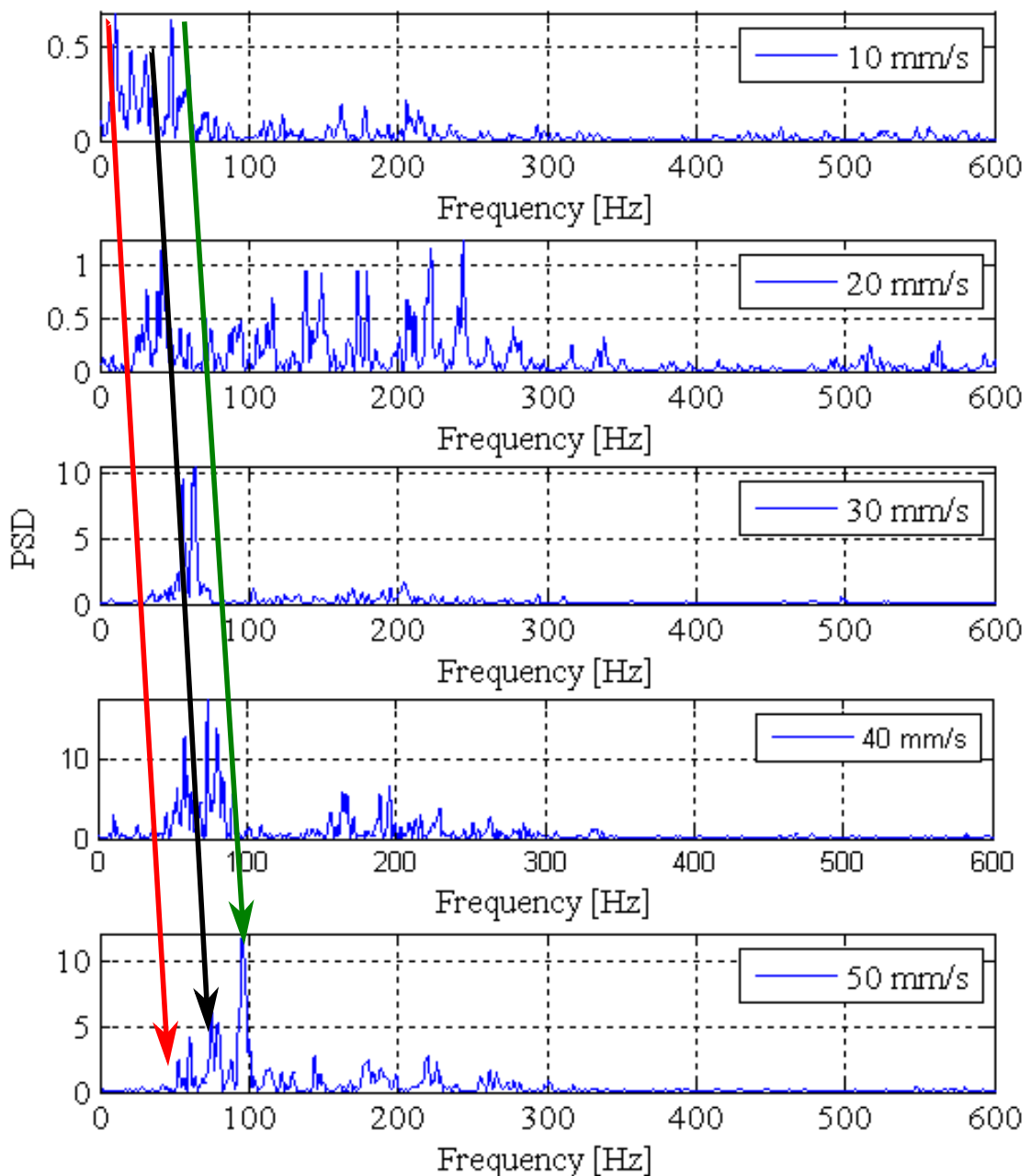
Figure 3.14: Acceleration PSD of the signals obtained from the accelerometer employing the tissue sample in Figure 3.12. The red arrow represents the position corresponding to the peak of the larger texture period, the black arrow is the finger one and the green arrow the smaller one.
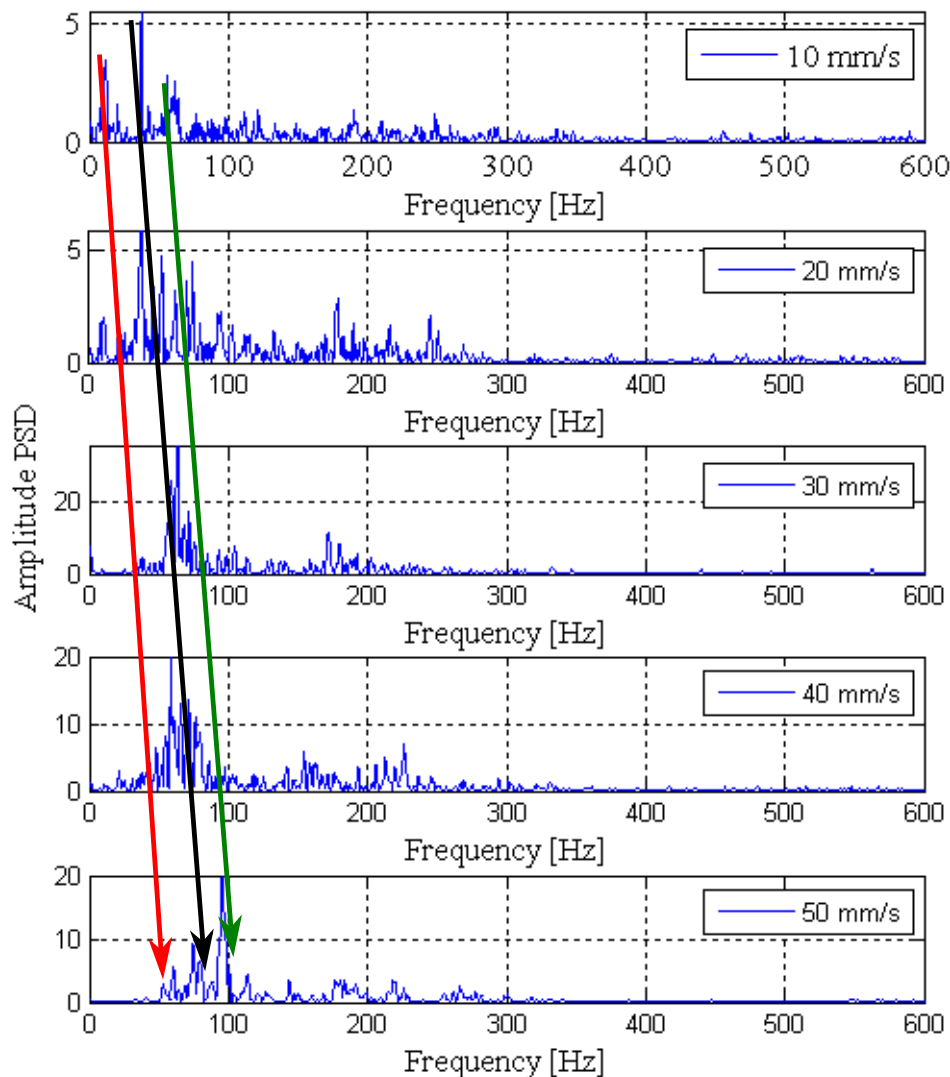
Figure 3.15: Acceleration PSD of the signals obtained from the accelerometer employing the tissue sample in Figure 3.13. The red arrow represents the position corresponding to the peak of the larger texture period, the black arrow is the finger one and the green arrow the smaller one.

3.7   Friction coefficient

The vibrations measured during the scanning of a finger on the object surface are originated by the sliding of the two surfaces in contact; while the frequency spectrum distributions are mainly determinate by the relative geometry of the two contact surfaces and the contact parameters, like scanning speed or mutual compliance. A major parameter effecting the amplitude of the induced vibration is the friction coefficient. Higher magnitude of friction forces corresponds to higher energy transferred to the generated acoustic field. For this reason a particular attention has been focused on the detection of the friction coefficient between fingertip and the tested surfaces. As described in chapter 2, the TriboTouch system is able to detect, during the contact, the normal (N) and tangential (T) loads by means of the triaxial force transducers, allowing for determining the

friction coefficient (μ) as their ratio:

$$\mu = \frac{T}{N} \tag{3.1}$$

With respect to the contact between finger and sample surface, tests have been performed to characterize the friction coefficient and its changes as a function of scanning speed and normal load, for the scanning on both aluminium samples and textiles. The skin is investigated in untreated conditions, meaning that the finger is cleaned with alcohol and dried, before each measure, so that the measured friction coefficient reflects comparable skin hydration state and lipid concentration.

Figure 3.16 shows an example of the friction coefficient obtained scanning the finger on the same aluminium surface sample (periodic roughness of period 0.3 mm and mean roughness of 4 μ) as a function of the applied load and for different scanning speed. The friction coefficient decreases when the contact force increases, highlighting that the skin/surface contact does not adhere to the Amonton's law [47] (because the skin relief deformations are mainly elastic, and increasing the load, these deformations rise until the relief is completely deformed and the contact area approximates to the contact of a large single relief [44, 4, 20]).
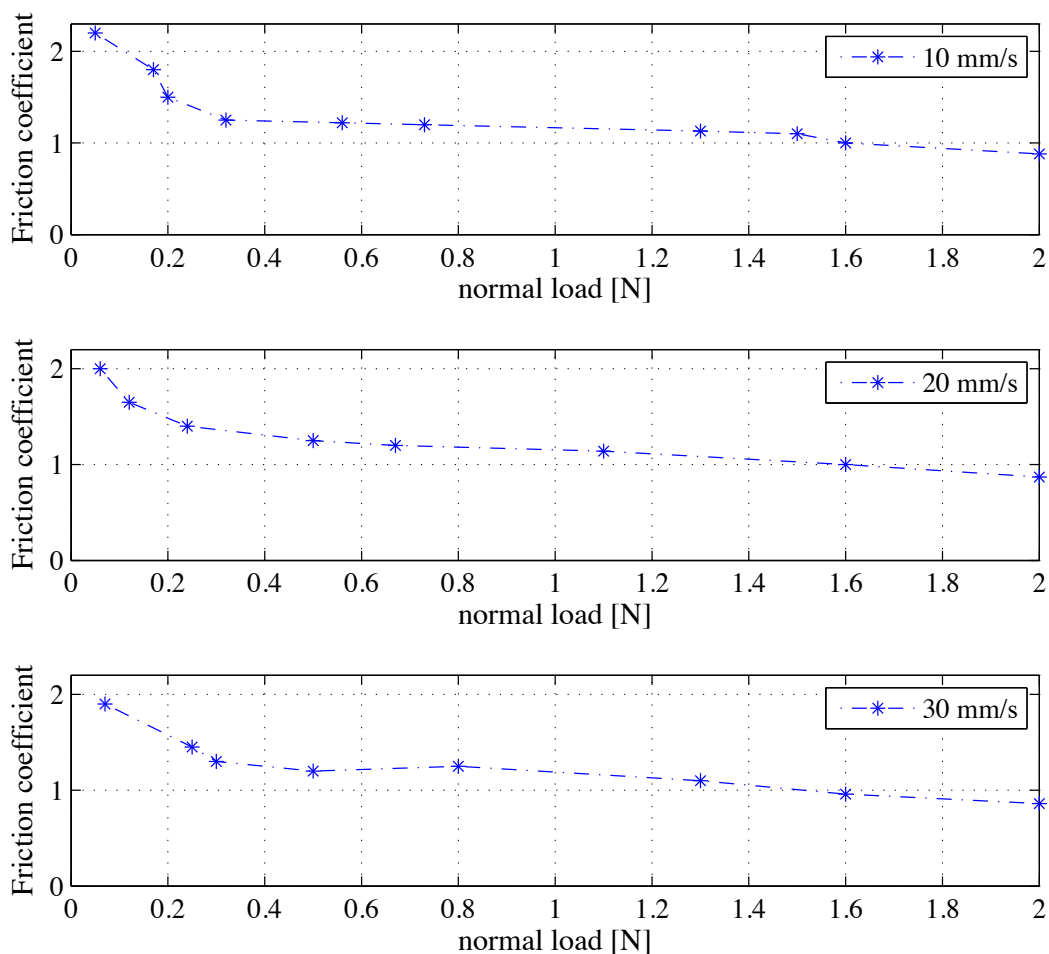

Figure 3.16: Normal load and scanning speed effects on the real finger friction coefficient on an aluminium sample.

Several authors [2, 1, 21, 20, 44, 54] have developed skin friction analysis supporting the Wolfram theory for a sliding surface on a distorting one (developed on the basis of Hertz contact model to account for the adhesion that mainly affects the skin friction), that allows for calculating the friction coefficient as:

$$\{\mu\} \propto S(\frac{K}{E})^{\frac{2}{3}} N^{-\frac{1}{3}} \tag{3.2}$$

where N is the applied load, E is Young's modulus of the skin, K is a colligative term including average dimension of adhesive contacts, their number, and frequency per unit areas, and S is the shear strength of the adhesive contacts.

These experimental studies, very consistent with the adhesion model, show little variation in the load power value, related to the experimental conditions and the body site where the skin is analyzed. Specifically, the Wolfram theory suggests that μ is proportional to $N^{-0.33}$ while e.g. [21] found out a dependence on $N^{-0.32}$ for middle finger hairy skin and [44] on $N^{-0.28}$ for forearm skin.

The presented results (Figure 3.16) show a proportionality of the friction coefficient to a power of the normal load varying from -0.27 (for a scanning speed of 10 mm/s) to -0.25 (for a scanning speed of 30 mm/s), for the glabrous skin of the right hand index finger, in agreement with the Wolfram theory.

Figure 3.17 and Figure 3.18 show the friction coefficient as a function of the scanning speed when the finger scans respectively on fabrics with a well defined texture periodicity and small yarn roughness, and on fabrics with high hairiness.

Regarding the effect of the scanning speed effects on the friction coefficient, from the comparison between Figure 3.16 (friction coefficient obtained scanning on the same aluminium surface sample), Figure 3.17 and Figure 3.18 (representing the values obtained from the scanning on fabrics with different speed but same normal force) it is possible to assert that in every case the friction coefficient tends to decrease with the increasing of the scanning speed.
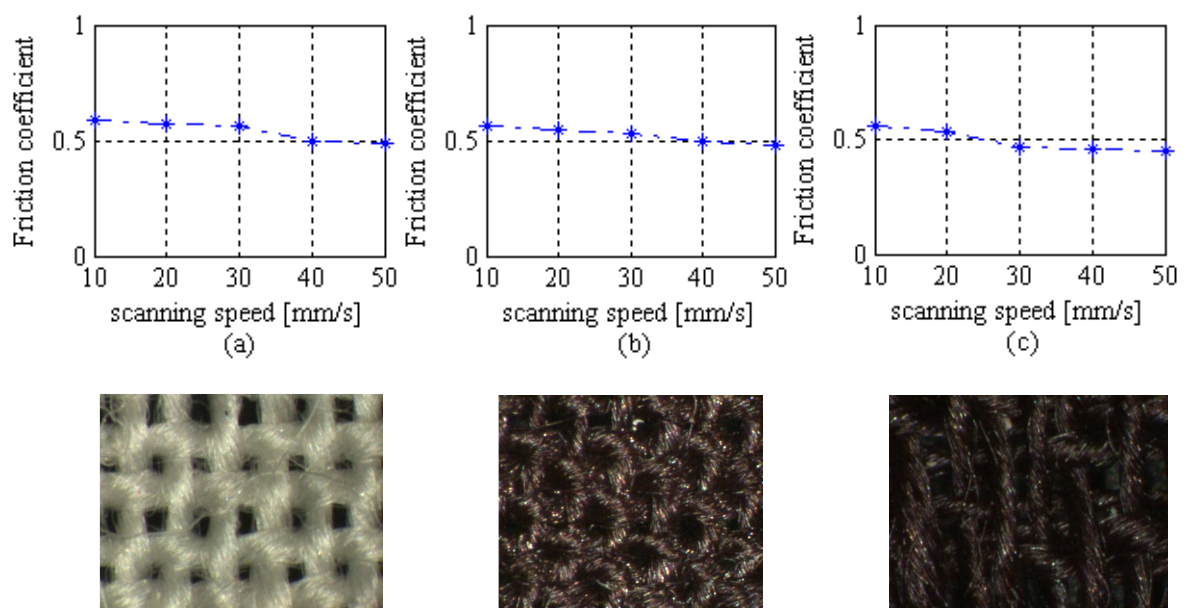

Figure 3.17: Scanning speed effects on the friction coefficient between finger and fabric samples with regular texture. The fabric figures are in scale 13:1.
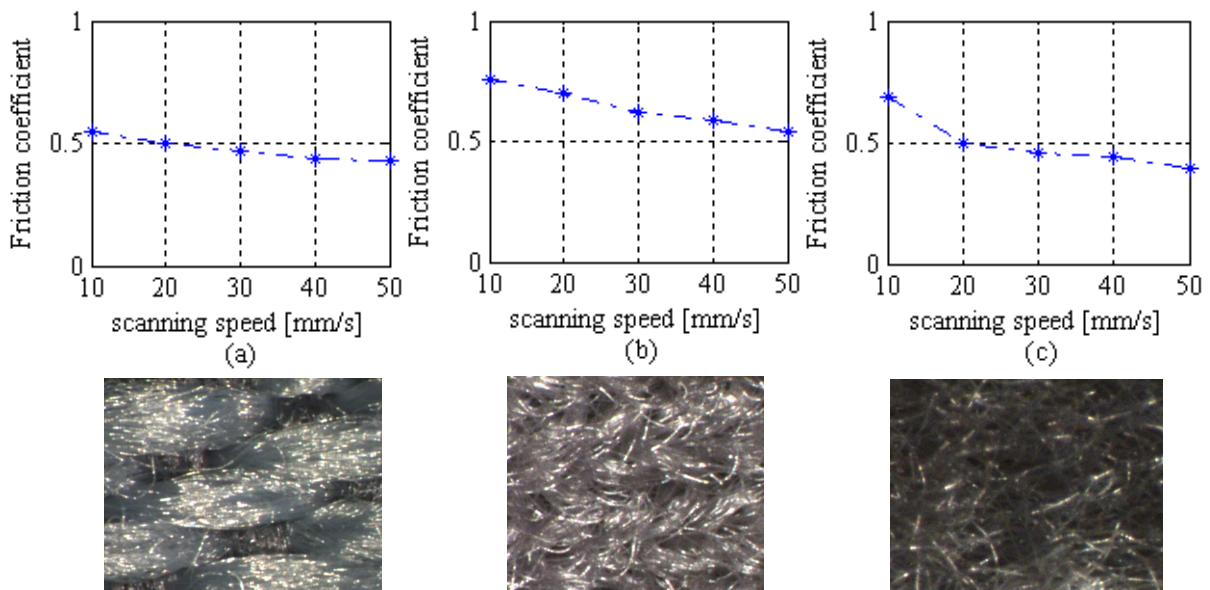
Figure 3.18: Scanning speed effects on the friction coefficient between finger and fabric samples without a regular texture and with a high hairiness. The fabric figures are in scale 13:1.

The friction coefficient decrease occurs in a different manner depending on the surface sample: the decrease is slight for the rigid aluminium sample, while it becomes significant for textiles. When dealing with textile, the decrease seems to be affected by the fabric yarn characteristics: higher hairiness corresponds to higher variations of the friction coefficient with the scanning speed(as shown from the increasing hairiness of the tissues (a), (b) and (c) in Figure 3.18). This different friction behavior is probably due to the fact that, when scanning on a rigid sample, the slight variation of the friction coefficient is due mainly to the finger compliance, while with textiles it is necessary to account for the textile compliance and accommodation phenomena. The aluminium-skin friction is minimally affected by speed changes and the observed small variation are related mainly to the decrease of the skin viscosity with the increasing of the shear rate at cause of natural skin lipid film and hydration [1]. For the tissue-skin contact, the yarn deformations play an important role in the friction process changing the contact area and characteristics. The same friction tests, presented above, have been performed with the silicone fake finger. In fact, if the obtained results on real finger friction coefficient are consistent with the adhesion model, generally accepted for the skin, the frictional features of the polymer, treated with lubricant oil (vaseline) for reproducing the effect of human sebum, have to be verified.

Figure 3.19 shows an example of the friction coefficient values obtained when the silicone finger scans on a aluminium surface sample (periodic roughness of period 0.3 mm and mean roughness of 4 μm). The trend of the friction coefficient with respect to the normal load is very close to the real skin one. This is due to the polymer viscoelastic properties and to the hydration introduced by lubricant oil. In fact, to reduce the silicone adhesion (highlighted from preliminary tests) it has been decided to exploit the polymer permeability treating the finger model with oil. In this way, it is possible to obtain a contact behavior closer to the real finger one (as explained in chapter 2). The process is not permanent and it is necessary to repeat the bath avoiding the progressive finger dryness and ensuring the measurements reproducibility (mainly for the lubricant that remains on the finger surface). The quantity of absorbed oil depends on the bath time.

Controlling the time of permanence of the polymer in the oil bath, it is possible to modify the resulting frictional coefficient.
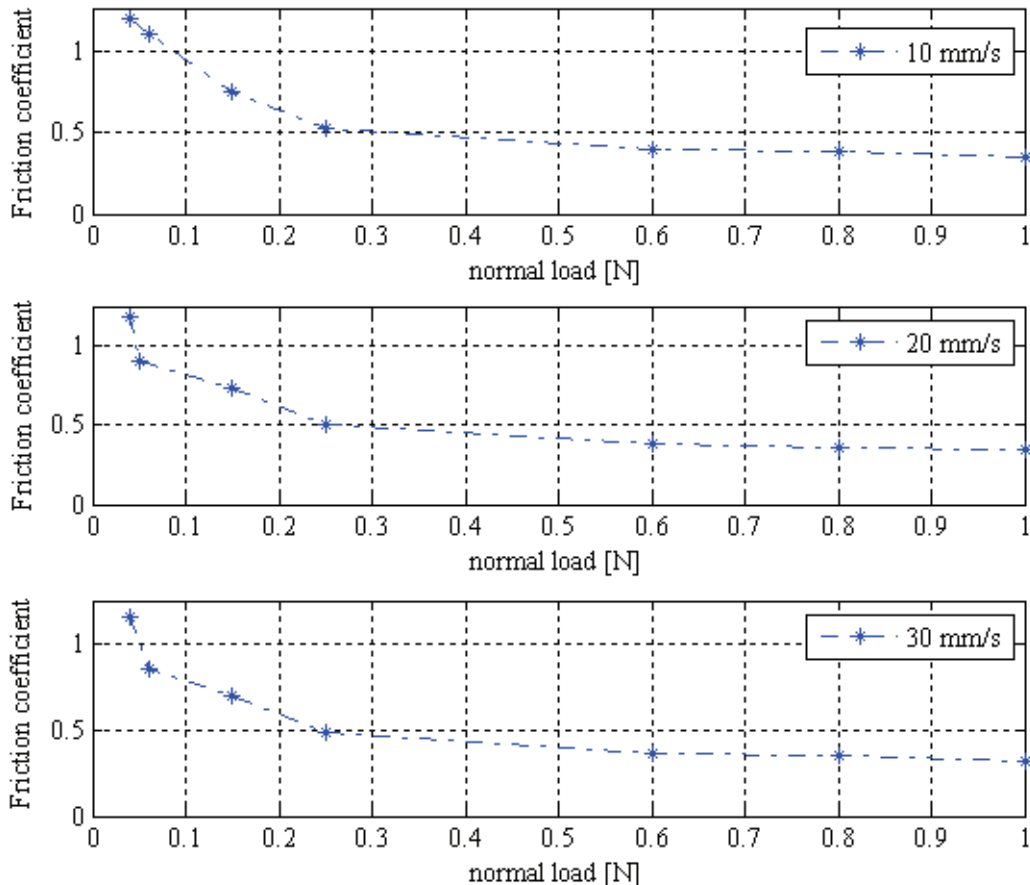
Figure 3.19: Normal load and scanning speed effects on the silicone finger model friction coefficient on an aluminium sample.

For example, in Figure 3.20 is shown a comparison between the friction coefficient obtained scanning on a surface aluminium sample with the silicone finger that has been treated with a different time of oil bath. The first test was made with an oil bath of one day and leaving the fingertip on a paper for five hours to eliminate oil excess on the finger surface (Figure 3.20(a)). The second test, in the same scanning conditions, was made with the fake finger treated in the same manner but for a permanence in the bath oil of five days (Figure 3.20(b)). For the same contact load (0.25 N) the polymer that has remained longer in oil bath shows a lower friction coefficient. Moreover, its decreasing trend with the increase of the scanning speed is stronger than the one obtained with the finger model treated just for one day on the oil bath.

The first treatment (one hour of oil bath) allows to reproduce the friction coefficient obtained with the real finger, and it is the one adopted for the tests made with the fake finger. Anyway, during tests, the friction coefficient is always monitored to verify the stability of the treatment with the lubricant oil during the duration of the tests.
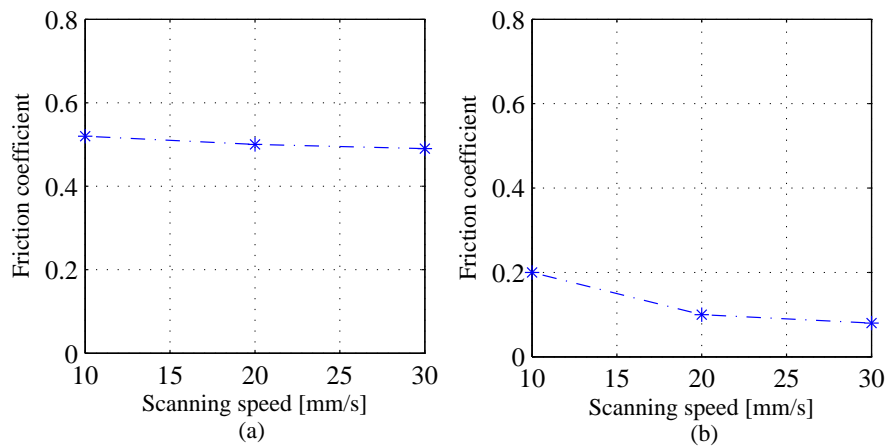
Figure 3.20: Lubricant oil effect on the silicone finger model friction coefficient on an aluminium sample, for a permanence time in oil bath of 1 day (a), and of 5 days (b) and a contact load of 0.25 N.

3.8 Concluding remarks

The TriboTouch set-up has been used to develop an experimental investigation on the effects of the contact load, scanning speed and surface roughness characteristics on the spectra of the vibration induced by the scanning. To cover a wide range of surface features, with respect to the everyday object features, both rigid samples with periodical and random roughness and fabric samples have been retained for the investigation. The results obtained by the analysis of the vibration spectra agree with the neurophysiological and psychophysical works present into the literature and highlight the main role of the fingerprints on the tactile perception. The coherence between the objective data and subjective analysis suggests the possibility to objectively quantify the tactile perception of a surface. The experimental results show also a good agreement of the fake finger dynamic behavior with the real one, suggesting the possibility to measure the local vibrations employing the fake finger. Finally, the tests allowed for measuring the macroscopic friction coefficient and its dependence on normal load and scanning speed. A further analysis is needed to account for different parameters: materials stiffness (e.g. by molding the same surface with polymers of different stiffness), scanning direction (e.g. by controlling the angle between the surface and the finger), etc. A statistical analysis on a representative sample of human subjects have to be carried out to link the perceived surface features with the vibration spectra.

Chapter 4

Numerical simulation of the finger/surface scanning

The experimental tests presented in the previous sections show how the spectra of the vibrations measured at the finger nail can be related to the surface characteristics and to the scanning and contact parameters. Nevertheless, the measured vibrations are representative of the global vibration of the finger, i.e. they have been modified (filtered, damped) by the finger material and can differ from the vibrations induced at the local contact zone between the fingertip and the object surface, where the mechanoreceptors are located (a maximum depth, under the epidermis, of about 2 mm). Because the aim of this work is to relate the surface object characteristics with the tactile perception through the induced vibrations, which are perceived by the mechanoreceptors, it is necessary to investigate the local vibrations at the contact; this analysis is needed to verify the representativeness of the measured global vibrations at the fingernail and to investigate the influence of local parameters as the contact pressure distribution on the fingertip. A first attempt, aimed to have more representative vibration spectra at the contact zone, is made through the measurement of the finger transfer function that allows accounting for the effect of the finger material and structure. The finger transfer function (paragraph 2.2) shows an almost linear behavior between 2 and 500 Hz, corresponding to the mechanoreceptors activation range. Thus, it seems that the finger dynamic response does not modify the vibration frequency distribution; nevertheless, the amplitude and the distribution of the local vibrations can't be accounted for by the use of the transfer function. Moreover, it is impossible to measure the vibrations at the contact surface without introducing invasive transducers that would affect the contact itself. For this reason it is necessary to develop a numerical model able to simulate the finger/surface scanning. With this aim, the numerical model has to be able to reproduce both the local and global dynamics; the global measurements at the fingernail can be used for validating the simulations, which will be used for investigating the local dynamics at the contact.

First a simple numerical model reproducing the sliding between two sinusoidal surfaces has been developed(paragraph 4.1) for investigating the only effect of the roughness width; the aim is to highlight whether the trend of the induced frequency peaks as a function of the roughness sample, and the consequent "duplex perception model", can be attributed to the fingerprint roughness width.

Then, a 2D finite element model (presented in paragraph 4.2) has been developed for a first attempt to simulate the scanning of the fake finger on a surface; an explicit dynamic code, PLASTD, for transient simulation of contact problems between deformable bodies

has been used. The model reproduces the experimental tests, calculating the global dynamics to compare with the experimental results, and computes the local behavior at the contact surfaces.

4.1 Simplified numerical model

4.1.1 Modeling sinusoidal sliding surfaces

A first simplified model has been developed with Matlab to reproduce the vibrations induced by the contact between two sinusoidal surfaces as a function of the roughness wavelength, for different scanning speeds; the material and contact properties and the system geometry are not accounted for by the model.

Both the fingerprint and the surface sample are modeled as sinusoids. The roughness sinusoidal profiles are created using the wavelength and roughness arithmetic mean values of the periodical surface samples used for the experimental tests. The model simulates the relative motion, at a constant speed, of the sinusoid representing the fingerprint with respect to the sample sinusoid. The surfaces are considered as rigid and no material is introduced. The compliance of the finger (with respect to the aluminum) and its local deformation (which is directly linked to the local vibration) is approximated by the intersection areas of the two sinusoids. The global vibration signal is calculated as the integral of the interpenetration areas between the two surfaces (red area in Figure 4.1). The hypothesis retained by this model is that at each intersection between fingerprint and sample roughness, the skin "adapts" its geometry to follow the roughness profile, and that the measured global vibrations are the sum of the local deformations at the contact. Obviously this model is not able to reproduce the amplitude of vibration, which is related to the contact and material properties, but can be used for predicting the frequencies of the induced vibrations.

Two formulations of the simplified model are compared. A preliminary model (model I) accounts for a punctual contact between the finger and the surface sample; in this case the intersection areas are not integrated, but only the distance between the closest pair of points belonging to the two sinusoids is considered, at each time step. The second model (model II), as explained above, accounts for the contact distribution by integrating the intersection areas at each time step of the simulation. In consequence, the model II sums the contribution of several points of contact, corresponding to the intersection areas between finger and surface sample, for calculating the global vibration signal.

With both the models, the sliding contact between the finger and the nine surface samples with periodical roughness employed in the experimental measurements has been simulated for five different scanning speeds (10 mm/s, 20 mm/s, 30 mm/s, 40 mm/s, 50 mm/s).
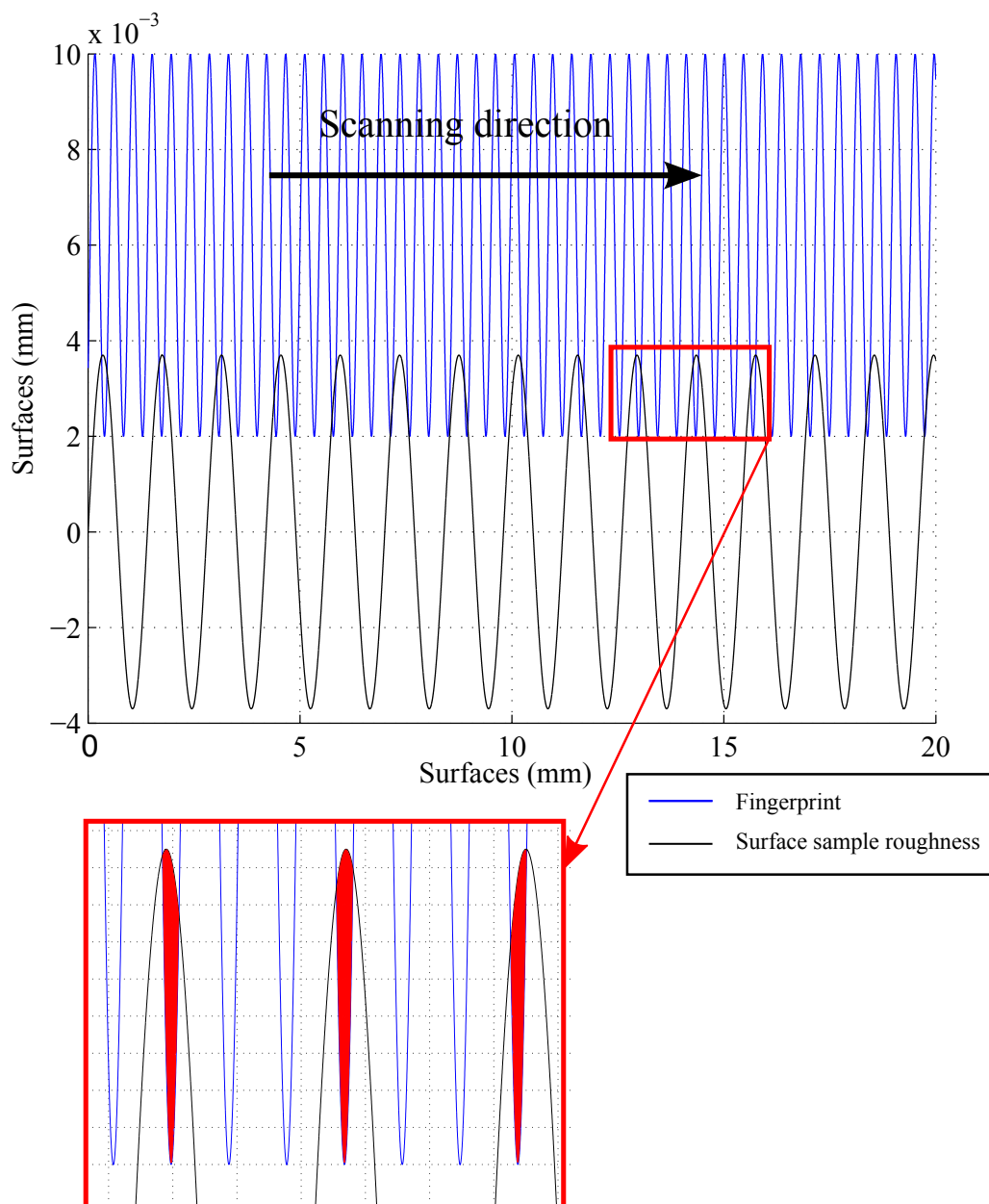
Figure 4.1: Example of the simulated contact between the two sinusoids.

4.1.2 Comparison between the numerical and experimental results

It is possible to compare the numerical results with the experimental ones on the relationship between the frequency of the induced vibration peaks and the sample roughness wavelength for the different scanning speeds.

Figure 4.2 shows the plots of the frequencies obtained with the model I, while Figure 4.3 represents the results given by the model II and finally Figure 4.4 shows the experimental results already described in section 3.4.

For both the models, the graphic of the frequency peaks as a function of the roughness wavelength has been divided into three zones, like for the experimental results: a first zone where the surface wavelength is smaller than the fingerprint one, and the frequency peak value is determined by the surface roughness period; a transition zone

where the two wavelength are comparable and the frequency peak is function of the ratio between the wavelengths of the sample and the fingerprint; a last zone where the fingerprint wavelength is smaller than the surface one, and the frequency value is due to the fingerprint period (chapter 3).

Figure 4.2: Relationship between the frequency main peaks and the scanning speed for different roughness samples obtained from the model I.

Figure 4.3: Relationship between the frequency main peaks and the scanning speed for different roughness samples obtained from the model II.

Figure 4.4: Relationship between the frequency main peaks and the scanning speed for different roughness samples obtained from the experimental results.

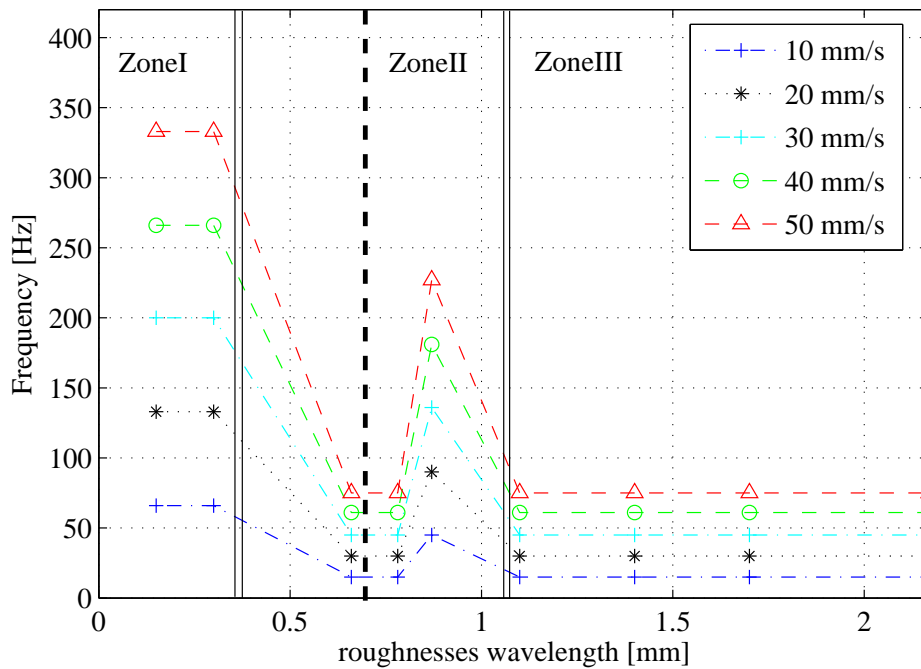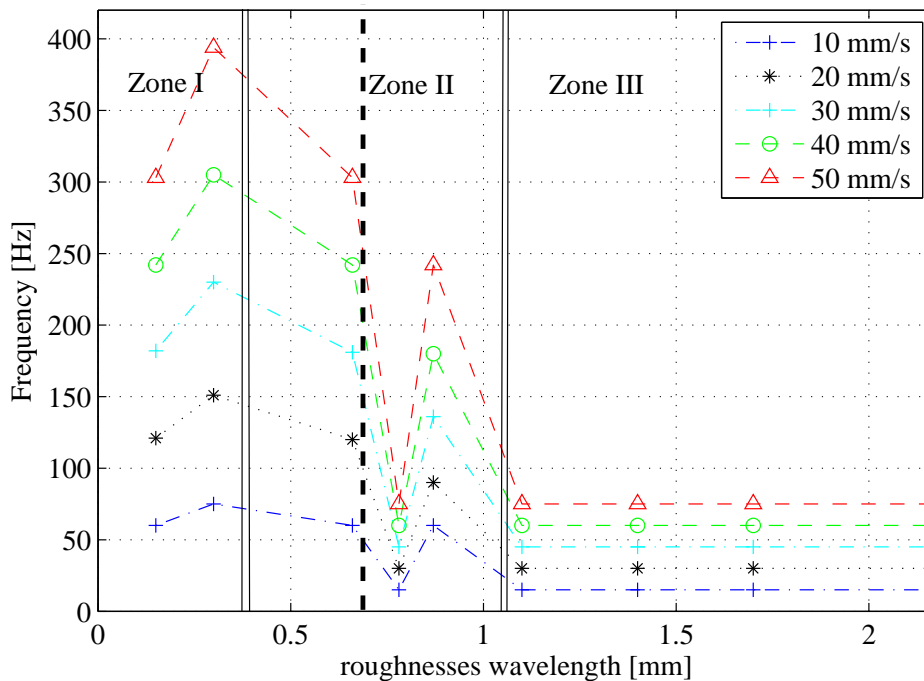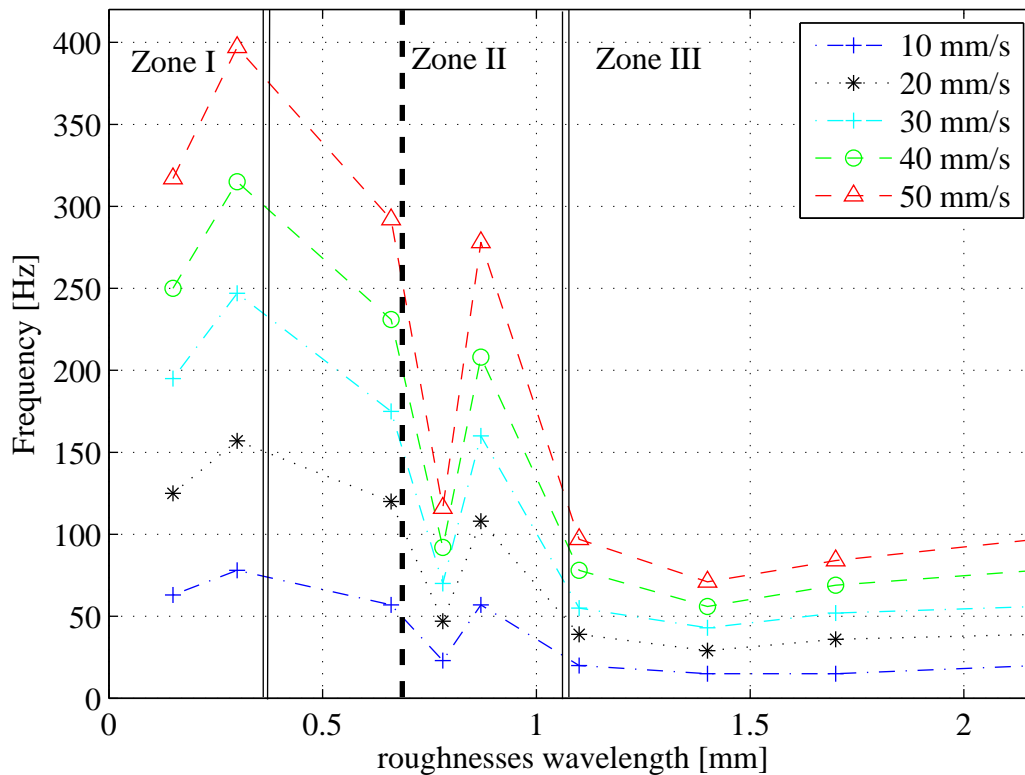Comparing Figure 4.2 and Figure 4.4 it is possible to see that even if there is a correspondence between the three zones of the frequency peak trends, model I does not allow for making distinction between different samples falling in the same zone. For example, no difference, in the frequency peak value, is found between the sample with roughness wavelength 0.15 mm and the one with wavelength 0.3 mm (Zone I). This divergence with the experimental results suggests that the signal generated from a single point of contact is not sufficient to reproduce the acceleration frequencies measured at the fingernail during the scanning.

The results obtained with model II, on the contrary (Figure 4.3), are well comparable with the experimental ones (Figure 4.4). The frequency trend is the same in both cases for each scanning speed, with the presence of the three main zones distinguished in function of the relationship between the wavelength of the surface sample and of the fingerprint one. The found frequency peaks are very similar to the experimental ones even if the real fingerprints and the sample roughness are not perfectly sinusoidal.

Thus, model II allows for confirming the experimental trend of the frequency peaks with respect to the fingerprints and the scanning speed, highlighting the role of the fingerprints in the tactile perception mechanism. The agreement between the experimental results and the results from the simplified model, which accounts only for the mutual periodicity of the fingerprints and sample surfaces, allows for asserting that the frequency information perceived by the mechanoreceptors is mainly function of the roughness profile and the filtering effect of the fingerprints.

On the other hand, this simplified numerical model does not give any information about the vibration amplitude because no material or contact properties are kept into account.

4.2   Finite element model

In order to account for material and contact properties, and to simulate the local dynamics at the contact, a finite element model of the finger has been developed is realized with the code PLASTD. This program, developed at the LaMCoS, allows for running mechanic, thermal and thermomechanic simulations. It is based on an explicit integration method for time simulation of contact problems by a forward Lagrange algorithm.

4.2.1   Numerical code

The explicit dynamic finite element code PLASTD (in 2D), is used to simulate the behavior of the system during the frictional contact. This software [87] is designed for large deformations and non-linear contact behavior, and applies a forward Lagrange multiplier method for the contact between deformable bodies. For the dynamic analysis, the formulation is discretized spatially by using the finite element method and temporally by using the β_2 method (Newmark). The contact algorithm uses slave nodes and target surfaces described by a four node quadrilateral element with 2x2 Gauss quadrature rule. The elementary target segments are described by two nodes and approximated by bicubic splines [88]. The forward Lagrange multiplier method is formulated by equations of motion at time ($t^i = i\Delta t$) with the displacement conditions imposed on the slave nodes at time t^{i+1}:

$$\begin{cases} M\ddot{u}^i + C\dot{u}^i + Ku^i + G^{i+lT}\lambda^i = F^i \\ G^{i+l}\{X^i + u^{i+1} - u^i\} \leq 0 \end{cases} \quad (4.1)$$

where M and K are respectively the symmetric and positively defined system matrices of mass and stiffness. C is the Rayleigh's proportional damping matrix:

$$C = (\alpha M + \beta K) \quad (4.2)$$

X^i is the coordinate vector at time t^i. u, $\dot{u}$, $\ddot{u}$ are respectively the vectors of nodal displacements, nodal velocities and accelerations. F is the vector of nodal external forces.

$\lambda = [\lambda_n \lambda_t]^T$ contains respectively normal and tangential contact forces acting on the nodes at the contact surface.

$G^T = [G^T{}_n G^t{}_n]$ is the global matrix of isplacement conditions ensuring non-penetration and the contact law of the bodies in contact.

The equations of motion 4.1 are discretized in time, by using an explicit Newmark scheme. The vectors $\ddot{u}^i$ and $\dot{u}^i$ are expressed at each time step using a time scheme of type β_2 (β_2 [0.5;1[ ):

$$\begin{cases} \ddot{u}^i = \frac{2}{\Delta t^2}(u^{i+1} - u^i - \Delta t\dot{u}^i) \\ \\ \dot{u}^i = \frac{1}{1+2\beta_2}\{\dot{u}^{1+1} + \Delta t(1 - \beta_2)\ddot{u}^{i-1} + \frac{2\beta_2}{\Delta t}(u^{i+1} - u^i\} \end{cases} \quad (4.3)$$

The stability of this method is assured when restriction on the critical time Δt_c is respected:

$$\Delta t_c \leq \frac{1}{\omega_{max}\sqrt{\frac{\beta_2}{2} - \beta}} \quad (4.4)$$

For the explicit Newmark β_2 scheme $\beta = 0$ and $\beta_2 > 1/2$, so Δt is:

$$\Delta t_c \leq \frac{1}{\omega_{max}\sqrt{\frac{\beta_2}{2}}} \quad (4.5)$$

The parameter β_2 is a numerical damping, equal to 0.5 for the central difference method and ω_{max} is the natural frequency of the smaller element. It is possible to approximate ω_{max} with the term $2*c/L$, where c is the longitudinal wave speed $\sqrt{\frac{E}{\rho}}$ and L is the element length. E and ρ are the material Young modulus and density. In consequence the approximated equation of the critical time is:

$$\Delta t_c \leq \frac{L}{2\sqrt{\frac{E\beta_2}{\rho 2}}} = \frac{\frac{L}{2}\sqrt{\frac{\rho}{E}}}{\sqrt{\frac{\beta_2}{2}}} \tag{4.6}$$

Thus, higher is the numeric dumping, smaller is the critical time. For the central difference method, where $\gamma > 1/2$:

$$\Delta t_c \leq \frac{L}{\sqrt{\frac{\rho}{E}}} \tag{4.7}$$

The critical time limits the time interval Δt and consequently affects the computational effort necessary for the simulation.

The displacements $^*u^{i+1}$ of the nodes situated on the contact surface are first computed with λ_i equal to 0. If β_2 is fixed to 0.5 (central difference method) the nodal displacements at time $^*t^{i+1}$ are obtained so that:

$$^*u^{i+1} = \Delta t^2 M^{-1}(F^i - Ku^i) + 2u^i - u^{i-1} \tag{4.8}$$

A constraint matrix G^{i+1} is formulated for the slave nodes if they have penetrated through a target segment. Calculations of contact forces λi and nodal displacements at time t^{i+1} are then performed:

$$\begin{cases} \lambda^i = (\Delta t^2 G^{i+1} M^{-1} G^{i+1^T})^{-1} \ G^{i+1}(^*u^{i+1}) \\ \\ u^{i+1} = {}^*u^{i+1} - (\Delta t^2 M^{-1} G^{i+1^T} \lambda^i) \end{cases} \tag{4.9}$$

Equations 4.9 are solved using the Gauss-Seidel method. During each iterations the following two contact conditions for each slave node k are checked:

$$\begin{aligned} I)\ \lambda_n^k \leq 0 \quad & \begin{cases} \lambda_n^k < 0 \quad (contact) \\ \\ \lambda_n^k = 0 \quad (separation) \end{cases} \\ \\ II)\ \|\lambda_t^k\| \leq \mu\,|\lambda_n^k| \quad & \begin{cases} if\ \ \|\lambda_t^k\| < \mu\,|\lambda_n^k| \ \rightarrow\ \dot{u}_t = 0 \quad (stick) \\ \\ if\ \ \|\lambda_t^k\| = \mu\,|\lambda_n^k| \ \rightarrow\ \lambda_t^k \cdot v_t \leq 0 \ (slip) \end{cases} \end{aligned} \tag{4.10}$$

where n and t are the normal and tangential vectors defining the contact, λn and λt are the normal and tangential contact forces at each node k and μ is the Coulomb friction coefficient. The first condition means that the contact force is a compression force (without adhesion components), while the second condition is associated with the use of a Coulomb friction law.

4.2.2 Finger model

The 2D model has been developed to be representative of the fake finger used for the measurements (see section 2.2.2): the body of the finger is made of RTV silicone that reproduces experimentally fingerprints and fingertip shape by molding technique; the central lever is made of aluminum and represents the finger bones, conferring stiffness to the finger; the surface of the aluminum sample with periodical roughness is modeled by a rigid surface (Figure 4.5).
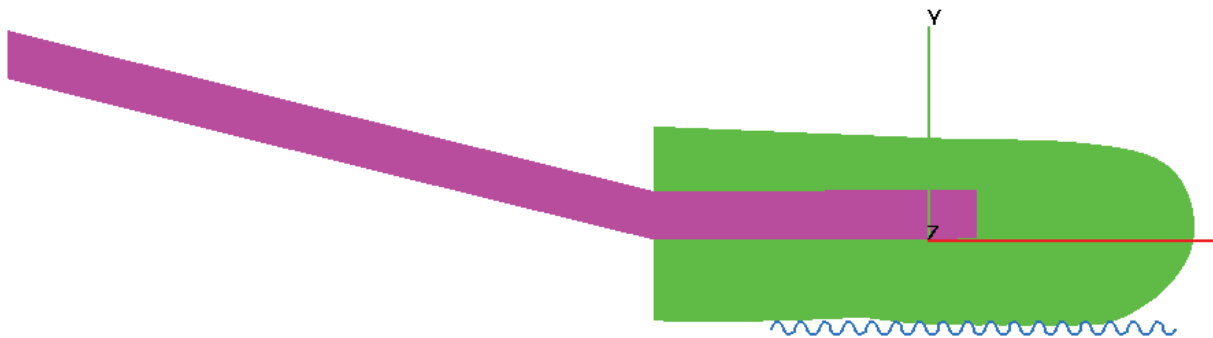
Figure 4.5: Numerical model.

The material parameters used for the simulations are the Young modulus E of the silicone equal to 1 MPa, its density γ=0.1E-05 Kg/mm^2 and the Poisson coefficient ν=0.4. With regard to the friction law, a Coulomb friction coefficient of 0.7 has been introduced. These properties are an approximation of the real material properties and have been used for a preliminary analysis.

With respect to the boundary conditions, the degrees of freedom of the nodes situated at the upper part of the aluminium lever are fixed to reproduce the connection between the real fake finger and its support; the surface sample is displaced at a constant speed.

Once the geometry and the mesh are created, the sinusoid representing the fingerprints is created displacing the first rows of nodes close to the finger surface; while the sinusoid representing the surface sample roughness is created by subsequent rigid segments. For this preliminary analysis it has been decided to use sinusoidal surfaces for both the finger and the sample surfaces; in further analysis it will be possible to introduce directly the surface profiles measured by profilometer. To reproduce the roughness of the finger and of the sample surface it is necessary to create a very fine mesh at the contact (the element size at the contact is about 0.001mm). At the same time, the global dynamics is also required, for correlating it to the local one. Consequently, refinement techniques have been used for having a coarser mesh away from the contact. This allows for reducing the dimension of the model (about 8542 nodes) and to decrease the computational effort. Therefore, the size of the model has been optimized for each surface sample and it increases with the decrease of the sample roughness wavelength.

To reduce the computational effort, for this preliminary tests the aluminium surface sample has been modeled by rigid surfaces, because the compliance of the skin is dominant. This greatly increases the critical time (0.1e-7 s) and, therefore reduces the simulation time.

The sinusoidal roughness of the finger and the surface sample are directly created in PlastD with the experimental roughness wavelength and arithmetic mean roughness value. In consequence, to avoid interpenetration between the two bodies and in order to reproduce the experimental loading conditions between finger and surface, at the beginning of the simulation they are not in contact. Figure 4.6 shows a force ramp up (phase I) to the desired normal load applied by the finger in the experimental set-up; as for the experimental test, the loading is obtained by a relative displacement of the finger along the normal direction to the sample surface. In order to avoid oscillations due to the system dynamic response and to reduce the loading time, a large α damping (100) is introduced in the model. In such way the stable contact condition can be reached and the sliding is initiated by the horizontal displacement of the surface sample. During the loading phase the tangential force changes its sign (Figure 4.6) because of the bending of the aluminum lever that has a component on the tangential direction. Then, the direction of the tangential force changes because of the sliding of the sample surface, reaching the final sliding state (phase II).
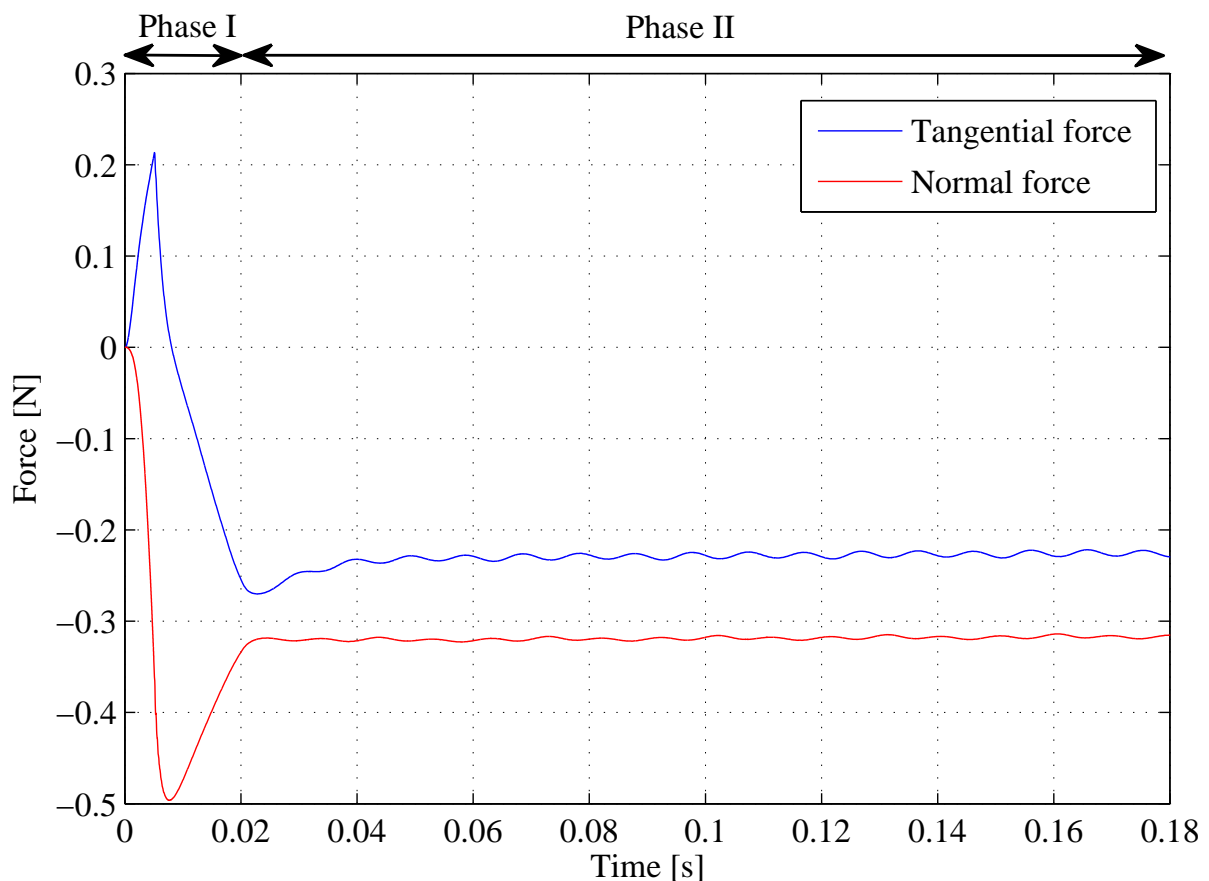
Figure 4.6: Contact tangential and normal forces (along the x and y axis).

Figure 4.7 and Figure 4.8 show the vonMises stress distribution at the contact surface during the sliding under a constant normal force and a zoom with the information about the node status (sliding, contact, adherence).
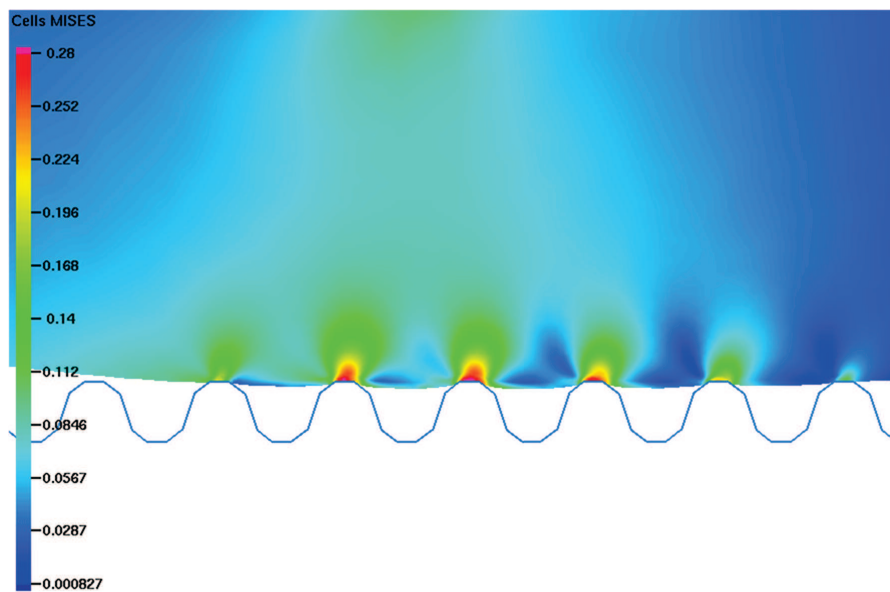
Figure 4.7: Example of the Von Mises deformation for the modeled contact between the finger meshed surface and the sinusoidal surface sample during the surface scanning at constant contact force of 0.25 N and a constant scanning speed of 50 mm/s.
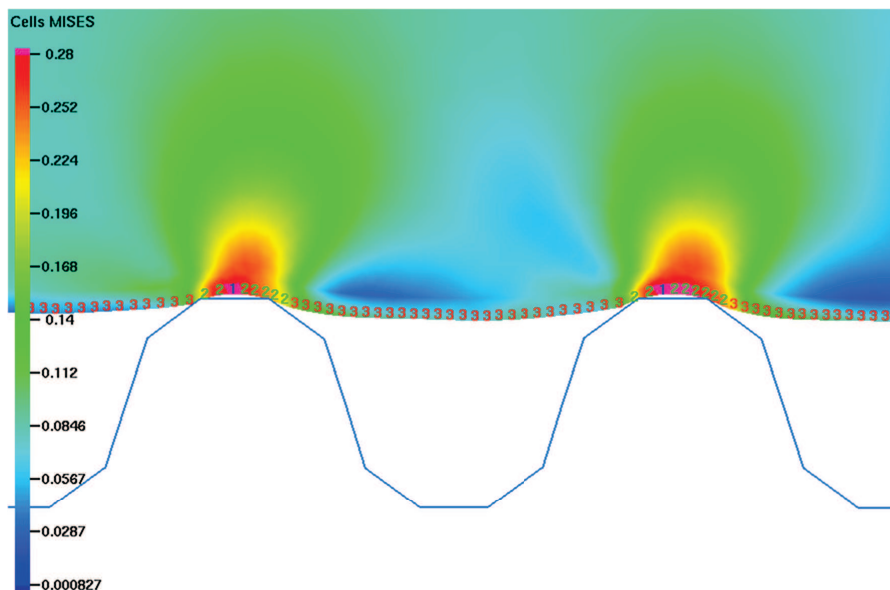
Figure 4.8: A zoom of the contact area shown in Figure 4.7 representing the contact node status: 1 adherence, 2 sliding, 3 detachment.

4.2.3 Comparison between numerical and experimental results

In order to compare experimental and numerical results, and to investigate the relationship between local and global dynamics, the acceleration of the nodes of the finger both at the contact surface and at the line corresponding to the accelerometer position are recovered during the numerical simulations.

Figure 4.9 there is an example of the acceleration signal obtained at the accelerometer position during the scanning of a surface sample with a roughness wavelength of 1.4

mm, while the finger wavelength is equal to 0.45 mm.
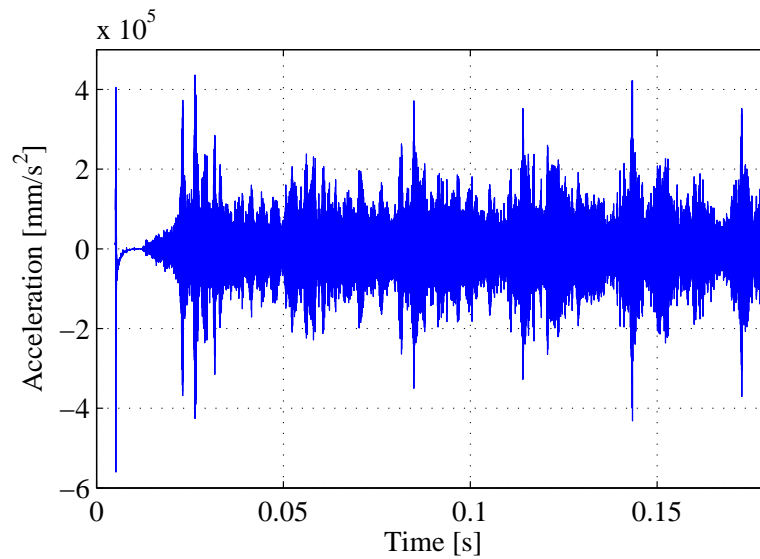
Figure 4.9: Example of the acceleration obtained from the numerical simulation at the accelerometer position for the scanning on a surface sample with a roughness period of 1.4 mm.

Figure 4.10 shows the corresponding acceleration at the contact zone between the finger and the sample. The larger amplitude of the vibration calculated at the fingernail can be explained by the fact that it is the sum of the local vibrations excited along all the interfaces and transmitted by the finger, while the acceleration at the contact surface is representative of the local vibration excited by the contact between the closest contact zones.
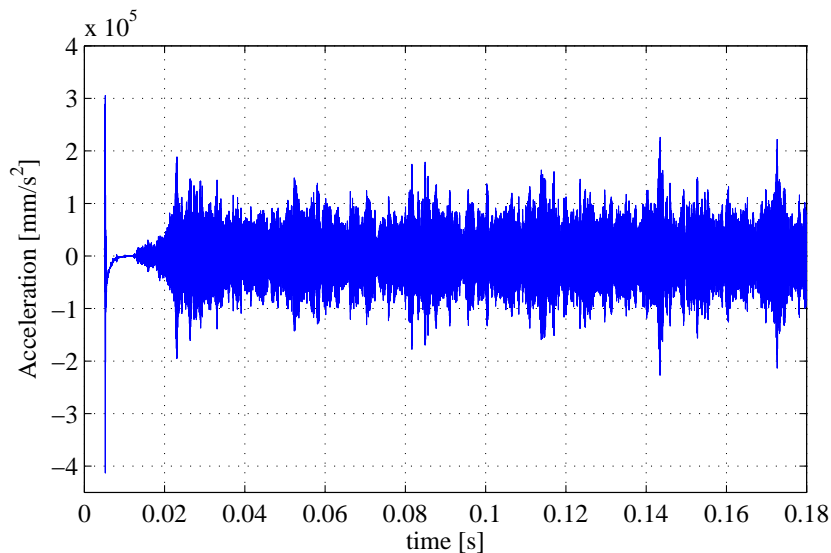
Figure 4.10: Example of the acceleration obtained from the numerical simulation at the finger/surface contact zone for the scanning on a surface sample with a roughness period of 1.4 mm.

Figure 4.11 (a) shows the FFT obtained from the acceleration at the fingernail position while Figure 4.11 (b) shows the FFT obtained from the acceleration recorded at the

contact zone (Figure 4.10). The main frequency peak value is the same for the two zones, about 120 Hz, and is the same obtained by the experimental measurements on the surface sample with a roughness wavelength of 1.4 mm.
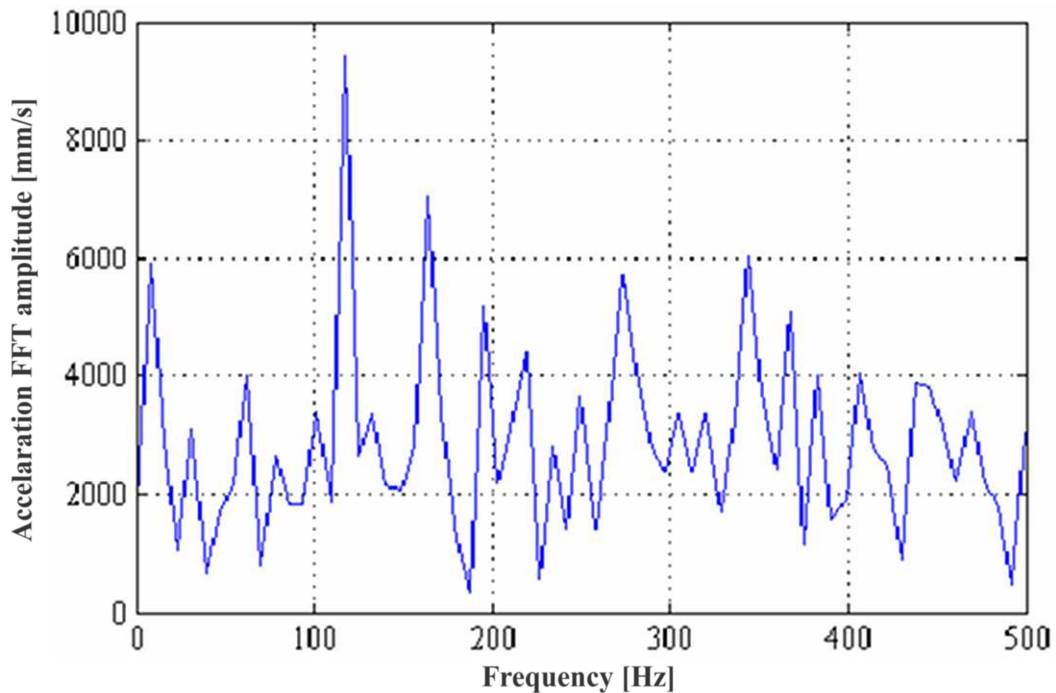
(a)
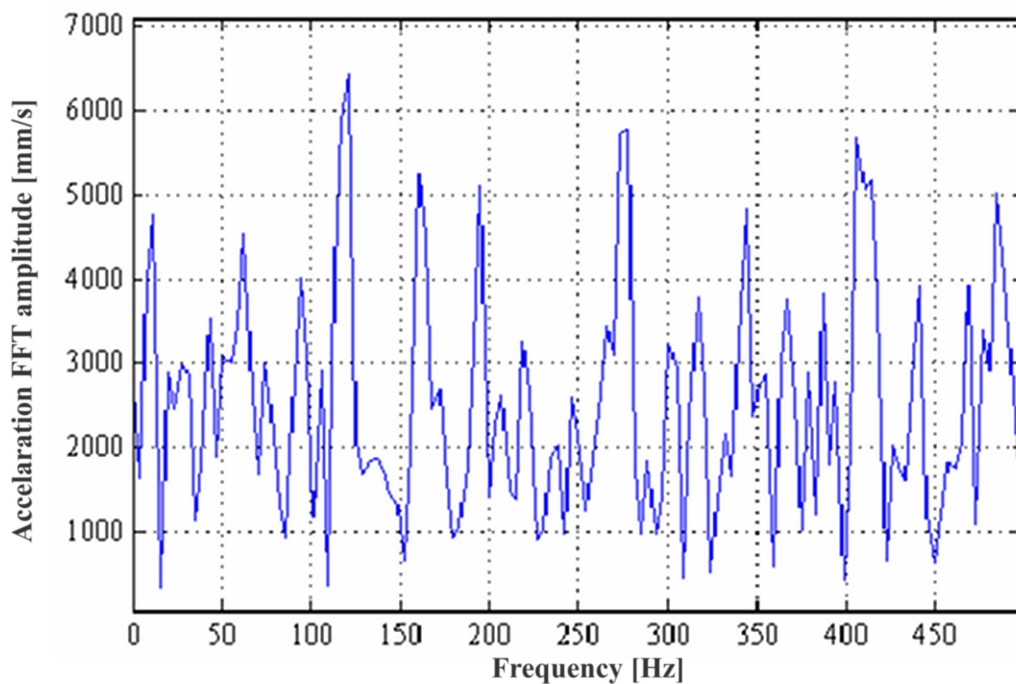
(b)

Figure 4.11: Example of the acceleration FFT obtained from the numerical simulation at the accelerometer position (a) and at the contact zone (b). The main frequency peak value is the same for the two zones, at about 120 Hz.

Comparing the spectra of the local and global vibrations, it can be asserted that the frequency distribution is quite similar, with an amplification of the main peak of the global vibration due to the contribution of all the contact zones. Further investigations are needed on this subject.

The resolution in frequency of the calculated spectra is poor, due to the small simulation time; nevertheless, these preliminary tests allow for recovering the same frequency peaks measured experimentally for the induced vibrations as shown in Figure 4.12, where the frequency peak values calculated by the numerical model agree with the ones measured by the experimental investigations on a finger with the same fingerprint wavelength used for the model. On the contrary the amplitude of vibration is not comparable to the experimental one. This because the material properties and in particular the material damping properties have not been updated by comparison with experimental tests.

The numerical results presented in this section are a first attempt to model and simulate the finger/surface scanning. The preliminary results show the capability of the numerical code to simulate the phenomenon and the possible interesting perspectives on the analysis of the local and global vibrations; a parametrical analysis will be performed as well for the understanding of the influence of material (damping) and contact (friction coefficient, adhesion, etc. . .) properties on the vibration induced by the surface scanning.
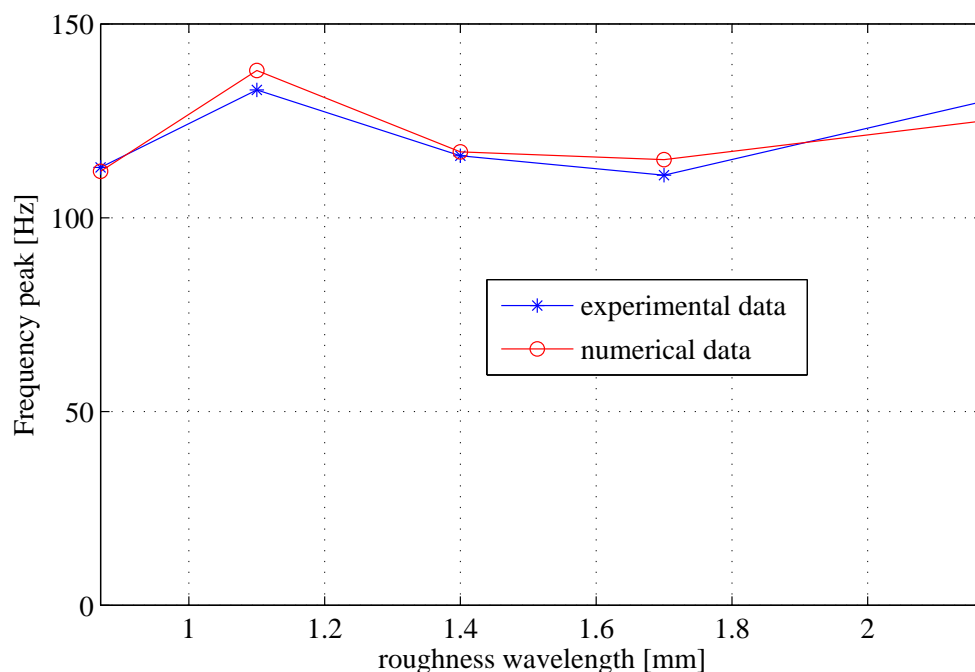
Figure 4.12: Relationship between the vibration FFT frequency peak values and roughness sample wavelength at a scanning speed of 50 mm/s for the experimental and the numerical results.

4.3   Measurements of local dynamics

Important data for updating and validating the numerical model will be recovered by the measurements of the local dynamics by image cross-correlation techniques. The TriboTouch has been designed to analyze the local vibrations at the contact surface using a fake finger and the image cross-correlation technique. The fake finger has been first

validated by comparison between the global vibrations measured at the fingernail of the real and fake finger (see chapter 2).

Then, the fake finger has been cut perpendicularly to the contact zone, and a fast camera is used to film the vibrations at the contact zone during the sliding (Figure 4.13). An image speckle is created on the fake finger surface (Figure 4.13(b)), creating a reference for the analysis of the images. A camera records the contact between the finger and the surface sample for the test duration and, throughout the image cross correlation, it is possible to know the displacement of the reference points chosen on the image speckle. At this time, only preliminary tests have been developed to verify both the feasibility of this experimental solution, and the image resolution reached with this technique. The preliminary results show the possibility to recover representative videos of the local vibrations. Results from the image cross-correlation are still not available.
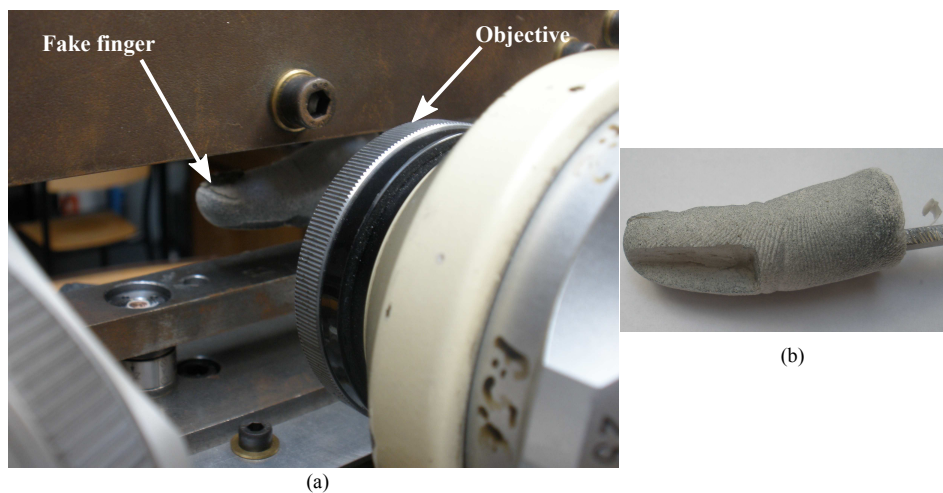
Figure 4.13: Experimental configuration for the measurements of the local dynamics on the finger model (a) and a zoom of the finger model with the image speckle (b).

4.4 Concluding remarks

A simplified numerical model and a finite element model have been developed to reproduce the scanning between the finger and the surface sample. The simplified model, simulating the sliding between two sinusoidal surfaces, allowed for highlighting the filtering role of the fingerprints on the vibrations. The aim of the FE model is to realize a parametrical study of the vibration induced from the scanning and to analyze the local vibrations and their link with the global ones. The frequency distribution obtained by the numerical model is comparable with the experimental one, while the same vibration amplitude is not attended. This difference is due to the material used in the models that is considered isotropic and to the material properties that are just a first approximation of the silicone ones. Nevertheless, even if these models are just a first attempt, they confirm the main role of the fingerprint in the tactile perception and show the capability of the numerical code to reproduce the phenomenon.

Chapter 5

Conclusions

This thesis is a first step of a project aimed at the definition of a quantitative characterization of the link between contact features, induced vibrations and tactile perception. The aim of the project is the analysis of the vibrations induced by the scanning of a finger on a surface, which are the direct cause of the mechanoreceptor excitation coded by the brain. The relationship among the features of the vibration spectra, the contact and scanning parameters, and the tactile perception is investigated in order to define objective indexes representative of the tactile sense.

Instead of focusing on each single feature of the contact pair (surface texture, material compliance, friction characteristics, etc...), the focus is moved directly to the induced vibrations, which are affected by contact characteristics and already contain the information perceived by the mechanoreceptors and coded by the brain. The aim is to keep into account the complexity of the phenomenon, which is affected by a large number of parameters interacting each other. In other words, to overcome the issue of neglecting the effect of a parameter or a combination of parameters (e.g. when accounting for only the texture of the object surface) the attention is focused to the consequence of the sliding contact, which are the direct element of activation of the human receptors, i.e. the induced vibrations.

Nevertheless, the investigation of the vibrations induced from the scanning of a finger on a surface involves several difficulties due to the contact characteristics and to the measurements themselves. Such issues are mainly related to the low amplitude of vibrations and to the impossibility of measuring the vibrations directly at the finger/object contact zone, without modifying the contact. The first issue is the reproduction of the scanning without affecting the measurements with external noise coming from the experimental test-bench. In fact the reproduction of the sliding contact between two surfaces implies the relative motion between them, which is obtained by appropriate mechanisms having a more or less complicated kinematics and including several sliding surfaces (bearings, sliders, etc...). In such a context it is quite difficult to distinguish between the vibrations coming from the reproduced sliding and the parasitic noise coming from the other sliding contact pairs.

With this aim, it has been decided, after preliminary measurements characterizing the main parameters involved in this study (like vibration magnitude and scanning speed), to develop a new experimental set-up, named TriboTouch. It is able to provide the relative motion between the contact surface by means of a compliant system and to recover the contact forces and the induced vibrations. The set-up can cover the full range of scanning speeds naturally used by human subject.

The test bench has been designed to guarantee measurement reproducibility and to avoid external noise. Indeed, the relative motion between finger and surface is obtained without any other interface under sliding contact by the compliant system and a linear voice coil actuator.

The TriboTouch allows for the development of measurements involving both real fingers and fake ones. The measurements on the real finger detect the global dynamics: an accelerometer is mounted on the finger to detect the induced vibrations and two triaxial force transducers are placed below the surface sample, to recover the contact forces and calculate the friction coefficient.

The use of a fake finger avoids the need to investigate each surface sample with the real finger, allows for the detection of the local vibrations (meaning at the contact area) by image cross correlation technique, and ensures constant boundary conditions (contact force, scanning speed, etc...).

After numerical and experimental validation of the new experimental set-up, the TriboTouch has been used to analyze the behavior of the right hand index finger, when scanning on rigid surface samples with periodical and isotropic roughness and on fabric samples.

To perform a parametric investigation of the vibration behavior with respect to the contact and scanning features and to analyze the link between the local and the global vibrations, both a simple numerical model, reproducing the sliding contact between two sinusoidal surfaces, and a finite element model, for transient simulation of the contact between finger and surface sample, have been developed.

5.1   Original contributions

Recent publications on virtual reality and augmented reality have highlighted the possibility of inducing the tactile sensation of surface ripples by exciting the finger nail with appropriate vibrations; several studies have investigated skin mechanical and frictional properties, pointing out the effects of skin natural production of sweat during the contact and finger scanning direction and inclination (with respect to the subject surface); on the contrary the link between induced vibrations features and surface characteristics perception has not been fully investigated yet and it constitutes a relatively new research field.

In this context, the thesis proposes a new approach to the study of the tactile perception through a complementary methodology, by developing experimental measurements and numerical models and accounting for the dynamic and tribological aspect of the problem. The main contributions introduced from the work object of this thesis are summarized in the following points:

– the development and the validation of a new experimental set-up, able to perform measurements of the induced vibrations and of the contact load, avoiding noise generation and without altering the measurements is one of the main goals of the thesis.

– In all the spectra obtained from the measurements on the real finger, the most significant part of the signals falls in the range between 2 and 500 Hz corresponding the whole reaction range of the mechanoreceptors. The measurements have been performed using roughness width and magnitude of everyday's object surfaces. The results show the correspondence between the mechanoreceptors acquisition

range and the roughness range of common surfaces.

– The analysis of the vibration detected on the real finger when scanning on rigid surface samples with periodical roughness, has highlighted the vibration linear trend with respect to the scanning speed and the non linear dependence from the roughness wavelength.

– The analysis of the relationship between the vibration frequency trend with respect to the surface sample roughness wavelength has highlighted the agreement of the experimental results with the "duplex perception model" presented in neurophysiologic literature. Specifically the experimental results show the possibility to distinguish among three different vibration behaviors on the basis of the relationship between the surface sample roughness width and the fingerprint one. When the surface sample wavelength is smaller than the fingerprint one, the frequency peak characterizing the spectra is affected by the sample width. When the fingerprint wavelength is smaller than the surface sample one, the frequency peak is independent by the sample roughness width and is affected by the fingerprint one; while a transition zone occurs when the two wavelength are comparable. These results suggest that the transition by a vibrational code (for the fine textures) to a spatial one (for coarse textures), affirmed by the "duplex model", is related to the fingerprint width.

– The role of the filtering effect of the fingerprints has also been confirmed from the numerical model developed to reproduce the sliding induced vibrations between two sinusoidal surfaces.

– The analysis of the vibration detected on the real finger when scanning on a rigid surface sample with isotropic roughness have highlighted that the corresponding spectra are characterized by a broadband distribution. This distribution rises in magnitude and shifts toward higher frequencies with the increasing of the scanning speed.

– The analysis of the vibration detected on the real finger when scanning on fabric samples has shown that the corresponding spectra are characterized by well defined peaks related to the fabric texture periodicity and a large frequency distribution related to the fabric yarn roughness. These two components are always present in the spectra, but their contribution depends on the fabric structure. When the fabric has a small yarn roughness, the most significant part of the spectra is represented by the frequency peaks, while the opposite happens when the fabric has high hairiness. A different behavior of the amplitude of the peaks can be observed as a function of the scanning speed: while the peak amplitude due to the finer texture periods (higher frequency) dominates for higher speeds, the amplitude of the vibrations due to the larger texture periods (lower frequency) dominates for low scanning speeds. This different behavior can be ascribed to the accommodation of the textile fibers occurring during the scanning changing the contact pattern. The frequency peak due to the fingerprints, which in this case are stiffer than the scanned surface, stays in the spectrum for all the scanning speeds.

– The study of the friction coefficient obtained from the skin/aluminium contact has proven, in agreement with the literature and the Wolfram theory for the contact between distorting surfaces, a decreasing friction coefficient with respect to the increasing of the contact load; a slight decreasing trend with respect to the scanning speed increase has been found. The decrease of the friction coefficient with the increase of the scanning speed is more significant for the contact between skin and

fabrics.

– The analysis of the global vibrations detected on the fake finger agrees with the one developed on the real finger, confirming the capability of the realized silicone polymer fake finger to reproduce the dynamical behavior of the real one.

– The representativeness of the fake finger is confirmed also by the similar values and trend (with respect to the normal load and the scanning speed) of the friction coefficient, thanks to the polymer permeability and to its bath on vaseline.

– The fake finger allows to slightly change the contact load, so that the effect of such variation in terms of vibration amplitude can be pointed out. The results have been compared with measurements on the real finger and allowed to quantitatively verify that the tactile perception is independent of the contact load for forces ranging between 0.2 and 1 N, while it rises for higher force values; similar results have been reported in literature on the base of neurophysiological studies on human subjects.

The development and validation of the TriboTouch set-up allowed to carry out a first analysis of the induced vibration spectra in function of some of the driving parameters. The presented results, in agreement with neurophysiologic analyses in literature, highlight the possibility to carry out objective indexes (frequency, spectral distribution, vibration amplitude, etc.) to quantify some of the subjective features of the tactile perception. Such results open interesting perspectives on the analysis of the tactile perception, with a particular focus on perception of fabrics.

5.2 Perspectives

As asserted above, this thesis is a first step of a project that is aimed to the definition of a quantitative characterization of the link between contact features, induced vibrations and tactile perception. The development and the validation of both the set-up and the measurements methodology and the obtained results will be the basis for further investigation:

– The results on the fabrics open a new interesting domain of investigation to link the different components of the vibration spectra to the quality perception of a fabric. In consequence, the next steps concern both further experimental campaigns to better characterize the fabric spectra and friction coefficient, and statistical investigations on human subjects to characterize the corresponding tactile perception.

– Both the experimental analysis and the numerical one have highlighted the role of the fingerprint in the frequency distribution of the vibration spectra. To better clarify this aspect and to extend the investigation of the role of the vibration amplitude, a parametrical analysis has to be developed improving the numerical model. This type of analysis is needed to understand the influence of material (damping) and contact (friction coefficient, adhesion, etc...) properties on the induced vibrations and the link between the local and the global vibrations.

– To this purpose, important data for updating and validating the numerical model need to be recovered by measuring, on the fake finger, the local dynamics by image cross-correlation techniques.

– Finally, a statistical analysis on human subjects is a necessary in order to draw a correlation between objective indexes, issue of the investigation of the induced vibrations, and tactile perception. Such analysis has to account for both the properties of the perceived surfaces (texture, material, adhesion, etc...) and the variety

of the human perception features (in function of subject age, gender, etc. . .).

Bibliography

[1] Tang W., Ge S., Zhu H., Cao X., Li N., The influence of normal load and sliding speed on frictional properties of skin, Journal of Bionic Engineering; 5: 33-38, 2008.

[2] Asserin J., H. Zahouani, Ph. Humbert, V.Couturaud, D. Mougin, Measurements of the friction coefficient of the human skin in vivo. Quantification of the cutaneous smoothness, Collids and surfaces, 19, 1-12, 2000

[3] Schrade U., Gerhardt L.C., Tribology of human skin and mechanical skin equivalents in contact with textiles, Journal of Wear, 263, 1112-1116, 2007.

[4] Tang W., Bhushan B., Adhesion, friction and wear characterization of skin and skin cream using atomic force microscope, Colloids and Surfaces B: Biointerfaces 76, 1-15, 2010.

[5] Hollins M., Bensmaïa S., Risner R., The duplex theory of tactile texture perception, Proceedings of fourteenth annual meeting of the international society for psychophysics , 115-120, 1998

[6] Lynette A. Jones and Susan J. Lederman. 2006. Human Hand Function, Oxford University Press

[7] Johansson R. S.,Tactile sensibility in man. A quantitative study of the population of mechanoreceptive units in the glabrous skin area of the hand, Umea university medical dissertations, new series no 35, 1978

[8] Maeno T., Kobayashi K., Yamazaki N., Relationship between the structure of human finger tissue and the location of tactile receptors, Bulletin of JSME international journal, vol 41, No 1, C, pp. 94-100, 1998.

[9] Hollins M., Bensmaïa S., Karlof K., Young F., Individual differences in perceptual space for tactile textures: evidence from multidimensional scaling, Perception and Psychophysics, 62, 1534-1544, 2000

[10] Hollins M., Bensmaïa S., Washburn S., Vibrotactile adaptation impairs discrimination of fine, but not coarse, textures, Somatosensory and Motor Research, 18, 253-262,2001

[11] Lederman S.J., Taylor M.M., Fingertip force, surface geometry, and perception of roughness by active touch, Perception & Psychophysics, 12 (5), 401-408, 1972.

[12] Lederman S.J., Loomis J. M., Williams D. A., The role of vibration in the tactual perception of roughness, Perception & Psychophysics, 32 (2), 109-116, 1982.

[13] Lederman S.J., Tactual roughness perception: spatial and temporal determinants, Canadian Journal of Psychology, 37(4), 498-511, 1983.

[14] T. Yoshioka, S. J. Bensamaïa, J. C. Craig, S. S. Hsiao, Texture perception through direct and indirect touch: an analysis of perceptual space for tactile textures in two modes of exploration, Journal of somatosens mot. res. ,24 (1-2), 53-70, 2007.

[15] Johnson K. O., Yoshioka T., Vega-Bermudez F.: Tactile functions of mechanoreceptive afferents innervating the hand, Journal of Clinical Neurophysiology, 17, 539-558, 2000

[16] Lederman S.J., Taylor M.M., Fingertip force, surface geometry, and Perception of roughness by active touch, Perception & Psychophysics, 12 (5), 401-408, 1972.

[17] Akay A., Acoustic of friction, Journal of Acoustical Society of America, 111(4): 1525-1548, 2002.

[18] Ando H., Watanabe J., Inami M., Sugimito M., Maeda T., A fingernail mounted tactile display for augmented reality systems, Electronics and communications in Japan, part 2, vol 90, no 4, 2007.

[19] Kajimoto H., Inami M., Kawakami N., Tachi S., SmartTouch augmentation of skin sensation with electrocutaneous display, Haptic interfaces for virtual environment and teleoperator systems, Proceedings of 11th symposium on haptics, 2003

[20] Derler A., Schrade U., Gerhardt L.C., Tribology of human skin and mechanical skin equivalents in contact with textiles, Journal of Wear, 263, 1112-1116, 2007.

[21] Sivamani R. K, Goodman J., Gitis N., Maibach H. I, Friction coefficient of skin in real-time, Skin Research and Technology, 9, 235-239, 2003.

[22] Sivamani R. K, Goodman J., Gitis N., Maibach H. I, Coefficient of friction: tribological studies in man-an overview, Skin Research and Technology, 9, 227-234, 2003.

[23] Lumpkin E. A., Caterina M. J., Mechanisms of sensory transduction in the skin, Nature, 445, 22 February 2007, doi:10.1038/nature05662

[24] Lynn B., Perl E. R., Afferent mechanisms of pain, Pain and touch, pp 213-241, 1996

[25] Spray D. C., Cutaneous temperature receptors, Annual reviews of physiology, 48, 625-638, 1986

[26] Johnson K. O, The roles and functions of cutaneous mechanoreceptors, Current Opinion in Neurobiology; 11: 455-461, 2001.

[27] Bolanowski S. J., Gescheider G. A., Verrillo R. T., Checkosky C. M.: Four channels mediate the mechanical aspects of touch, Journal of the Acoustical Society of America, 84, 1680-1694, 1988.

[28] Trulsson M., Francis S. T., Kelly E. F., Westling G., Bowtell R., McGlone F., Cortical Responses to Single Mechanoreceptive Afferent Microstimulation Revealed with fMRI, NeuroImage, doi:10.1006/nimg.2000.0723, 2000.

[29] Kelly E. F., Trulsson M., Folger S. E., Periodic Microstimulation of Single Mechanoreceptive Afferents Produces Frequency-Following Responses in Human EEG, The American Physiological Society, 0022-3077/97, 1997.

[30] Jenmailm P., Birznierks I., Goodwin A. W., Johansson R. S.: Influence of object shape on responses of human tactile afferents under conditions characteristic of manipulation, European journal of neuroscience, vol.18, 164-176, 2003

[31] Goodwin A. W., John K. T., Marceglia A. H.: Tactile discrimination of curvature by humans using only cutaneous information from the fingerpads, Experimental Brain Research, 86, 663-672, 1991.

[32] Goodwin A. W., Wheat H. E.: Magnitude estimation of contact force when objects with different shapes are applied passively to the fingerpad, Somatosensory and Motor Research, 9, 339-344, 1992.

[33] Vega-Bermudez F.,Johnson K. O.: SA I and RA receptive fields, responses variability, and population responses mapped with a probe array, Journal of Neurophysiology, 81, 2701-2710, 1999.

[34] Johansson R. S., Lofvenberg J., Regional differences and interindividual variability insensitivity to vibration in the glabrous skin of the human hand, Brain Research, 301:65-72, 1984.

[35] Birznieks I., Jenmalm P., Goodwin A. W., Johansson, R. S.: Encoding of direction of fingertip forces by human tactile afferents, Journal of Neuroscience, 21, 8222-8237, 2001.

[36] Talbot W. H., Darian-Smith I., Kornhuber H. H., Mountcastle V. B., The sense of flutter-vibration: comparison of the human capacity with response patterns of mechanoreceptive afferents from the monkey hand, Journal of Neurophysiology;31:301-334, 1968.

[37] Bolanowski S. J., Gescheider, G. A. and Verrillo R. T.: Hairy skin: Psychophysical channels and their physiological substrates. Somatosens Mot Res 11 , pp. 279-290, 1994.

[38] Olausson H., Wessberg J., Kakuda N., Tactile directional sensibility: peripheral neural mechanisms in man, Brain Research, 866, 178-187, 2000.

[39] Biggs J., Srinivasan M. A., Tangential versus normal displacements of skin: relative effectiveness for producing tactile sensations, IEEE, 2002.

[40] Napier J. R., The human hand, Burlington, NC: Carolina biology supply, 1976.

[41] Manuskiatti W., Schwindt D. A., Maibach H. I., Influence of age, anatomic site and race on skin roughness and scaliness, Dermatology, 196, 401-407, 1998.

[42] Qi Wang, Vincent Hayward: In vivo biomechanics of the fingerpad skin under local tangential traction,Journal of biomechanics, 40(4), pp. 851-860, 2007.

[43] Prevost A., Scheibert J., Debregeas G., Effect of fingerprints orientation on skin vibrations during tactile exploration of textured surfaces, Commununicative & Integrative Biology, 2009 Sep-Oct; 2(5): 422-4.

[44] Koudine A. A., Barquins M., Anthoine PH., Aubert L., Leveque J. L., Friction properties of skin: proposal of a new approach, International Journal of Cosmetic Science, n.22:11-20, 2000.

[45] Adams M. J., Briscoe B. J., Johnson S. A., Friction and lubrication of human skin, Tribology letters, vol 26, no 3 june 2007.

[46] G. Sheng : Friction Induced Vibrations and Sound. Principle and Applications, CRC Press Taylor and Francis Group,2007.

[47] El-Shimi A. F., In vivo skin friction measurements, J. Soc. Cosmet., Chem., 28, 37-51, February 1977.

[48] Scheibert J., Prevost A., Frelat J. and Rey P. and Debrégeas G., Experimental evidence of non-Amontons behaviour at a multicontact interface, arXiv:0806.1594v1 [cond-mat.soft] 10 Jun 2008.

[49] Adamson A. W., Physical chemistry of surfaces, Interscience, New York, 1965.

[50] Burwell J. T., Straug C. D., J. Appl. Phys., 20, 79, 1949.

[51] Appeldoorn J. K., Barnett G., Frictional aspects of emollience, Proc. Sci. Sect. Toilet Goods Ass., 40, 28-35, 1963.

[52] Prall J. K., instrumental evaluation of the effects of cosmetic products on skin surfaces with particular reference to smoothness, J. Soc. Cosmet. Chem., 24, 693-707, 1973.

[53] Comaish S., Bottoms E., The skin and friction deviations from Amonton's law, and the effects of hydration and lubrication, Brit. J. Dermatol., 84, 34-73, 1971.

[54] Han H. Y., Shimada A., Kawamura S., Analysis of friction on human fingers and design of artificial fingers, Proceedings of the 1996 IEEE International Conference on Robotics and Automation Minneapolis, Minnesota april 1996.

[55] Wolfram L. J, Friction of skin, J. Soc. Cosm. Chem., 34, 465-476, 1983.

[56] Wolfram L. J, Frictional properties of skin, Cutaneous investigation in health and desease, pp. 49-57, Marcel Dekker, New York, 1986.

[57] Raja K. Sivamani, Jack Goodman, Norm V. Gitis, Howard I. Maibach: Coefficient of friction: tribological studies in man-an overview, Skin research and technology, 9: pp. 227-234,2003.

[58] Klatzky R. L., Lederman S. J., Relative availability of surface and object properties during early haptic processing, journal of experimental psychology: human perception and performance, 23, 1680-1707, 1997.

[59] Klatzky R. L., Lederman S. J., Reed C., There is more to touch than meets the eye: relative salience of object dimensions for touch with and without vision, Journal of experimental psychology: human perception and performance, 15, 45-57, 1989.

[60] Srinivasan M. A., LaMotte R. H., Tactual discrimination of softness: Abilities and mechanisms, Somesthesis and the neurobiology of the somatosensory cortex, 123-136, 1996.

[61] Rhodes D., Schwartz G., Lateralized sensitivity to vibrotactile simulation: individual differences revealed by interaction of threshold and signal detection tasks, Neuropsychologia, 19, 831-835, 1981.

[62] Birznieks I., Jenmalm P., Goodwin A. W., Johanson R. S., Encoding of direction of fingertip forces by human tactile afferents, the journal of neuroscience, october 15, 21(20):8222-8237, 2001.

[63] Birznieks I., Jenmalm P., Johanson R. S., Goodwin A. W., Responses in human tactile afferents to fingertip forces with tangential force components in distal and proximal directions, Acta universitatis latviensis, 631:7-23, 2001.

[64] Hollins M., Bensmaïa S., Karlof K., Young F., Individual differences in perceptual space for tactile textures: evidence from multidimensional scaling, Perception and Psychophysics, 62, 1534-1544, 2000.

[65] Hollins M., Risner R, Evidence for the duplex theory of tactile texture perception., Percept Psychophys., 62(4):695-705, 2000.

[66] Hollins M., Fox A., Bishop C., Imposed vibration influences perceived tactile smoothness. Perception, 29, 1455-1465, 2000.

[67] Hollins M., Lorenz F., Harper D., Somatosensory coding of roughness: The effect of texture adaptation in direct and indirect touch. Journal of Neuroscience, 26, 5582-5588, 2006.

[68] Gescheider G. A., Wright J. H., Effects of sensory adaptation on the form of the psychophysical magnitude function for cutaneous vibration. Journal of Experimental Psychology, 77, 308-313, 1968.

[69] Bensmaia S. J., Hollins M, 2003, The vibrations of texture, Journal of Somatosens Mot. Res. ,20 (1), 33-43.

[70] Martinot F., "The Influence of Surface Commensurability on Roughness Perception With a Bare Finger", in proc. of Eurohaptics 2006, Paris, France, 2006.

[71] Young J. J., Yang K. U., Kwon D. S., Kang S. C., Factors affecting discrimination of surface property using an integrated display: roughness perception, ICCAS 2004.

[72] Biet M., Conception et contrôle d'actionneurs élelectro-actifs dédiés à la stimulation tactile, these pour l'obtention du Doctorat de l'Université des Sciences et Technologies de Lille (spécialité Génie électrique),décembre 2007

[73] Jeong Y., Yang G., Kyung K., Kwon D., Kang S., Factors affecting discimination of surface property using an integrated tactile display: roughness and vibration, IC-CAS2004

[74] Yoshika T., Bensmaia S. J., Craig J. C., Hsiao S.S., Texture perception through direct and indirect touch: An analysis of perceptual space for tactile textures in two modes of exploration, Somatosensory mot res, 24 (1-2): 53-70, 2007

[75] Lederman S.J., 1981, The perception of surface roughness by active and passive touch, Bulletin of the Psychonimic society, vol 18(5), 253-255.

[76] Wandersman E., Candelier, R., Debrégeas G., Prevost A., Texture-induced modulations of friction force: the fingerprint effect, arXiv:1107.2578v1 [cond-mat.soft] 13 Jul 2011

[77] Martinot F., Caractérisation du rôle de la dynamique du toucher dans la perception de textures, thése présentée et soutenue publiquement le 10 Octobre 2006 pour l'obtention du doctorat de l'université des sciences et technologies de lille (spécialité instrumentation et analyses avancées)

[78] Breugnot C., Contribution à la caractérisation mécanique du toucher des surfaces textiles à partir de critéres neurosensoriels, these pour l'obtention du titre de docteur de l'université de haute alsace discipline : sciences pour l'ingénieur, ecole nationale superieure des industries textiles de mulhouse laboratoire de physique et mecanique textiles, 2005.

[79] Praene J. M., Bueno M. A., Pense A. M., Etude phénoménologique du frottement des matériaux fibreaux souples, 18me Congrès français de méchanique, Grenouble, 27-31 août 2007.

[80] Fagiani R., Massi F., Chatelet E., Berthier Y., Sestieri A., Experimental analysis of friction induced vibrations at the finger contact surface, Proceedings of the Institution of Mechanical Engineers, Part J: Journal of Engineering Tribology, Vol.224, Issue 9, pp. 1027-1035, 2010.

[81] Phillips J. R., Johansson R. S., K.O. Johnson K.O., Responses of human mechanoreceptive afferents to embossed dot arrays scanned across fingerpad skin, Journal of neuroscience, 12(3), 827-839, 1992.

[82] Barnes C. J., Childs T. H. C., Henson B., Soutee C. H., Surface finish and touch-a case study in a new human factors tribology, Journal of wear, 740-750, 2004.

[83] Fagiani R., Massi F., Chatelet E., Berthier Y., Sestieri A., Dynamic analysis of surface scanning for tactile perception, Proceedings of the 10th Biennial Conference on Engineering Systems Design and Analysis, ASME 2010.

[84] Fagiani R., Massi F., Chatelet E., Berthier Y., Sestieri A., Design and validation of an experimental set-up for the analysis of friction induced vibrations at the finger contact surface, AIMETA, 2011.

[85] Lobontiu N., Compliant Mechanisms Design of Flexure Hinges, CRC PRESS, 2002.

[86] Henein S, "Conception des guidages flexibles" , Presses polytechniques et universitaires romande, ISBN : 2-88074-481-4, (2004).

[87] Baillet L., Sassi T., "Finite Element method with Lagrange multipliers for contact problems with friction", Comptes rendus mecanique, 334, 917-922 (2002).

[88] Baillet L., Sassi T., "Mixed finite element formulation in large de-formation frictional contact problem", Revue Européenne des Eléments Finis, 14 (2-3), 287-304 (2005).